TRANSPORTATION RESEARCH RECORD 982

Bridges and Foundations

TRB
TRANSPORTATION RESEARCH BOARD
NATIONAL RESEARCH COUNCIL
WASHINGTON, D.C. 1984

Transportation Research Record 982
Price $10.80
Editor: Elizabeth W. Kaplan
Compositor: Joan G. Zubal
Layout: Betty L. Hawkins

modes
1 highway transportation
3 rail transportation

subject areas
25 structures design and performance
33 construction
62 soil foundations

Transportation Research Board publications are available by ordering directly from TRB. They may also be obtained on a regular basis through organizational or individual affiliation with TRB; affiliates or library subscribers are eligible for substantial discounts. For further information, write to the Transportation Research Board, National Research Council, 2101 Constitution Avenue, N.W., Washington, D.C. 20418.

Printed in the United States of America

Library of Congress Cataloging in Publication Data
National Research Council. Transportation Research Board.
Bridges and foundations

(Transportation research record; 982)
1. Bridges–Foundations and piers–Addresses, essays, lectures. I. National Research Council (U.S.). Transportation Research Board. II. Series.
TE7.H5 no. 982 380.5 s 85-4969 [TG320] [642.2]
ISBN 0-309-03764-6 (pbk.) ISSN 0361-1981

Sponsorship of Transportation Research Record 982

GROUP 2–DESIGN AND CONSTRUCTION OF TRANSPORTATION FACILITIES
Robert C. Deen, University of Kentucky, chairman

Structures Section
John M. Hanson, Wiss, Janney & Elstner & Associates, chairman

Committee on General Structures
Clellon Lewis Loveall, Tennessee Department of Transportation, chairman
John M. Kulicki, Modjeski & Masters, secretary
John J. Ahlskog, Dan S. Bechly, Neal H. Bettigole, Edwin G. Burdette, Martin P. Burke, Jr., Jack H. Emanuel, Dah Fwu Fine, Richard S. Fountain, Frederick Gottemoeller, J. Leroy Hulsey, Walter J. Jestings, Robert N. Kamp, Heinz P. Koretzky, Celal N. Kostem, Wendell B. Lawing, Richard M. McClure, Gordon R. Pennington, David R. Schelling, Arunprakash M. Shirole, Marcello H. Soto, Robert F. Victor, Stanley W. Woods

Committee on Steel Bridges
Frank D. Sears, Federal Highway Administration, chairman
Chris S. C. Yiu, Pavlo Engineering Company, secretary
Pedro Albrecht, Dan S. Bechly, Chester F. Comstock, J. Hartley Daniels, David A. Dock, Jackson L. Durkee, Nicholas M. Engelman, John W. Fisher, Karl H. Frank, Louis A. Garrido, Wayne Henneberger, Robert B. Jarvis, B. F. Kotalik, Richard W. Lautensleger, Albert D. M. Lewis, Abba G. Lichtenstein, Joseph M. McCabe, Jr., Roy L. Mion, W. H. Munse, Robert H. Scanlan, Frederick H. Sterbenz, Carl E. Thunman, Jr., Carl C. Ulstrup

Committee on Concrete Bridges
Robert C. Cassano, California Department of Transportation, chairman
T. Alberdi, Jr., Craig A. Ballinger, W. Gene Corley, C. S. Gloyd, John M. Hanson, James J. Hill, Ti Huang, Cornie L. Hulsbos, Roy A. Imbsen, Hubert Janssen, Heinz P. Koretzky, H. G. Kriegel, John M. Kulicki, R. Shankar Nair, Edward G. Nawy, Walter Podolny, Jr., Adrianus Vankampen, Julius F. J. Volgyi, Jr., Donald J. Ward W. Jack Wilkes

Committee on Dynamics and Field Testing of Bridges
James W. Baldwin, Jr., University of Missouri-Columbia, chairman
Charles F. Galambos, Federal Highway Administration, secretary
Baidar Bakht, Furman W. Barton, David B. Beal, Harold R. Bosch, John L. Burdick, William G. Byers, Gene R. Cudney, Bruce M. Douglas, Ismail A. S. Elkholy, Hota V. S. GangaRao, David William Goodpasture, Roy A. Imbsen, F. Wayne Klaiber, Celal N. Kostem, Robert H. Lee, Fred Moses, M. Noyszewski, Gajanan M. Sabnis, R. Varadarajan, William H. Walker, Kenneth R. White

Construction Section
Garland W. Steele, West Virginia Department of Highways, chairman

Committee on Construction of Bridges and Structures
Robert M. Barnoff, Pennsylvania State University, chairman
Mrinmay Biswas, John K. Bright, John F. Cain, David A. Dock, Jackson L. Durkee, Thomas H. Ellis, George A. Harper, Marvin H. Hilton, Frank J. Kempf, Andrew Lally, John P. Rutter, Michael M. Sprinkel, Man-Chung Tang, J. R. Wilder, Thomas G. Williamson, Kenneth C. Wilson

Lawrence F. Spaine and William G. Gunderman, Transportation Research Board staff

Sponsorship is indicated by a footnote at the end of each paper. The organizational units, officers, and members are as of December 31, 1983.

NOTICE: The Transportation Research Board does not endorse products or manufacturers. Trade and manufacturers' names appear in this Record because they are considered essential to its object.

Contents

TENSION ARCH STRUCTURE
Sam G. Bonasso and Lyle K. Moulton 1

OVERVIEW OF THE PENNSYLVANIA STANDARD PLANS FOR LOW-COST BRIDGES
Fred W. Bowser, Fred S. Faber, Jr., Heinz P. Koretzky, and M. G. Patel 9

PERFORMANCE OF SLIDING BRIDGE BEARINGS
Ali Mazroi and Thomas M. Murray 12

EARTHQUAKE PRECURSERS AND POTENTIAL DAMAGE IN THE UNITED STATES (Abridgment)
Stewart C. Watson, Edward R. Fyfe, and Ronald J. Watson 21

HORIZONTALLY CURVED I-GIRDER BRIDGE ANALYSIS: V-LOAD METHOD
Michael A. Grubb 26

PRESTRESSED STEEL BEAM-CONCRETE SLAB COMPOSITE BRIDGE UNITS FOR COUNTY ROAD USE
Thomas Hendrick, Clifford Clottey, and Thomas M. Murray 36

TEMPERATURE PROBLEM IN A PRESTRESSED BOX-GIRDER BRIDGE
P. C. Hoffman, R. M. McClure, and H. H. West 42

SEASONAL AND DIURNAL BEHAVIOR OF CONCRETE BOX-GIRDER BRIDGES
K. Nam Shiu 50

FOUNDATION DESIGN: WEST SEATTLE BRIDGE
John H. Clark 57

PRESTRESSED CONCRETE HIGHWAY BRIDGES IN THE FEDERAL REPUBLIC OF GERMANY–CONSTRUCTION METHODS AND EXPERIENCES
Kurt Rahlwes 64

Addresses of Authors

Bonasso, Sam G., Alpha Associates, Inc., 209 Prairie Avenue, Morgantown, W. Va. 26505
Bowser, Fred W., Bureau of Design, Pennsylvania Department of Transportation, Harrisburg, Pa. 17120
Clark, John H., Andersen-Bjornstad-Kane-Jacobs, Inc., 1300 Dexter Horton Building, Seattle, Wash. 98104
Clottey, Clifford, School of Civil Engineering and Environmental Science, University of Oklahoma, Norman, Okla. 73019
Faber, Fred S., Jr., Buchart-Horn, Inc., 55 South Richland Avenue, P.O. Box M-55, York, Pa. 17405
Fyfe, Edward R., Watson Bowman Associates, Inc., 95 Pineview Drive, P.O. Box 9, Getzville, N.Y. 14068
Grubb, Michael A., Technical Center, U.S. Steel Corporation, Monroeville, Pa. 15146
Hendrick, Thomas, School of Civil Engineering and Environmental Science, University of Oklahoma, Norman, Okla. 73019
Hoffman, P. C., Department of Civil Engineering, Villanova University, Villanova, Pa. 19085
Koretzky, Heinz P., Bureau of Design, Pennsylvania Department of Transportation, Harrisburg, Pa. 17120
Mazroi, Ali, School of Civil Engineering and Environmental Science, University of Oklahoma, Norman, Okla. 73019
McClure, R. M., Department of Civil Engineering, The Pennsylvania State University, University Park, Pa. 16802
Moulton, Lyle K., Department of Civil Engineering, West Virginia University, Morgantown, W. Va. 26506
Murray, Thomas M., Fears Structural Engineering Laboratory, University of Oklahoma, Norman, Okla. 73019
Nam Shiu, K., Construction Technology Laboratories, Portland Cement Association, 5420 Old Orchard Road, Skokie, Ill. 60077
Patel, M. G., Bureau of Design, Pennsylvania Department of Transportation, Harrisburg, Pa. 17120
Rahlwes, Kurt, Philipp Holzmann AG, Taunusanlagel, 6000 Frankfurt am Main 1, Federal Republic of Germany
Watson, Ronald J., Watson Bowman Associates, Inc., 95 Pineview Drive, P.O. Box 9, Getzville, N.Y. 14068
Watson, Stewart C., Watson Bowman Associates, Inc., 95 Pineview Drive, P.O. Box 9, Getzville, N.Y. 14068
West, H. H., Department of Civil Engineering, The Pennsylvania State University, University Park, Pa. 16802

Tension Arch Structure

SAM G. BONASSO and LYLE K. MOULTON

ABSTRACT

The Tension Arch structure is introduced and explained. The Tension Arch principle, when incorporated in an innovative bridge structure, has the potential for solving many of the problems that have plagued conventional bridge designs over the years. It offers more efficient use of materials; can be used with a variety of materials, including steel, concrete, and timber; can achieve lower construction costs through reduced design cost, mass production of compressive and tensile components, minimum shop and field custom fabrication, and reduced erection time and erection equipment costs; and provides a geometry that is relatively insensitive to a variety of support movements along any or all three axes.

Throughout the years the American bridge builder has made steady progress in designing and building bridges to serve an ever expanding federal highway system, as well as state, county, and municipal roadways. Many design innovations have been introduced and bridge building techniques have been refined. This has led to longer spans; higher load carrying capacity; and, in many instances, bridges that are aesthetically pleasing. Unfortunately, however, neither bridge maintenance techniques nor the funds required to maintain this bridge system have kept pace with these modern advancements.

Consequently, the highway bridge system has fallen into disrepair and many bridges are in need of major repair, rehabilitation, or replacement. In fact, it has been estimated that almost a quarter of a million bridges in the United States are structurally deficient or functionally obsolete (1,2). More than half of these are off the federal-aid highway system. The cost of rehabilitation and replacement has been estimated at roughly $50 billion, and the funds required for such a massive program of replacement and rehabilitation are simply not available. This is especially true at the local level where the needs are particularly acute.

In an effort to make the most of available funds, there has been a trend in recent years toward the use of improved bridge maintenance techniques and the rehabilitation of existing bridges, in order to forestall the need for full-scale bridge replacement (2-7). For those bridges that must be replaced, efforts have been made to devise standardized short-span bridge replacement systems that can be constructed more quickly and economically than can custom-designed bridges (8). In addition, FHWA has attempted to encourage highway agencies to strive to integrate bridge maintenance needs into preconstruction procedures (9,pp.100-135). Although these efforts certainly constitute a move in the right direction, for the most part they have not attempted to address one of the most fundamental and continuing problems embodied in the conventional design and construction of bridges in the United States. This is the tendency to design bridge systems that are costly to build initially and that contain features that make continued maintenance difficult and expensive.

For example, in the design of conventional highway bridge systems, the cost savings that can be achieved by making the superstructure continuous over the piers has long been recognized. In fact, in many states, a relatively large percentage of the multispan bridges are designed for partial or total continuity. However, in recognition of the fact that these continuous bridges may be more sensitive to differential settlements than simply supported bridges, the majority of states found these structures on piles, or other deep foundations, unless rock or some other hard foundation material is located close to the proposed foundation level (10). In many instances, the cost of these deep foundations may be substantially greater than the savings achieved by making the superstructure continuous. Consequently, it has been suggested that substantial savings may be achieved in some instances by designing bridges to tolerate the total and differential settlements to which they may be subjected (10).

Another frequent consequence of conventional bridge design practice is the occurrence of bridge deck joints and bearings that continually require maintenance in order to prevent deterioration of the bridge superstructure (11). Although considerable effort has been devoted to solving this problem, a substantial number of highway agencies have concluded that it is better to avoid the problem than to try to solve it. For this reason there has been a trend toward the use of integral-abutment bridges, which contain no conventional joints or bearings (9, 12). However, at present the behavior of these bridges is not well understood, and, to remove at least some of the uncertainties, there has been a tendency to also found these structures on piles or other costly deep foundations (12).

These limited examples represent only a few of the many technical and financial problems facing those who are charged with maintaining and upgrading the highway bridge system in the United States. However, even if solutions to these particular problems are found, the fact remains that most conventional bridge designs do not incorporate even a limited capability for handling long-term increases in live load stresses or temporary overloads without costly overdesign, rehabilitation, or retrofitting (13).

Consequently, there is a need to redirect efforts to the development of innovative bridge systems that attempt to solve these problems. The Tension Arch bridge described in this paper is the result of one such effort that shows promise of producing reduced initial construction costs, less maintenance, better capability to adjust to total and differential settlements, and the capability to handle limited increases in live loads without excessive overdesign or future costs for rehabilitation.

TENSION ARCH CONCEPT

It is a known mathematical principle that the arch and the catenary are the inverse of each other. The funicular shape taken by a chain subject to a given series of loads, a tensile structure, is the mathematical opposite of the arch formed by those same

loads, the compressive structure (see Figure 1) (14, 15). On the basis of this, it may be said that a structure that supports a load through both tension and compression, such as the simple beam with a point load at the center, would tend to create a triangular funicular polygon of compression, such as

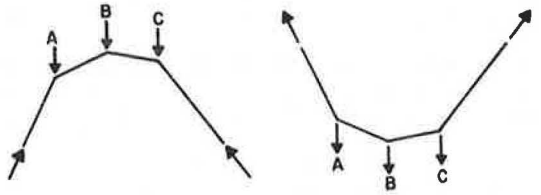

FIGURE 1 A series of loads, if supported by compression, will assume a certain funicular shape (left), and the same loads supported by tension will assume the inverse of that shape (right).

the solid line shown in the beam in Figure 2. But it is known from photoelastic tests that a beam-type structure subject to a point load exhibits stress behavior as shown in Figure 3. So a dashed funicular polygon of tension (shown in Figure 2) also tends to occur in the beam.

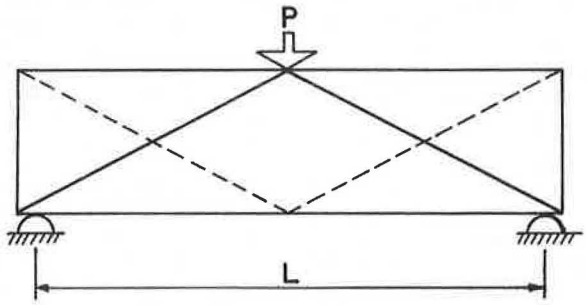

FIGURE 2 Simple beam funiculars of tension and compression.

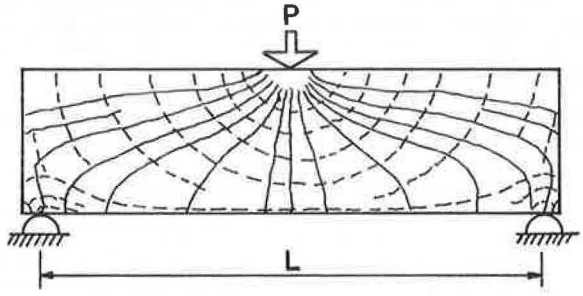

FIGURE 3 Simply supported beam showing photoelastic stress trajectories, with the tensile stress trajectories (dashed lines) curved upward, and the compression stress trajectories (solid lines) curved downward.

Concept of Moment

When a beam, an arch, or a truss is viewed as a moment resistant structure, this view has to do with the ability of the structure to transfer the energy created by the load's geometry, mass, and gravity to the earth. It is generally assumed that structures must be moment resistant to support loads. However, pure compressive structures such as segmental arches and pure tensile structures such as cables or chains are generally not considered moment resistant structures because they have no internal moment. They create rather an "external" moment. The resisting couple is internal to the geometry of the whole structure but external to the cross section. These structures support loads based on their overall geometry and stress resultants. For example, in Figure 4, $M_C = PL/4 = T_H \cdot Yc$, where T_H is the horizontal internal tension at the center line and Yc is the sag at that point. Moment resistant structures like beams or trusses, on the other hand, resist loads based on moment resisting properties of cross section, that is, area and moment of inertia. Any special overall shape geometry of a beam or a truss is a consideration only as it affects the moment of inertia.

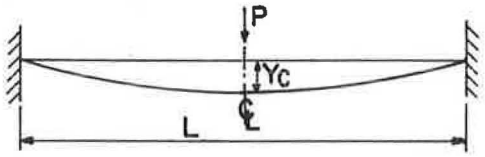

FIGURE 4 Parabolic cable with concentrated load.

The moment energy, PL/4, generated by the load, P, which must be supported and transmitted by the structure, is related to the overall geometric properties of the span and is based on the ratioed gravitational energy generated by the mass of P. PL/4 is not only the maximum moment of a simply supported beam with the load, P, at the center, but also the moment energy created by a load, P, midway between two points in space, L distance apart, supported by any structure.

CURRENT FREE-BODY DIAGRAM

From Newtonian mechanics and the theory of elasticity, an approach to analyzing structures using a tool called a free-body diagram has been developed. The usual free-body diagram cut through a simple beam is shown in Figure 5.

The three vectors shown in this free-body diagram represent mathematical abstractions. They represent reality as viewed from an orthogonal three axes system. However, they are visually inaccurate because the moment vector is the effect of a force acting at a distance and not itself a cause. Moments and forces do not really exist; they are symbols for reality. Engineering and science educators for many years have wrestled with communicating these abstract concepts, particularly moments, to students.

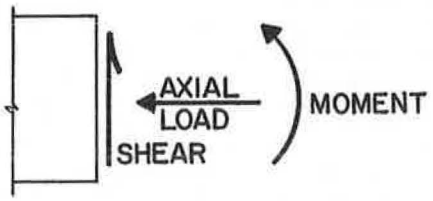

FIGURE 5 Traditional free-body diagram of a beam.

Through this free-body diagram (Figure 5), a mathematical abstraction is allowed to direct the approach to structural design. This free-body diagram is equated with basic structural behavior. One result of this is that the overall stress level efficiency of structures is not measured. In fact, structures are created, on the basis of the overall average stress levels in the materials used, that are grossly inefficient. For example, designing steel beams based on controlling maximum moment, generally at the center of the span, makes the rest of the material throughout the beam understressed, or half the concrete in a reinforced concrete beam is unused and merely supports the reinforcing steel. Prestressed and posttensioned structures are an effort to overcome this inefficiency. Trusses also are a more efficient use of materials. But due to the high cost of manufacture and construction their application has declined.

Let us view the energy created by a force P acting midway between two points L distance apart as PL/4. This is a mass-gravity geometric relationship independent of structure. The ability of a beam's cross section to transmit this energy could be described by M = f(I/c), where I and c are the geometric properties of moment of inertia and distance, and f is stress level, a material property.

However, a more holistic view of the beam describes its moment carrying capacity by the relationship M = K x d, where K is the stiffness and d is the deflection at the center due to the load P. K contains geometric properties including the length as well as the cross section and the material property of elastic modulus. In the current design paradigm one is prone to say M = PL/4 = f(I/c) = K x d, but only PL/4 is exact. The other relationships are based on a variety of simplifying assumptions and varying physical properties and conditions.

In Figure 3, the plot of stress trajectories in a simple beam, it can be observed that the compressive stress trajectories formed take an arching shape (solid lines) and the tensile stress trajectories formed take a catenary shape (dashed lines). With a view to these stress trajectories, a more visually accurate free-body diagram of a section through this structure would be the polar representation of Figure 6.

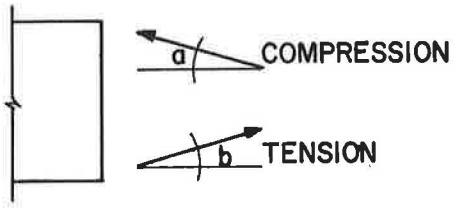

FIGURE 6 Free-body diagram of what actually occurs in a beam and in the Tension Arch.

Geometry

Structures are analyzed and designed on the basis of the fundamental assumption that the geometry of the structure remains unchanged while it supports the load (plane sections remain plane sections). This is true of suspension bridges, arches, beams, trusses, and everything in between. However, the suspension bridge without the stiffening truss, or other means of stiffening, is a dynamically sensitive string, a swinging bridge, or a musical string (plane sections do not remain plane). Roebling was among the first to realize this and to incorporate adequate techniques for stiffening into his designs. On the other hand, techniques for preserving arch geometry under load were first used perhaps by the Romans or earlier peoples and were later used by the modern French and the Swiss and then worldwide.

Modern suspension bridge builders are aware that the solution to the problem of dynamic sensitivities is based on the preservation of the original geometry, through stiffening trusses or beams or energy absorption techniques. Pure tensile structures such as ski lifts and aerial tramways are restricted by custom and standard to a ratio of hanging load to internal tension (16). For example, if the internal tension is 1,000 lb, the maximum hanging load is 50 lb (a ratio of 1:20). The ultimate purpose of this ratio is to ensure the geometry of the operating system. Thus the structure that will exist in the field is analyzed.

Structure as Energy Conduit

Structures do act as transmitters of energy. The moment energy, that is, the ratioed or levered gravitational energy created by the load in the span, can be thought of as analogous to electricity in the wire, with the load as a generator or dynamo and the wire as the structural section. The energy created by the load is transmitted by the structure to the earth. But the earth is a purely compressive structure with negligible tensile resistance. So each basic structural system must transform any inherent tensile energy to compression so that it can be absorbed by the earth. This occurs generally at or near reactions, or their direct extension from the earth. Thus beams and other structural systems whose reactions occur along tensile flanges or sections require longer bearing lengths or stiffeners. Figure 7 shows where these tension-to-compression transfers occur in a variety of structures.

Man and Tension

The ability of man to devise means and methods for resisting tension has been a vital part of his growth and of that of his civilization. This can be seen in his weapons, housing, structures, clothing, and almost everything that man has developed in the last 20 centuries. It is particularly visible in his structures or his shelter. The suspension bridge dates back to antiquity and is one of the ways that even primitive man used to span the chasm. But just what is tension? How does it originate? Where does it go? Let us consider the segmented arch, a pure compressive structure, and its funicular polygon. As load is increased above a certain level, the cracks in the arch open, and the funicular tends to move outside the structural cross section. Energy must be applied in opposition to the load to close these cracks and restore the funicular to its original geometry. If the original resisting structure was a funicular of compression, then the necessary opposing structure must be a funicular of tension. Thus tension may be defined as the energy component necessary to overcome a deficiency in compression.

With the development and understanding of tension resisting materials, man proceeded from wood to steel structures, to reinforced concrete, and ultimately to the skyscraper, which gets man higher and higher from the compressive earth. Finally the airplane with tensile structures as a vital part of its composition transmits its load to the earth through a form of compressed air.

The ability to resist tension is thus a vitally important part of the rise of human civilization. Today more than ever, a great deal of technical tal-

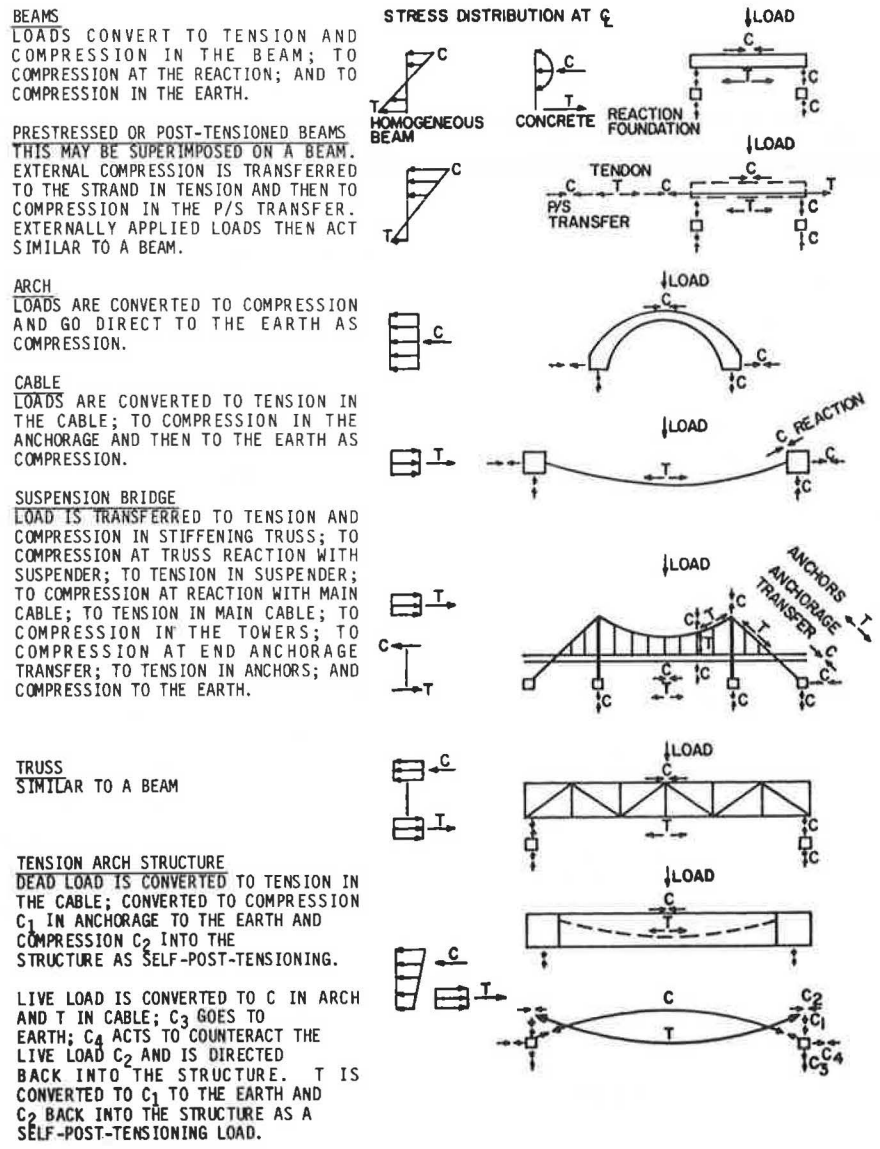

FIGURE 7 Tension to compression transfers in some typical structures.

ent is spent merely trying to resolve the question of how to resist tension--how it will be controlled, directed, and transformed into compression so that it can be absorbed by the earth.

TENSION ARCH STRUCTURE

The Tension Arch structure is a combination of the arch and the catenary. It is a structure that transports loads to the earth through segregated unbonded tensile and compressive structural components. It is basically a suspension structure whose horizontal tensile forces are resisted by a compressive strut. This strut or prop contains an internal saddle to preserve the parabolic shape of the cable or tensile component (see Figure 8).

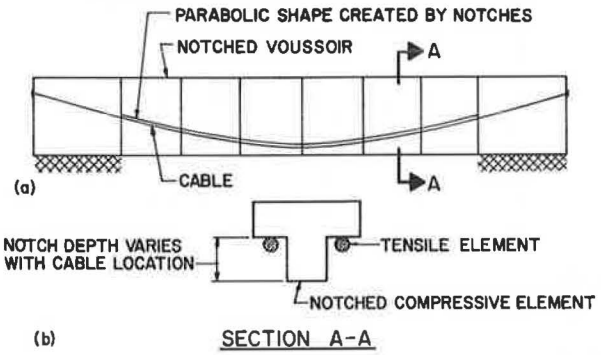

FIGURE 8 Typical Tension Arch structure in elevation (a) and section (b).

Compressive Structures

When considering pure compressive structures, we usually think of a Roman or concrete arch spanning between two points. There is something in the arch that strikes a personal intuitive chord. It is a structure that we somehow know is dependent on geometry and proportion to support its load. If the geometry fails, the structure is no longer a purely compressive structure and buckles and collapses. All beautiful arches exhibit a delicate sense of propor-

tion; it is hard to imagine an arch that is not beautiful. But, due to the mass of most arch structures, we endow them with a certain degree of stiffness or ability to resist a moment-type energy, whether they have it or not. This is true not only of arches but also of prestressed and posttensioned segmental structures that are literally flat arches whose segments are compressed by external energy. The abstract concept of moments directs the approach to design, whereas tensile and compressive forces (i.e., directional energy components) alone or together transmit the load's energy to the earth.

Catenaries or Suspended Structures

When a purely tensile structure, such as a chain or cable, is considered, it is easy to understand that the applied load can change the shape of the chain and that the catenary geometry must be preserved to support the load effectively and efficiently. A chain or a cable is a structure that is obviously dependent on geometry and proportion working with axial stress resultants to support its loads. No internal moments can be supported because these structures can only resist tension. It was observed earlier that very specific ratios of hanging load to interior tension of the cable, as well as stiffening systems, are important to all tensile structures, from suspension bridges to aerial tramways, to ensure catenary or parabolic geometry.

But when we see an arch structure or a suspension cable, what do we see? Are we seeing just a structure or are we also seeing energy being transformed and transmitted? This is not so obvious with the arch, but consider the cable. In no structure is the concept of visible energy so apparent as in the pure tensile structure. A variety of catenary shapes, from utility lines to bridges, makes up our everyday environment. We have been taught that it is the shape of a cable that supports its loads through pure tension. However, the shape of a cable or chain is generally any shape we would like it to have. It will assume a shape based on a particular use, for example, around a wheel or over a saddle. What is seen in a suspended cable structure is the shape of the tensile energy that is transmitted through the cable to its supports, where it is changed to compression and transmitted to the earth. Change the tension in the cable and its shape changes. The tension inside controls the external geometric shape. The physical composition of the cable or chain is merely a visual characteristic of the material and is secondary to the structure's property as an energy transmitter.

Tension Arch = Arch + Catenary

A conclusion that may be drawn from these observations is the classical concept that structures tend to assume a shape based on the loads they support or the energy they transmit--the point made in the first paragraph of this paper. But, from another perspective, it is not the structures that tend to assume the shape but the tensile and compressive energy within the structures that tends to assume a specific shape due to its own nature. If structures are viewed from this perspective, a structure's behavior takes on a vitally different appearance.

With this as a basis, the Tension Arch structure combines (a) the stress-strain properties of materials as energy transmitters; (b) the geometric properties of levered or ratioed loads, that is moments; and (c) the geometric properties of the arch and catenary. This combination is a structure that will resist the external load's moment energy. The Tension Arch, in effect, takes two structures with no "moment resistive capacity," the cable and the segmental arch, and combines them to create a structure that can resist moment energy and preserve the parabolic geometry of the tensile element (see Figure 8).

The Tension Arch is both a cable-stiffened arch and an arch-stiffened cable. It is at once a suspension structure, which dissipates its horizontal tension through a flat arch or prop, and a flat arch structure, which dissipates its horizontal thrust through a parabolic shaped tensile tie. It may also be viewed as the mathematical inverse of a tied arch. It combines and displays the properties of posttensioned, suspension, and arch structures. The inherent geometry of the system makes it different from what is sometimes referred to as "tied" or unbonded concrete.

This structure further takes advantage of the energy created by the load itself to add to the ability of the structure to support that load. It does this by rerouting a portion of the tensile energy (the cable's horizontal tension component) back into the structure instead of dissipating it into the earth as do the ties on the traditional suspension bridge. This portion of the load, the horizontal tension, posttensions the structure.

For example, a cable that spans 100 ft with a 2 ft sag (a 2 percent sag ratio) creates an internal tension of 12.5 lb for each 1 lb supported by the cable at the center of the span. If the 12.5 lb of internal horizontal force per pound of vertical external load must be dissipated into the earth, massive anchorages are required, as with suspension bridges. However, if the 12.5 lb can be redirected back into the structure, in effect to posttension the structure, the mechanical advantage inherent in the cable's geometry can be used to support the load. This is what occurs in the Tension Arch. The horizontal forces generated by vertical load and the cable's geometric form are levered and used to assist in supporting the load.

Negative Moment Resistance at the Supports--Effect of Parabolic Shape

Figure 9 is a free-body diagram of a single-span Tension Arch structure in which the supports are restrained from rotating. Summing the forces in the Y direction yields

$$\Sigma F_Y \,{}^{+}\uparrow = C \sin\beta + T \sin\alpha - (w\ell/2) = 0 \qquad (1)$$

In this structure the angle α is known because the shape of the tensile element is formed on the inside of the compression component. The tension, T, is also known because it can be controlled and selected on the basis of loads and design parameters. That

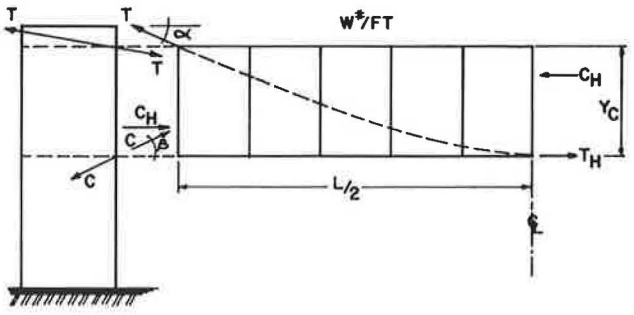

FIGURE 9 Free-body diagram of beam.

leaves C and β as the unknowns. Summing the forces in the X direction yields the following equation:

$$\Sigma F_X \stackrel{+}{\rightarrow} = -C_H + C \cos \beta + T_H - T \cos \alpha = 0 \quad (2)$$

because at the center line

$$|C_H| = |T_H|.$$

This gives

$$C \cos \beta = T \cos \alpha$$

The following expression can be generated from Equation 1:

$$C \sin \beta = (w\ell/2) - T \sin \alpha \quad (3)$$

Squaring Equation 3 yields the following relationship:

$$C^2 \sin^2 \beta = (w^2\ell^2/4) - w\ell\, T \sin \alpha + T^2 \sin^2 \alpha \quad (4)$$

Squaring Equation 2 and adding it to the preceding relationship yields the following equation:

$$C^2 = (w^2\ell^2/4) - w\ell\, T \sin \alpha + T^2 \quad (5)$$

It is known from basic cable theory (Figure 10)

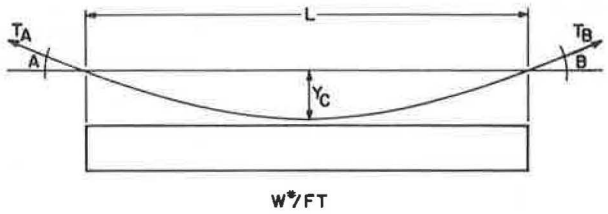

FIGURE 10 Parabolic cable with uniform load.

that for a symmetrically loaded structure Angle A = Angle B. If the shape of the cable is restricted to a parabolic shape, it is known that

$$TA = TB = w\ell/2 \text{ tangent A}$$

It is also known that for small angles

$$\sin A = \text{tangent A}$$

and from the properties of the parabola that this equals 4Yc/ℓ. Therefore,

$$\tan \alpha = 4Yc/\ell = \sin \alpha \quad (6)$$

It is further known that the horizontal component of tension in the cable is

$$T_H = w\ell^2/8Yc \quad (7)$$

Substituting Equation 6 into Equation 5 yields the following expression:

$$C^2 = (w^2\ell^2/4) - 4 \cdot w \cdot T_H \cdot (Yc) + T^2 \quad (8)$$

It is known that C must equal T to preserve equilibrium. By inspection, in order for $C^2 = T^2$ the value of $T_H(Yc)$ must be equal to $w\ell^2/16$. But $T_H(Yc)$ is the "moment" at the center of the span resisted by the cable. It is only with $T_H(Yc)$ equal to $w\ell^2/16$ that this equality will exist and the system will be in equilibrium. It can be inferred that if M at the center is $w\ell^2/16$ then M at the ends is also equal in value to $w\ell^2/16$ and opposite in sign.

It is known that the end moments must vary between the limits of 0 and $w\ell^2/12$ and the center line moment must vary between the limits of $w\ell^2/8$ and $w\ell^2/24$. But $w\ell^2/8$ is a measure of the energy. The total moment value or energy to be resisted is the quantity in question when it is said that

$$|M_A| = |M_B| = |M_C| = w\ell^2/16.$$

What this simplified analysis implies is that half of the moment energy created by the load is carried by the cable and half of the load's moment energy is carried by the compression component. The analysis further considers the development by the Tension Arch of negative bending at the abutment regions as long as they are designed to dissipate it. With the existence of the $w\ell^2/16$ relationship, the implication is that the moment at the center line and the moment at the abutments are the same and these sections may be designed for precisely the same forces, only acting in different directions. The natural shape of the cable allows this to conveniently occur so that the design of this section at the center line yields the same section at the abutments.

The approach to designing the first Tension Arch structure has been to ensure that compressive stress distribution exists at all times in the compression component cross section. No tensile stress, or crack opening, is allowed. What this means is that the location of compression resultant is restricted by adding a small amount of additional posttensioning.

Design and Analysis

On the basis of the previous discussion it is assumed that for a single span, one-half the simple-span moment is taken at the center of the span and one-half is taken at the ends. This considers both dead and live loads. Early laboratory tests at West Virginia University indicate that the system behavior is similar to that of a partly fixed end beam on a series of spring supports. The laboratory structure also exhibited a sensitivity to the ratio of dead load to live load, a characteristic of most tensile structures. This information will be used in the design and analysis of the full-scale experimental project now being developed in conjunction with the West Virginia Department of Highways.

The analysis of the compressive elements is made using the traditional combined axial load and bending relationship:

$$(T_H/A_C) \pm (T_H \cdot E_C/I_C) \pm (M_L \cdot C/I_C) \quad (9)$$

where A_C, I_C, E_C, and C are geometric properties of the compression section. No tensile stresses are allowed in the compression element and additional tension is provided to ensure this condition. The resulting cross section for a bridge designed to span 100 ft is shown in Figure 11.

Erection--Dead Loads

The level of T_H during construction can be critical before the compression element is in place. Several erection schemes have been developed; the most effective one appears to be the arch crane. It will be used to support half of the dead load during construction with the other half supported by the tensile element. In this way the horizontal tensile

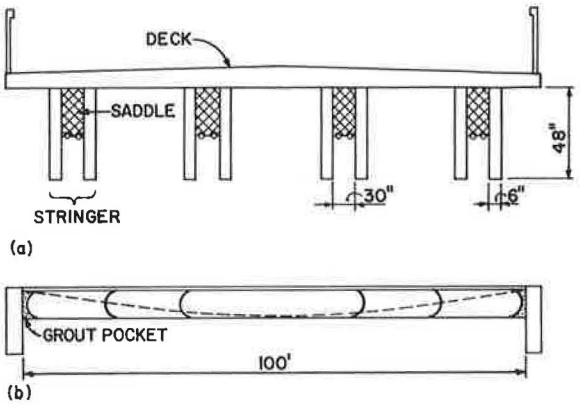

FIGURE 11 Schematic of an experimental Tension Arch structure that will be built by the West Virginia Department of Highways during 1984.

force T_H directed toward the center of the span is counteracted by a horizontal compressive force C_H directed away from the center (see Figure 12). Another obvious approach is for all of the dead load during construction to be supported by falsework from above or below.

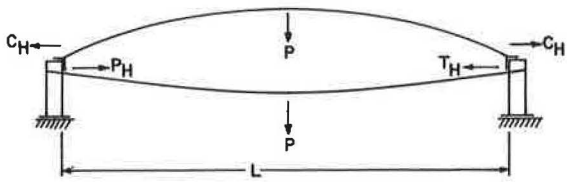

FIGURE 12 Compressive arch crane and tensile elements support dead load by both tension and compression.

Each stringer (see Figure 11) will be erected and completed before moving to the next if only one arch crane is used. A grout pocket is left at the end of each stringer and filled with chemically expanding grout. When the grout is set the stringers are post-tensioned to the appropriate energy level to receive the deck and other loads.

Movements and Deflections

Thermal loads are handled through the raising and lowering of the whole structure. This movement and other movements, such as differential settlement, are absorbed by the circular joints located at the center and at the abutments. These joints appear to be hinges; however, moment energy is transmitted across these joints, inasmuch as tension and compression both exist at these locations. The result is a structure that can withstand substantial movement through settlement and rotation and at the same time transmit moment energy within the framework of its original design geometry and assumptions. A temperature expansion or seismic load or settlement would all generally be experienced and handled similarly by this structure. Such movements would be viewed as a translation, a rotation, or a combination of the two at these joints.

Abutment Design

In the experimental project, abutments will be designed to resist lateral earth pressures. The negative moments resisted by this structure at the abutment interface are dissipated into the old abutment structure. What better way to make use of this energy dissipation than to use the structure behind the abutment? The Tension Arch structure geometry is designed to allow some abutment rotation to occur. Additional soil compaction due to lateral earth pressures will occur on the face of the abutment. The resulting minor rotations would not affect the overall structure's capacity to support loads. What the Tension Arch does is create a bent integral with the abutment. It simply makes use of the natural shape of the cable to build a structure that can resist positive and negative moment energy.

Origin of Concept

While viewing the natural shape of the cable as it appears in a ski lift (see Figure 13), one can observe that it is similar to the natural shape of tension in a continuous beam over several supports. For example, if one had to provide a single piece of reinforcing steel for a concrete beam continuous over several supports, it would assume a shape similar to this sinusoidal wave. Not only would this be appropriate for the moment energy involved, it would also be positioned for many of the basic shear problems that exist in reinforced concrete. By marrying with this ski lift cable a group of compression components with the inverted saddle shape of the cable incorporated into their cross section, it is ensured that the natural shape of the cable, the catenary or parabolic shape, will be preserved for all loads. When the last piece was mentally installed, a rigid structure ensued. Extensive patent searches indicate no similar structures. Literature searches had similar results and patents were applied for in the spring of 1982.

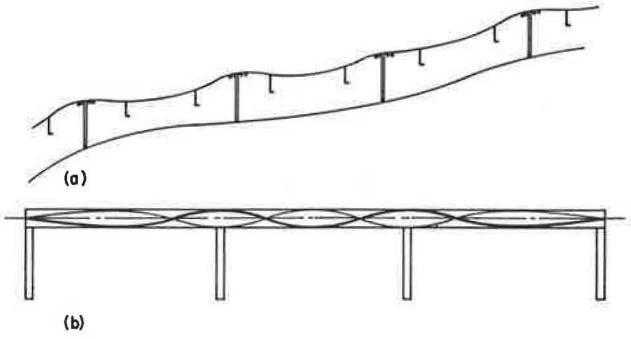

FIGURE 13 Natural shape of the tensile cable of a ski lift (a) reflects the natural shape of tension in a beam [solid line in (b)]; the natural shape of compression [thin line in (b)] is the opposite of this tensile shape.

CONCLUSIONS

The Tension Arch concept will potentially allow all types of structures to maximize the use of material at higher overall stress levels. Half of the concrete in a beam need not be used merely to position and bond the reinforcements necessary to withstand the tensile load. Nor will the midheight area cross section of beams be used at low stress levels. The concrete can all be devoted to compression. Wood beams could easily be made continuous with this system, inasmuch as they would no longer have to resist

anything but localized tensile and bending stresses. Wood beams of 200 ft or more could be conveniently designed with this technique and assembled at the site from small modular pieces.

The only things that need to be continuous are the tensile elements. They can be wires, rods, plates, or anything that can conveniently be shipped to the site and made continuous.

Continuous tension is considerably different from continuous compression. It is easy to make a variety of materials continuous in compression; however, continuous tension must be handled selectively and only the highest quality materials can be used. Although at first the problem of deflections was considered serious due to the sensitive geometry, this has not proved to be the case. The ratio of dead load to live load is of more importance. An expression for deflection is available that is consistent with cable theory and virtual work, and reasonable deflection has been calculated and experienced (17).

This system can achieve construction cost reductions in structural systems of 20 percent or more as a result of (a) reduced design cost, (b) mass production of the compressive and tensile structural components, (c) minimum shop and field custom fabrication, and (d) reduced erection time and erection equipment costs. Finally, the Tension Arch is a structure whose geometry is relatively insensitive to a variety of support movements along any or all three axes.

The West Virginia Department of Highways and FHWA are currently considering the construction of the first Tension Arch structure. Testing will continue through West Virginia University during the construction of this project.

REFERENCES

1. To Rebuild America--$2.5 Trillion Job. USNews and World Report, Sept. 27, 1982, pp. 57-61.
2. Bridges on Secondary Highways and Local Roads--Rehabilitation and Replacement. NCHRP Report 222. TRB, National Research Council, Washington, D.C., 1980, 132 pp.
3. Rehabilitation and Replacement of Bridges on Secondary Highways and Local Roads. NCHRP Report 243. TRB, National Research Council, Washington, D.C., 1981, 46 pp.
4. Proc., Bridge Maintenance and Rehabilitation Conference, Morgantown, West Virginia, August 13-16, 1980, 775 pp.
5. Bridge Inspection and Rehabilitation. Transportation Research Record 899. TRB, National Research Council, Washington, D.C., 1983, 76 pp.
6. Bridge Maintenance. Organization for Economic Cooperation and Development, Paris, Sept. 1981, 131 pp.
7. Manual for Bridge Maintenance. AASHTO, Washington, D.C., 1976.
8. N.B. Taly and H.V.S. GangaRao. Development and Design of Standardized Short-Span Superstructural Systems. Report FHWA-WV-76-5, West Virginia Department of Highways Research Project 50. West Virginia University, Morgantown, Nov. 1976, 220 pp.
9. D.H. Beeson. Integration of Maintenance Needs Into Preconstruction Procedures. Report FHWA-TS-77-216. Federal Highway Administration, April 1978.
10. L.K. Moulton, H.V.S. GangaRao, and G.T. Halvorsen. Tolerable Movement Criteria for Highway Bridges, Volume I: Interim Report. Report FHWA/RD-81/162. Federal Highway Administration, Dec. 1981, 127 pp.
11. Howard Needles Tammen and Bergendoff. Bridge Deck Joint-Sealing Systems. NCHRP Report 204. TRB, National Research Council, Washington, D.C., June 1979, 46 pp.
12. J.L. Jorgenson. Behavior of Abutment Piles in an Integral Abutment Bridge. Report ND(1)-75(B). North Dakota State Highway Department; North Dakota State University, Fargo, Nov. 1981.
13. R.H. Berger. Extending the Service Life of Existing Bridges by Increasing Their Load Carrying Capacity. Report FHWA-RD-78-133. Federal Highway Administration, June 1978, 152 pp.
14. H.M. Irvine. Cable Structures. The MIT Press, Cambridge, Mass., 1981, 259 pp.
15. P. Sandori. The Logic of Machines and Structures. Wiley, New York, 1982, 180 pp.
16. D. Marocchi. Aerial Tramways and Ski Lifts--Theory and Planning, S. Bonasso, ed., Alpha Associates, Inc., Morgantown, W.Va., 1983, 164 pp.
17. T. Au. Elementary Structural Mechanics. Prentice Hall, Englewood Cliffs, N.J., 1963, 521 pp.

Publication of this paper sponsored by Committee on General Structures.

Overview of the Pennsylvania Standard Plans for Low-Cost Bridges

FRED W. BOWSER, FRED S. FABER, Jr., HEINZ P. KORETZKY, and M. G. PATEL

ABSTRACT

As one of several steps to address the massive and worsening bridge problem, the Pennsylvania Department of Transportation decided to develop ready-to-use, low-cost bridge design standards for small bridges. Buchart-Horn, Inc., retained by the department, developed the standardized bridge plans for 18-35 ft, 30-90 ft, and 90-130 ft span ranges, using steel, concrete, and prestressed concrete materials. The standards for timber and buried structures will be published soon. Three types of superstructures and two or three types of substructures, including pile-supported footings for each series, have been incorporated. Each set of standards includes and illustrates step-by-step procedures for developing a set of bridge plans from the standards. The data assembly (computations) sheets and blank plan sheets for a bridge with spaces provided for dimension insertion are included. The user completes them based on field information, geometry, and soil conditions. The completed sheets become construction plans. The contractor, when preparing bids, has the option of building the structures specified in the contract or developing an alternate structure from the standards based on the predefined parameters in the contract. The plans are approved for federally funded projects. The ultimate goal is to expedite and economize bridge replacement efforts while minimizing inconvenience to the public. Although this is not an ultimate answer, it is a step in a positive direction. The productivity realized using these standards will be enhanced when they are incorporated in the Computer Aided Design and Drafting system.

Because the structural portion of bridge engineering is nearly a perfect science, several attempts have been made to standardize bridge design, drafting, and construction. However, because of the uniqueness of each bridge, due to such things as variations in soil condition, highway geometry, required waterway opening, traffic conditions, and environmental aspects, each bridge is nearly custom tailored. During the early years when bridges were constructed at certain alignments and the approaches were built to meet the bridges, standardizing bridges was relatively simple. The Pennsylvania Department of Transportation (then the Department of Highways) in the 1920s and 1930s had developed and used bridge standards for width, span, skew, and vertical opening. Design standards for concrete arches, as an example, were published as early as March 1924. Bridges were constructed using these standards without developing custom-tailored detailed drawings. Even though the standardized bridge plans lost their popularity due to geometric constraints, the design standards continued to evolve to simplify, expedite, and economize the bridge design process.

In the 1960s, when alternate bidding for bridges was in full swing, detailed standards for prestressed concrete structures were issued that simplified and virtually eliminated the need for longhand superstructure design. These standards were further refined and updated in the 1970s.

In 1981 the department contracted with Buchart-Horn, Inc., consulting engineers from York, Pennsylvania, to develop ready-to-use standard plans for bridges spanning from 18 to 130 ft. These plans were to be developed to reflect low life-cycle construction cost, ease and speed of construction, and attention to safety, volume, and type of traffic and availability of materials. The consultant initiated a study to determine the current state of the art of "standard bridges." Federal and neighboring state agencies, vendors, material suppliers, and contractors and their societies were contacted to collect data on readily available products, bridge types, and innovative fabrication and construction practices (1). Site visits were also made by the consultant to inspect actual structures for study and evaluation. After analyzing the collected data, the consultant was required to narrow down superstructure types to five. Based on the consultant's study, projected life-cycle costs, and considering competitive materials, the department selected three types of superstructure for standardization. This in practice reduced the choice from 19 possible bridge superstructure types to three each for the 18-35 ft, 30-90 ft, and 90-130 ft span ranges. The substructure types were narrowed down from seven to three for the 18-35 ft span, to two for the 30-90 ft span, and to four for the 90-130 ft span ranges. The selection was based primarily on ease of construction, fabrication, and erection; economy; and proven performance.

The 18-35 ft and 35-90 ft span range standards were developed using the working stress design (WSD) method and published in June 1982 and October 1982, respectively. Since then the department has switched to load factor design (LFD) combined with increased live load and other design criteria modifications.

The time schedule given in Table 1 has been established for completion of the series. During 1980 the department reintroduced an alternate bidding policy under which contractors are permitted to bid on their own design in lieu of the department-supplied design that is part of the contract proposal. The bridge low-cost (BLC) standards were introduced in time to assist the contractors in designing alternates. Not only do these standards save substantial design and drafting time for the department, they also permit the contractor to quickly develop biddable bridge quantities for an alternate bridge of his choice, from the standards, without fear of rejection of his design after the project is awarded.

FORMAT OF STANDARDS

The standards are composed of design sheets and con-

TABLE 1 Time Schedule

Steel and Concrete Structures			Buried Structures			Timber Structures		
Span Range (ft)	Bridge Low-Cost Standard	Issue Date	Span Range (ft)	Bridge Low-Cost Standard	Issue Date	Span Range (ft)	Bridge Low-Cost Standard	Issue Date
18-35	520	10/83	6[a]	530	8/84	18-35[b]	550	5/84
30-90	510	7/83				30-90[b]	540	2/84
90-130	500	11/83						

[a]Will be dictated by the physical limitations of the buried structure types selected for presentation.
[b]Only working stress design (WSD) criteria will be used.

struction sheets. The design sheets include (a) general information, design criteria, instructions for use, and design examples for each type of substructure and superstructure and (b) data assembly sheets for each superstructure and substructure type. The construction sheets include (a) detailed drawings for each superstructure type with left and right skews, (b) detailed drawings for each substructure type with left and right skews, and (c) stakeout sheet.

To provide maximum versatility, these standards accommodate (a) any curb-to-curb width between 22 and 48 ft and (b) any structure skew angle between 45 and 90 degrees. Standardized substructures are provided with variable heights (bottom of footing to top of stem) from 4 to 16 ft for 18-35 ft spans, from 4 to 20 ft for 35-90 ft spans, and from 5 to 22 ft for 90-130 ft spans.

The bridge superstructure and substructure types given in Table 2 were selected for the bridge standards. With three types of superstructures and two to four types of compatible and interchangeable substructures from which to choose, the designer is able to adapt the standards to fit most applications.

TABLE 2 Superstructure and Substructure Types

Superstructure Types	Substructure Types
18-35 ft Span Range *(2)*	
Adjacent prestressed box beam	Concrete breastwall
Adjacent precast channel beam	Concrete stub abutment
Concrete deck on steel beams	Concrete pile cap
30-90 ft Span Range *(3)*	
Adjacent prestressed box beam	Spread footing cantilever
Concrete deck on prestressed spread box beams	Pile-supported stub
Concrete deck on steel beams	
90-130 ft Span Range *(4)*	
Composite steel I-beam	Spread-footing stub
Composite prestressed I-beam	Pile-supported stub
Composite prestressed adjacent box beams	Spread-footing cantilever
	Pile to supported cantilever

All superstructure types employ a cast-in-place concrete safety parapet that is cost-effective on a life-cycle basis because of minimal maintenance costs.

DESIGN PROCEDURE

Because the drawings cannot be reproduced here, the descriptive design procedure method has been used. The standards can be obtained, however, by writing to PennDOT Publication Sales Store, Room 110, T&S Building, Harrisburg, Pa. 17120.

Before using these standards, the designer must obtain basic survey and geometric data for the proposed construction site. Information concerning the foundation material and elevation of potential foundation bearing areas must also be obtained. When the necessary data assembly and construction sheets have been selected, the designer is ready to begin producing final contract drawings. The following simple steps are followed in the plan preparation process:

1. Complete the data assembly sheet for the superstructure type selected: (a) Answer the listed questions. (b) Fill in the control stations and elevations table. (c) Complete the control dimensions table; reference to supplemental tables, figures, and geometric equations is required; work the table from top to bottom. (d) Determine the deck geometric condition by making the test comparison indicated under "Deck Configuration" (for steel beam structures only). (e) Complete the reinforcing steel table as required. (f) Complete the superstructure quantities table. (g) Compute elevations and dimensions for substructure design by filling out the appropriate tables.
2. Complete the data assembly sheets for the substructure type selected: (a) Enter the abutment number in the drawing title block (a separate data assembly sheet is required for each abutment). (b) Complete the control dimensions table; refer to geometric equations and supplemental tables and figures as required. (c) Compute the work point station at the front face of the abutment stem and enter in the stakeout control table. (d) Complete the reinforcing steel table. (e) Complete the substructure quantities table.
3. Transfer the appropriate information from the data assembly sheets to the fill-in spaces on the standard construction sheets: (a) Information from the superstructure data assembly sheet should be placed in the appropriate fill-in slots in the standard superstructure drawings; coded letters and numbers are provided to facilitate the correct placement of dimensions and other data. (b) Elevations and dimensions for substructure design must be transferred from the superstructure data assembly sheet to the standard substructure drawings. (c) Information from the substructure data assembly sheets must also be transferred to the standard substructure drawings through the use of the codes provided. (d) Complete the appropriate stakeout drawing by reference to the substructure data assembly sheets.
4. Add titles and complete quantity estimates and add miscellaneous information: (a) Customize the standard drawings by adding necessary location and route number information to the title block of each sheet. (b) Compute quantities for excavation, structure backfill, and other items not specifically provided for on the data assembly sheets; all quantities should be posted in the quantity estimate block of the general plan sheet for the structure. (c) Add necessary information pertaining to utilities, hy-

draulic data, and roadway alignments. (d) Add subsurface exploration information as required.

The completed set of drawings assembled from these standards should be reviewed and signed by a registered professional engineer before the plans are submitted to the department for approval. In the case of a contractor's alternate design, the approval of the plans by the department will officially allow the contractor to begin construction.

ADVANTAGES AND DISADVANTAGES

Advantages to the preparation of bridge design and construction plans using the BLC standards are that the standards

1. Give on the average a most economical structure based on life-cycle cost;
2. Allow expeditious design and drawings development (1 day bridge design and drawing are possible, if a computer is used);
3. Reduce project design costs;
4. Permit quick and reliable alternate design by contractors;
5. Induce keen competition among contractors and suppliers, and thus economize on initial construction costs;
6. Make a modified turnkey concept achievable;
7. Standardize details and thereby simplify construction; and
8. Reduce potential for costly errors.

Disadvantages of using the BLC standards are that

1. Standards are not usable for complex geometries and outside the preestablished parameters;
2. Designers lose the feel for the "right" proportioning of a structure and lose their proficiency in making the tedious computations required for conventional design;
3. Dimensional computation errors may not be caught because drawings are not to scale;
4. Regular supplementary geometry computations are needed for bridges having vertical or horizontal geometry or both; the standards can hardly be used for bridges with sharp horizontal curves;
5. Some earthwork computations require scale drawings; and
6. Use of such detailed standards retards innovation.

WHAT LIES AHEAD

In the future the equations are to be computerized to achieve 1-day bridge design and drawing. This is a part of the consultant's assignment. However, completion of all the standards is the first priority. In addition, the standards will be incorporated in Computer Aided Design and Drafting to develop instant designs and drawings to scale.

The ultimate goal of this effort is to expedite any bridge replacement efforts and accomplish the project in an economical, cost-effective manner while minimizing the inconvenience to the traveling public. Although this is not an ultimate answer for dealing with the many bridge problems in the commonwealth, it is a step in the right direction. Complex structures will continue to require custom design by knowledgeable professional engineers.

REFERENCES

1. Phase A Summary Report--Data Gathering. Buchart-Horn, Inc., York, Pa., Oct. 1981.
2. Standard Plans for Low Cost Bridges (BLC-400). Publication 182. Pennsylvania Department of Transportation, Harrisburg, June 1982.
3. Standard Plans for Low Cost Bridges (BLC-410). Publication 183. Pennsylvania Department of Transportation, Harrisburg, Oct. 1982.
4. Standard Plans for Low Cost Bridges (BLC-500)--Load Factor. Publication 17. Pennsylvania Department of Transportation, Harrisburg, Dec. 1983.

Publication of this paper sponsored by Committee on General Structures.

Performance of Sliding Bridge Bearings

ALI MAZROI and THOMAS M. MURRAY

ABSTRACT

An experimental program to evaluate the performance of sliding bridge bearings is described. Tests were conducted in a fixture specially constructed to simulate actual field conditions. Vertical load, up to 250 kips, was applied through a roller nest to the top flange of a 33-in.-deep girder directly over the test bearing. A closed-loop hydraulic testing system was used to apply the horizontal (friction) force. Data were accumulated and processed in real time using a microcomputer-based data acquisition system. Results are presented for three types of tetrafluoroethylene (TFE) elements on two steel surfaces with two backing types, and for new and used self-lubricating bronze expansion bearings. Comparison of results with published design recommendations shows that the recommendations are not conservative for certain TFE-type bearings but are adequate for self-lubricating bronze expansion bearings.

The purpose of this study was to determine experimentally the effective coefficient of friction of two classes of sliding bridge bearings--tetrafluoroethylene (TFE) and self-lubricating bronze expansion bearings. Both new bearings and bearings removed after approximately 20 years of service were used in the testing program.

From previous research (1) it was known that few studies of the behavior of complete bearing assemblies have been conducted and that specification provisions have been based on classic values of coefficients of friction between sliding parts without regard to effects of manufacturing tolerances or environmental effects. This study was an attempt to assess these effects and to provide guidelines to establish accurate estimates of horizontal force requirements for the type of bearings tested. The TFE bearing tests were conducted under sponsorship of the Research Division of the Oklahoma Department of Transportation (ODOT) and the self-lubricating bronze expansion bearing tests under the sponsorship of the Engineering Department Materials Division, the Port Authority of New York and New Jersey.

For the purpose of this study the effective coefficient of friction, μ_{eff}, is defined as

$$\mu_{eff} = F/N \quad (1)$$

where F is horizontal force to overcome the resistance to allow motion and N is normal force applied to the bearing. The value of F was determined experimentally for the entire assembly for an applied normal force, N, from which μ_{eff} is calculated.

BACKGROUND

Few experimental studies of full-scale bridge bearings using simulated field conditions were found in the course of a thorough literature review (1). Specification requirements seem to have been developed from classic values of friction coefficients or from test setups normally used for quality control (small specimens loaded using standard testing machines). Only two significant papers on TFE bearings were found and none on self-lubricating bearings.

Jacobson (2) has conducted experimental work to investigate the potential use of TFE as a sliding surface. He concludes that TFE bearings are suitable for use in highway bridges but recommends that only unfilled TFE be used for bridge bearings. A substantial increase in the coefficient of friction for filled TFE was found after 7,000 cycles of testing. The use of 15-25 percent glass filler resulted in a 35-50 percent increase in the values for the coefficient of friction under applied normal loads between 200 and 800 psi. He also tested several fabric-backed specimens with filled TFE surfaces that failed by delamination of the fabric pad. He concludes that the fabric-backed materials are suitable only when used in conjunction with unfilled TFE.

Taylor (3) has found that the coefficient of friction of polymerized tetrafluoroethylene (PTFE) is influenced by a number of parameters, including pressure across sliding surfaces, rate of movement, presence or absence of lubrication, previous loading and movement history, and temperature. Most of the tests were made on unlubricated and unfilled PTFE. The maximum value of the coefficient of friction of all unlubricated bearings occurred during the first cycle of movement. The coefficient of friction decreased with higher compressive stress across the bearing, but increased slightly at lower temperature. He discusses the theory of the real area of intimate contact between the PTFE and slider, and the shear force required to break the junctions in these areas.

For unspecified reasons, in Recommended Design Loads or Bridges (4), the following recommendations to replace the last paragraph of Article 1.2.13 of the AASHTO specification (5) are made:

> The longitudinal force due to friction at expansion bearings or shear resistance at elastomeric bearings shall also be provided for in the design as follows. For sliding type bearings, this force shall be based on the following percentages of the dead load supported:
>
> | Bearing Type | Average Static Friction Coefficient |
> |---|---|
> | Steel bearing on steel | 0.2 |
> | Steel bearing on self-lubricating bronze plate | 0.1 |
> | Polytetrafluorethylene (PTFE) on polytetrafluorethylene or stainless steel | 0.06 |
>
> For rocker type bearings, this force shall be based on a 20% friction coefficient on the pin, and shall be reduced in

> proportion to the radii of the pin and the rocker ... (4,p.1173).

SCOPE OF STUDY

The results of two series of tests on sliding bridge bearings are reported. Tests of typical TFE bearings were conducted to determine the effects of varying amounts of glass fiber, size of contact area, type of backing element, and nonparallel conditions on the effective coefficient of friction. All tests were done at room temperature (approximately 70°F) and no lubrication was used. In addition, tests of both new and used self-lubricating bronze expansion bearings were conducted. Both flat plate and curved plate bearings were tested at room temperature.

To achieve confidence in the experimental results, several increments of normal load were used and at least three tests were conducted at each load level for each bearing.

TEST DETAILS

To determine the experimental coefficient of friction of bridge bearings, a test setup that simulates an actual bridge was built as shown in Figures 1 and 2. The normal force is applied with a 750,000-lb-capacity hydraulic ram and the horizontal force with a 55,000-lb-capacity closed-loop hydraulic testing system. The data are recorded using a microcomputer system.

The test setup was erected inside the Fears Structural Engineering Laboratory on the laboratory reaction floor. The floor is a concrete slab 30 ft x 60 ft x 3 ft 6 in. deep with four W36x150 steel beams embedded in the concrete. The slab weighs 1 million lb and is capable of reacting 320,000 lb in any one location. The setup was erected directly over two of the embedded W36 beams spaced 8 ft apart. The setup consisted of three parts: (a) an H-frame (Figure 1) that was designed for 250,000 lb maximum vertical reaction and that supported the hydraulic ram, (b) a triangular frame (Figure 2) that was designed for 55,000 lb maximum horizontal reaction and that supported the closed-loop hydraulic testing system, and (c) a W33x130 15-ft-long girder, which simulated the actual bridge girder.

The vertical load chain consisted of the H-frame, hydraulic ram, load cell, swivel head, roller nest with a known effective coefficient of friction, a steel plate with a highly polished surface, the simulated bridge girder, the test bearing, a steel reaction plate, and the reaction floor, as shown in Figure 1. The horizontal load chain consisted of the triangular frame, the actuator of the closed-loop hydraulic testing system, the load cell, a loading linkage to prevent out-of-plane forces, and the simulated girder, as shown in Figure 2. Lateral brace mechanisms were used to stabilize the girder against out-of-plane rotations and a pipe roller was used to support the unloaded end of the bridge girder.

Instrumentation consisted of the two calibrated load cells, a horizontal displacement transducer, an analog-to-digital signal converter, and a microprocessor. The applied normal force was measured using the calibrated 300,000-lb-capacity load cell; the horizontal force was measured using the calibrated 100,000-lb-capacity load cell; and the horizontal movement (girder movement) was measured using a calibrated transducer that is part of the closed-loop hydraulic testing system.

The analog signals from the three instruments were digitized using a 16-channel differential input AC/DC converter with direct interface to the micro-

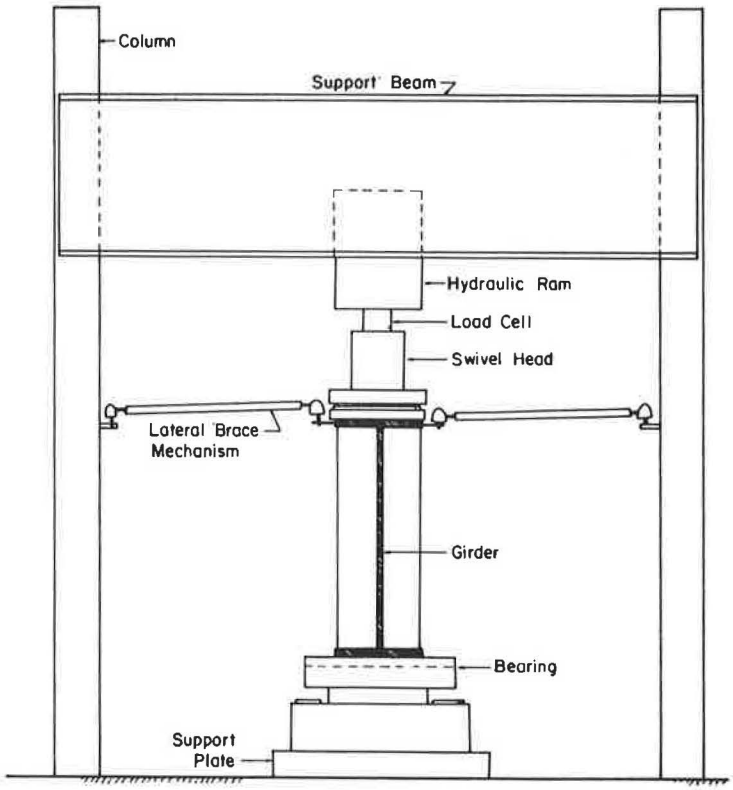

FIGURE 1 Vertical load chain.

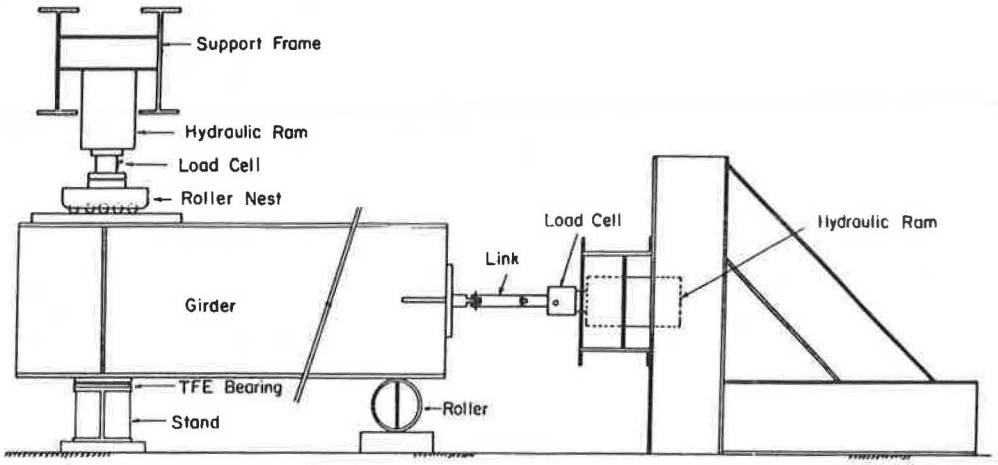

FIGURE 2 Side view of test setup.

processor. The microprocessor was used to reduce and plot the data in real time. In this manner, changes in normal force due to uncontrollable vertical movement in the vertical force chain were accounted for, and the instantaneous relationship of the two force and one displacement variables was known.

The microprocessor was programmed to account for the coefficient of friction of the roller nest, for the effects of the weight of the girder and other test setup parts not accounted for by the load cell in the vertical load chain, and for uplift effects caused by the horizontal force couple. In Figure 2 it can be seen that a force couple results from the application of the horizontal force and the resisting force at the bearing sliding surface. This couple tends to reduce the applied normal force at the bearing.

Tests of each TFE bearing assembly were conducted at nominal contact pressures ranging from 200 to 6,000 psi depending on the configuration. Tests of the self-lubricating bearings were conducted at nominal load increments of 25 kips starting at 175 kips and decreasing to 50 kips. A second test series was then conducted at 175 kips. At each normal force level three tests were conducted.

Approximately 100 data sets (each set consisted of two force readings and one displacement reading) were recorded for each test. The effective coefficient of friction was automatically calculated by the microprocessor taking into account the initial force on the bearing due to the weight of the system, the horizontal force-couple effect, and the effective coefficient of friction of the roller nest. The graphics capabilities of the microprocessor system were used to plot results. Typical plots for TFE and self-lubricating expansion bearing tests are shown in Figure 3. Normal forces vary from the nominal load increments because of uncontrollable vertical movement as the girder is pulled. These changes are recorded by the microprocessor. The normal force corresponding to the maximum horizontal force is used to calculate the effective coefficient of friction for the test. The initial linear displacement is caused by elastic deformation of the test fixtures and does not affect test results.

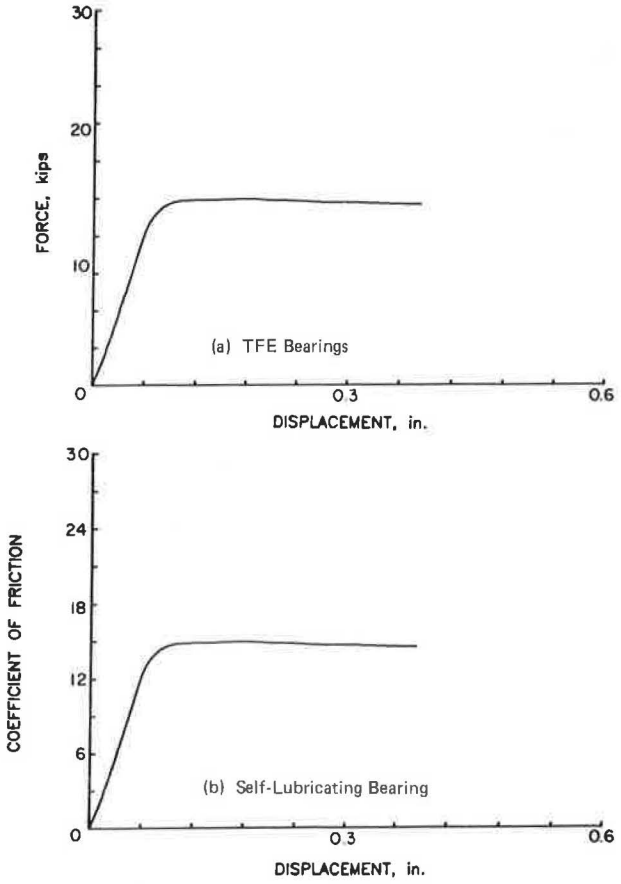

FIGURE 3 Typical horizontal movement versus friction force plots.

TEST RESULTS FOR TFE EXPANSION BEARINGS

In this study, three types of TFE elements (unfilled, 25 percent glass filled by weight, and woven unfilled and glass-filled fibers), two steel surfaces (stainless steel and mirror-finish stainless), and two backings (carbon steel plate and 70 Durometer elastomeric material vulcanized to a steel plate) were tested in appropriate combinations. Table 1 gives the seven element types and Table 2 gives the eight combinations tested. In each test the bottom element was tack welded to the stand (Figure 2) and the top element was tack welded to the girder so that movement could occur only between the element surfaces. The interface was moved at least 0.15 in. horizontally in a direction parallel

TABLE 1 TFE Test Elements

Element No.	Description
1	3/32" Glass filled* TFE bonded to 1/4" A-3 carbon steel
2	3/32" Glass filled* TFE, mechanically locked to 1/4" carbon steel
3	1/4" Mirror finish stainless steel
4	3/32" Glass filled* TFE bonded to #10 gage carbon steel hot vulcanized to 3/4" 70 Durometer AASHTO grade neoprene
5	1/16" Unfilled TFE bonded to 1/4" carbon steel
6	Unfilled TFE fibers and glass fibers woven and bonded to 1/4" carbon steel
7	1/8" Stainless steel

*Glass filled 25% by weight

TABLE 2 TFE Test Element Combinations

Test Series	Top Element	Bottom Element
I	Glass Filled TFE (#1)	Glass Filled TFE (#1)
II	Mirror Finish Stainless Steel (#3)	Glass Filled TFE (#1)
III	Glass Filled TFE (#2)	Mirror Finish Stainless Steel (#3)
III-A	Unfilled TFE (#3)	Mirror Finish Stainless Steel (#3)
IV-N	Glass Filled TFE (#1)	Glass Filled TFE w/Neoprene Backing (#4)
V	Woven TFE (#6)	Mirror Finish Stainless Steel (#3)
VI-N	Stainless Steel (#7)	Glass Filled TFE (#1)
VII-N	Unfilled TFE (#5)	Glass Filled TFE (#1)

N - nonparallel

to the short side of the elements at a speed of 1 in. per minute.

Tests were conducted in either parallel or nonparallel conditions. For the former, the girder and rigid stand were leveled as accurately as possible. For the nonparallel condition, the girder was shimed so that a 1/32 in. per foot (0.15 degree) slope was induced. Contact area between elements was varied for Test Combination I (glass-filled TFE versus glassfilled TFE) only. Table 3 gives the complete variation of test parameters. All tests were done at room temperature (approximately 70°F) on new elements (0 cycle). The effect of dirt or sand in the interface was not investigated.

Effect of Contact Area and Contact Pressure

To determine the effect of contact area on the effective coefficient of friction, a series of tests was conducted using Test Combination I, glass-filled TFE versus glass-filled TFE. Contact area was varied from 20 in.^{2} (Tests I-20) to 100 in.^{2} (Tests I-100) and contact pressure was varied from 250 to 2,000 psi. The average coefficient of friction from at least three tests for each combination of area and pressure is shown plotted in Figure 4.

It is clear from Figure 4 that contact area has little effect on the effective coefficient of friction. However, the effective coefficient of friction for this combination was found to decrease with increasing contact pressure. At low contact pressure, 250 psi, the effective coefficient of friction is approximately 10 percent, decreasing sharply to approximately 8.25 percent at 500 psi and then at a slower uniform rate to approximately 6.75 percent at 2,000 psi. Because of these results only contact pressure was varied in subsequent testing.

TABLE 3 Summary of Test Combinations

Series	Top Element	Bottom Element	Dimension (in)	Contact Area (in^2)	Parallel*
I-20	#1	#1	3 x 6.6	20	no
I-40	#1	#1	5 x 8	40	no
I-60	#1	#1	6 x 10	60	no
I-100	#1	#1	8.7 x 11.5	100	no
I	#1	#1	2.93 x 7	20.5	yes
I-N	#1	#1	2.93 x 7	20.5	no
II	#3	#1	5 x 8.91	44.55	yes
II-N	#3	#1	5 x 8.91	44.55	no
III	#2	#3	5.45 x 9.4 4.2 x 7.6	51.8 31.90	yes
III-A	#5	#3	5 x 9	45	yes
IV-N	#1	#4	5 x 8.91	44.55	no
V	#6	#3	4.9 x 9	44.1	yes
VI-N	#7	#1	6 x 10	60	no
VII-N	#5	#1	4.9 x 9	44.10	no

*Yes - Parallel Interface
No - Nonparallel (1/32" per 12" slope) Interface (N)

Results for Glass-Filled TFE Versus Glass-Filled TFE

Twenty-two tests were conducted using glass-filled TFE elements, top and bottom. The contact area for all tests was 20.5 in.^{2} and the contact pressure was varied from nominally 200 psi to 2,000 psi. The effective coefficient of friction was found to de-

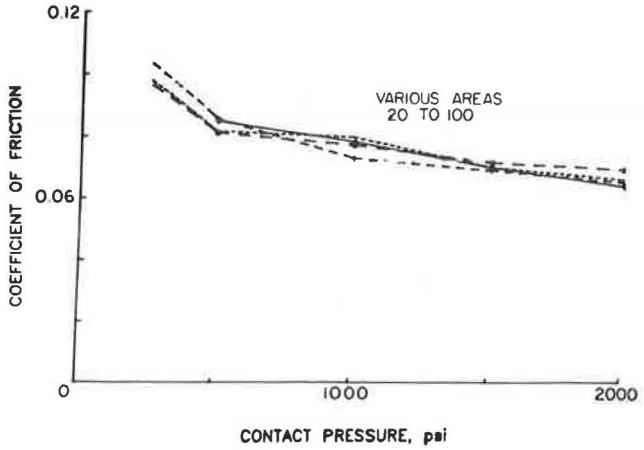

FIGURE 4 Coefficient of friction versus vertical pressure with variation of contact area (Series I).

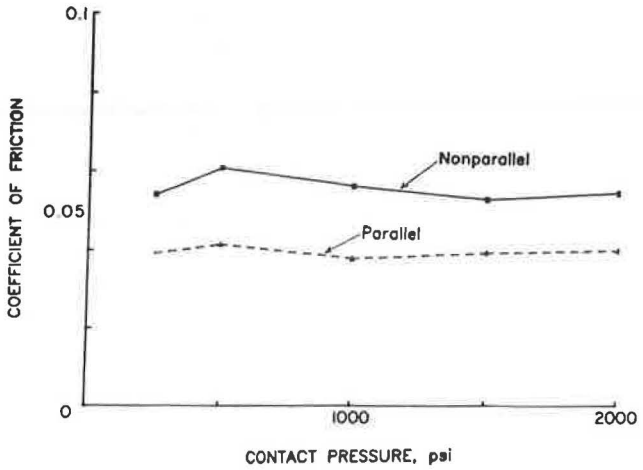

FIGURE 6 Coefficient of friction versus contact pressure, mirror-finish stainless steel versus glass-filled TFE (Series II).

crease abruptly from 5.5 to 3.6 percent between 500 and 1,000 psi and then to increase gradually to 3.9 percent at 2,000 psi as shown in Figure 5, Test Series I (parallel).

Test Series I was repeated with nonparallel interfaces with the results shown in Figure 5. Both the magnitude and relationship to contact pressure of the effective coefficient of friction were influenced by the nonparallel interface. When the nonparallel interface was used, the effective coefficient of friction increased approximately 50 percent.

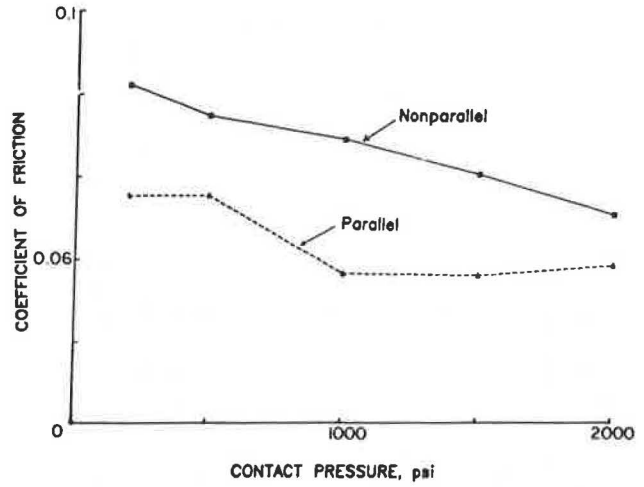

FIGURE 5 Coefficient of friction versus contact pressure, glass-filled TFE versus glass-filled TFE (Series I).

Test with Mirror-Finish Stainless Steel

Test Series II, III, III-A, and V were conducted with one TFE element and one mirror-finish stainless steel element. Glass-filled TFE was used for Series II and III, unfilled TFE for Series III-A, and woven TFE for Series V. Both parallel and nonparallel interfaces were used in Test Series II and III.

Figure 6, Series II test results, shows the effect of nonparallel interfaces on the effective coefficient of friction. The average increase is approximately 40 percent for a slope of 1/32 in. per foot. From Figure 6 it is clear that contact pressure has little effect on the coefficient of friction of glass-filled TFE sliding on mirror-finish stainless steel.

Test Series III varied from Series II only in that the mirror-finish stainless steel element was placed on the bottom and glass-filled TFE mechanically locked to a 1/4-in.-thick steel plate was used for the upper element. This type of TFE element has a significantly higher allowable contact pressure than does glass-filled TFE bonded to carbon steel plates, 6,000 psi versus 2,000 psi. Only the parallel condition was tested. For this series, the effective coefficient of friction decreased slightly with increasing contact pressure from approximately 4 percent at 1,000 psi to 3 percent at 6,000 psi.

Test Series III-A was identical to Series III except that the top element was unfilled TFE bonded to 1/4-in.-thick carbon steel. The allowable contact pressure for this combination was 5,000 psi. A significant decrease in the effective coefficient of friction, compared to Series III, was found. The effective coefficient of friction using the unfilled TFE element is approximately 64 percent of that for the glass-filled TFE element. Little effect was found when the contact pressure was varied from 1,000 to 5,000 psi (2.6-2.2 percent).

Unfilled TFE fibers and glass fibers woven and bonded to 1/4-in.-thick carbon steel were used as the top element in Test Series V. The bottom element was mirror-finished stainless steel. The allowable contact pressure for this combination was 2,000 psi. The effective coefficient of friction was found to be essentially the same as that for unfilled TFE versus mirror-finish stainless steel, Series III-A.

Miscellaneous TFE Tests

Test Series IV-N was conducted using glass-filled TFE bonded to 1/4-in.-thick carbon steel as the top element and glass-filled TFE bonded to No. 10 gauge carbon steel hot vulcanized to 3/4-in.-thick 70 Durometer AASHTO grade neoprene as the bottom element. This combination was tested in the nonparallel condition with a limiting contact pressure of 500 psi. The effective coefficient of friction varied from 9.2 to 6.8 percent when the contact pressure was varied from nominally 250 psi to 500 psi.

Test Series VI-N used an unfinished stainless steel top element and a glass-filled TFE bottom ele-

TABLE 4 Summary of TFE Expansion Bearing Test Results

Test No.	Elements	Parallel	Average Effective Coefficient of Friction				
			250 psi	500 psi	1000 psi	1500 psi	2000 psi
I-60-N	Glass Filled TFE vs Glass Filled TFE	no	0.096	0.081	0.077	0.072	0.070
I	Glass Filled TFE vs Glass Filled TFE	yes	0.055	0.055	0.037	0.036	0.039
I-N	Glass Filled TFE vs Glass Filled TFE	no	0.082	0.075	0.069	0.061	0.051
II	Glass Filled TFE vs Mirror Finish Stainless Steel	yes	0.039	0.041	0.038	0.039	0.040
II-N	Glass Filled TFE vs Mirror Finish Stainless Steel	no	0.054	0.061	0.056	0.053	0.055
III	G.F. Mechanically Locked TFE vs Mirror Finish Stainless Steel	yes	-	-	0.040	-	0.042[1]
III-A	Unfilled TFE vs Mirror Finish Stainless Steel	yes	-	-	0.026	-	0.024[2]
IV-N	Glass Filled TFE vs Glass Filled TFE with Neoprene	no	0.092	0.068	-	-	-
V	Woven TFE and Glass vs Mirror Finish Stainless Steel	yes	0.025	0.022	0.026	0.020	0.020
VI-N	Glass Filled TFE vs Stainless Steel	no	0.123	0.102	0.082	0.077	0.075
VII-N	Unfilled TFE vs Glass Filled TFE	no	0.069	0.062	0.059	0.053	0.056

*Minimum of 3 tests.
1. Tested to 6000 psi: 0.040 @ 3000 psi, 0.031 @ 4000 psi, 0.030 @ 5000 psi, 0.031 @ 6000 psi
2. Tested to 5000 psi: 0.024 @ 3000 psi, 0.021 @ 4000 psi, 0.022 @ 5000 psi

ment. The series was conducted in the nonparallel condition and the contact pressure was limited to 2,000 psi. The effective coefficient of friction was found to be higher than that for any other combination, as high as 12.3 percent, and was found to vary considerably with contact pressure, 12.3 percent at 275 psi to 7.5 percent at 2,000 psi.

Test Series VII-N was conducted with an unfilled TFE top element and a glass-filled TFE bottom element in the nonparallel condition with a limiting contact pressure of 2,000 psi. The effective coefficient of friction varied from 6.9 percent at 250 psi to 5.3 percent at 1,500 psi to 5.6 percent at 2,000 psi.

Summary of TFE Tests

A summary of all TFE expansion bearing tests is given in Table 4. The average effective coefficient of friction from at least three tests for each contact pressure in the range 250-2,000 psi is shown. The highest values were found for the lowest contact pressure and the lowest for the highest contact pressure. Values varied from 12.3 to 2.0 percent.

A comparison of the results for the four most commonly used element combinations is shown in Figure 7: glass-filled TFE versus stainless steel, glass-filled TFE versus glass-filled TFE, glass-filled TFE versus mirror-finish stainless steel, and unfilled TFE versus mirror-finish stainless steel. The effective coefficient of friction decreases with increasing contact pressure for all combinations. The highest values were obtained for glass-filled TFE versus stainless steel and the lowest for unfilled TFE versus mirror-finish stainless steel. For contact pressure greater than 500 psi, the effective coefficient of friction does not vary with contact pressure. Note that Figure 7 shows results for parallel and nonparallel conditions.

In all of the tests, the lowest effective coefficient of friction was found for the combination of

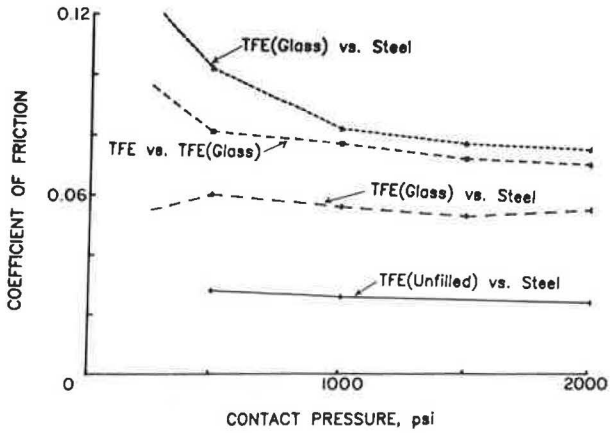

FIGURE 7 Comparison of results for various TFE elements.

unfilled TFE fibers and glass fibers woven and bonded to carbon steel versus mirror-finish stainless steel. However, when tests using the nonparallel condition were attempted, the woven element tended to dig into the opposite element causing damage and a very high effective coefficient of friction. Consequently, this combination is not recommended unless a perfectly parallel interface can be guaranteed.

TFE bearings backed with rubber (neoprene) are commonly recommended for nonparallel surfaces. Test Series IV-N was conducted using 3/32-in.-thick glass-filled TFE bonded to No. 10 gauge carbon steel that in turn was hot vulcanized to 3/4-in.-thick 70 Durometer AASHTC grade neoprene versus 3/32-in.-thick glass-filled TFE bonded to 1/4-in.-thick carbon steel. The bearing was tested at 250, 500, and 700 psi contact pressure. At 700 psi, the allowable contact pressure, the neoprene failed with a sub-

stantial increase in effective coefficient of friction. A possible cause was poor-quality neoprene.

TEST RESULTS FOR SELF-LUBRICATING BRONZE EXPANSION BEARINGS

Two types of bearings were used in this portion of the study (6): flat plate and curved plate. Details are shown in Figure 8. Each bearing consists of three parts: a machined steel base plate, a machined bronze plate, and a machined steel sole plate. The bronze plate contains recesses on both sides that are filled with a solid lubricant applied under heat and pressure. The recesses are arranged in a geometric pattern so that overlap in the direction of movement is achieved. The total area of the recesses is approximately 50 percent of the total surface area of the bronze plate.

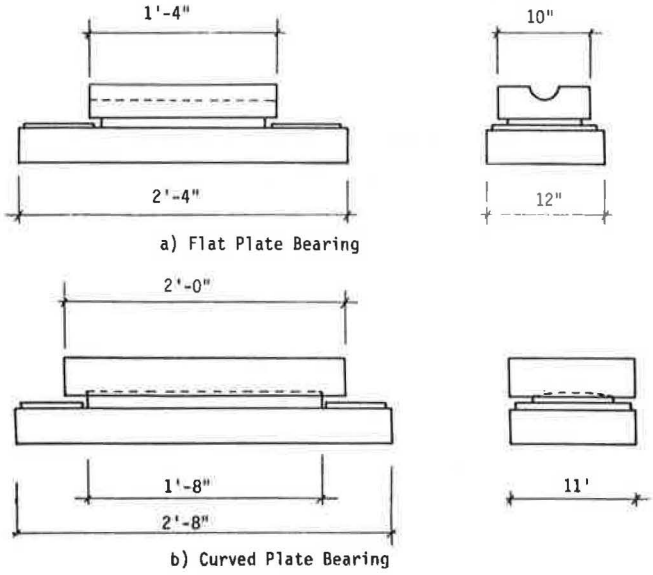

FIGURE 8 Self-lubricating bronze expansion bearings used in testing.

The flat plate bearing used in the testing program is only part of the entire bearing assembly. A separate pin and upper bearing plate are normally provided to permit rotation at the bearing location. Longitudinal expansion is accommodated through movement of the bronze plate. Because of the configuration of the test setup used in this research, the lack of rotation capability in the flat bearings did not affect test results. The curved plate bearing provides allowance for both expansion and rotation.

One new and two used bearings of each type were tested for a range of normal forces. The four used bearings were removed from a bridge after 20 years of service. The two new bearings were manufactured to specifications identical to those of the used bearings.

All bearings were initially tested at a nominal normal force of 175 kips. Subsequent tests were conducted in decreasing increments of nominally 25 kips to 50 kips. A final test at 175 kips was then conducted At each normal force level three tests were conducted. For the first two tests, the bridge girder was carefully positioned so that the centerline of the sole plate was directly over the centerline of the bearing plate. The girder was then pulled approximately 0.35 in. toward the horizontal reaction frame. For the third test, the centerline of the sole plate was positioned 1 in. beyond the centerline of the bearing plate and then the girder was pulled toward the horizontal reaction frame. Travel was again approximately 0.35 in. To check this procedure, in two tests the centerline of the sole plate was positioned 1 in. beyond the centerline of the bearing plate and the girder pulled 2 in. toward the horizontal reaction frame. The original procedure was found to be adequate.

Results of the 123 tests are summarized in Tables 5, 6, and 7 and are discussed in the following paragraphs. A more complete description of the test results is found in Mazroi et al. (6).

Curved Plate Bearing Test Results

For the new curved plate bearing, the maximum effective coefficient of friction was obtained in the first test (nominal normal force of 175 kips). The effective coefficient of friction then decreased with decreasing load until 75 kips normal force, whereupon the values increased slightly. For the used curved plate bearing No. 1, a somewhat similar pattern was found; however, the effective coefficient of friction values for this bearing were lower than those for the new bearing. For the used curved plate bearing No. 2, the effective coefficient of friction values decreased until the nominal normal force was decreased to 100 kips and then increased. The highest value obtained in any test was 0.1232 (new bearing, Test 1) and the lowest was 0.0561 (curved plate bearing No. 1, Test 4) (Table 5). The average value for all tests was 0.0905 with a standard deviation of 0.0171 (Table 6).

Flat Plate Bearing Test Results

The maximum effective coefficient of friction for this bearing type was from the first test of flat plate bearing No. 2. For all three bearings, the effective coefficient of friction decreased with decreasing normal force until 100 ± 25 kips was reached and then the coefficient increased slightly. The highest value obtained in any test was 0.1772 (flat plate bearing No. 2, Test 1) and the lowest

TABLE 5 Highest, Average, and Lowest Results of Expansion Bearing Tests

Bearing	Effective Coefficient of Friction		
	Highest	Average	Lowest
Curved Plate			
New	0.1232	0.0946	0.0831
No. 1	0.1023	0.0711	0.0561
No. 2	0.1206	0.1052	0.0907
All	0.1232	0.0905	0.0561
Flat Plate			
New	0.1334	0.0961	0.0869
No. 1	0.1150	0.1004	0.0867
No. 2	0.1772	0.0833	0.0643
All	0.1772	0.0933	0.0643
All Tests	0.1772	0.0919	0.0561

TABLE 6 Summary of Expansion Bearing Test Results

Bearing	Average Effective Coefficient of Friction	Standard Deviation	Coefficient of Variation	Least Square Method	
				Slope	Intercept
Curved Plate					
New	0.0946	0.0090	0.000077	0.1001	-0.636
No. 1	0.0711	0.0115	0.000125	0.0754	-0.523
No. 2	0.1052	0.0094	0.000084	0.0931	1.231
All	0.0905	0.0171	0.000089		
Flat Plate					
New	0.0961	0.01083	0.000110	0.1094	-1.425
No. 1	0.1004	0.00877	0.000073	0.1093	-0.944
No. 2	0.0833	0.02510	0.000599	0.1232	-4.166
All	0.0933	0.01785	0.000313		
All Tests	0.0919	0.01747	0.000303		

TABLE 7 Summary of Expansion Bearing Test Results Excluding First Test of Each Bearing

Bearing	Average Effective Coefficient of Friction	Standard Deviation	Coefficient of Variation
Curved Plate			
New	0.0934	0.00666	0.000042
No. 1	0.0695	0.00905	0.000078
No. 2	0.1052	0.00966	0.000088
All	0.0895	0.01682	0.000278
Flat Plate			
New	0.0942	0.00641	0.000039
No. 1	0.0996	0.00830	0.000065
No. 2	0.0784	0.01223	0.000142
All	0.0907	0.01288	0.000163

was 0.0643 (flat plate bearing No. 2, Test 11) (Table 5). Both the high and the low values occurred with bearing No. 2. The average value for all tests was 0.0933 with a standard deviation of 0.01785 (Table 6).

Summary of Self-Lubricating Bearing Tests

For all tests the highest effective coefficient of friction found was 0.1772 and the lowest was 0.0561. The average value for all flat plate bearings was 0.0905, for all curved plate bearings 0.0933, and for all bearings 0.0919. The corresponding standard deviations are 0.0171, 0.01785, and 0.01747. Hence, the expected effective coefficient of friction for all bearings 95 percent of the time is approximately 0.09 ± 0.02.

The effective coefficient of friction for the first test of each bearing was, in general, higher than that for the remaining tests. Table 7 gives average values, standard deviations, and coefficients of variation for the test results excluding the first test of each bearing. From this data the expected effective coefficient of friction 95 percent of the time is approximately 0.09 ± 0.01. Insignificant difference was found between old and new bearings.

SUMMARY

From test results of various TFE expansion bearing configurations, the effective coefficient of friction was found to be less consistent when both elements were TFE, as opposed to one element being mirror-finish stainless steel. The highest values of effective coefficient of friction were obtained for glass-filled TFE versus stainless steel (7.5-12.3 percent) and the lowest for unfilled TFE fibers and glass fibers woven versus mirror-finished stainless steel (2.1-2.6 percent). Tests using a nonparallel condition showed that the effective coefficient of friction increases about 50 percent for only 1/32 in. per foot (0.15 degree) slope.

The effective coefficient of friction, in general, was found to decrease with increasing contact pressure. However, the change was found to be very small when the contact pressure was 50 percent or greater of the maximum contact pressure, except for Series I-N (glass-filled TFE versus glass-filled TFE with nonparallel interfaces) where the coefficient of friction continued to decrease and Series V (unfilled TFE fibers and glass-filled fibers woven versus mirror-finish stainless steel) where little change was found as the contact pressure was varied.

The results of this study show that the recommendation in Recommended Design Loads for Bridges (4), that the design longitudinal force due to friction at sliding expansion bearings composed of TFE on TFE or stainless steel should be based on a coefficient of friction of 0.06, is not conservative for all combinations of elements used in this study. Of the combinations tested, (a) glass-filled TFE versus glass-filled TFE, (b) glass-filled TFE versus mirror-finish stainless steel, (c) glass-filled TFE mechanically locked to steel plate versus mirror-finish stainless steel, (d) unfilled TFE versus mirror-finish stainless steel, and (e) unfilled TFE fibers and glass fibers woven and bonded to carbon steel plate versus mirror-finish stainless steel satisfied the design recommendation for all contact pressures. The criterion was also satisfied with unfilled TFE versus glass-filled TFE for contact pressures of 1,000 psi and greater. The design assumption was satisfied for nonparallel conditions using (a) glass-filled TFE versus mirror-finish stainless

steel and (b) unfilled TFE versus glass-filled TFE for contact pressure of 1,000 psi and more. The design recommendation was not satisfied for (a) nonparallel tests of glass-filled TFE versus glass-filled TFE, (b) nonparallel tests of glass-filled TFE versus stainless steel, and (c) nonparallel tests of unfilled TFE versus glass-filled TFE for contact pressures less than 1,000 psi. Thus, it is concluded that the suggested design assumption (4) must be used with caution.

Recommended Design Loads for Bridges (4) also recommends that the design coefficient of friction for steel bearing on self-lubricating bronze plate be taken as 0.1. For both the new and used self-lubricating bronze expansion bearings tested, the effective coefficient of friction was found to be 0.09 ± 0.02 with a confidence interval of 95 percent for all tests. Hence, the recommendation is judged to be adequate.

ACKNOWLEDGMENTS

This paper was developed from research projects sponsored by the Oklahoma Department of Transportation and by the Port Authority of New York and New Jersey. The authors wish to thank Tim Borg, Jim Schmidt, and Dwight Hixon of the ODOT Research and Development Division and Veldo Goins of the ODOT Bridge Division for their helpful suggestions and assistance during the course of the TFE bearing portion of the study and Ray Finnegan and Anthony Shaw of the Engineering Department Materials Division of the Port Authority of New York and New Jersey for their help and guidance during the self-lubricating bronze expansion bearing portion of the study. The assistance of Leon R.L. Wang, Bryant E. Davidson, and Lori Creech of the Fears Structural Engineering Laboratory in performing the testing and completing the research reports is acknowledged.

REFERENCES

1. A. Mazroi, L.R.L. Wang, and T.M. Murray. Effective Coefficient of Friction of Bridge Bearings. Research Report FSEL/ODOT. Oklahoma Department of Transportation, Oklahoma City; Fears Structural Engineering Laboratory, University of Oklahoma, Norman, Feb. 1982.
2. F.K. Jacobson. TFE Expansion Bearings for Highway Bridges. Physical Research Report 71. Illinois Department of Transportation, Bureau of Materials and Physical Research, Springfield, April 1977.
3. M.E. Taylor. PTFE in Highway Bridge Bearings. Report LR491. Transport and Road Research Laboratory, Crowthorne, Berkshire, England, 1975.
4. Recommended Design Loads for Bridges. Journal of the Structural Division of ASCE, Vol. 107, No. ST7, July 1981, pp. 1161-1213.
5. Standard Specifications for Highway Bridges. American Association of State Highway Officials, Washington, D.C., 1977.
6. A. Mazroi, B.E. Davidson, and T.M. Murray. Effective Coefficient of Friction of Certain Self-Lubricating Bronze Expansion Bearings. Research Report FSEL/PANYNJ 83-01. Port Authority of New York and New Jersey, New York; Fears Structural Engineering Laboratory, University of Oklahoma, Norman, March 1983.

Publication of this paper sponsored by Committee on General Structures.

Abridgment

Earthquake Precursers and Potential Damage in the United States

STEWART C. WATSON, EDWARD R. FYFE, and RONALD J. WATSON

ABSTRACT

FHWA has issued earthquake design guidelines for new structures and for retrofitting. These guidelines follow the recent work product, published in October 1981, of the study done by the Applied Technology Council. Effective March 1, 1983, AASHTO has similarly adopted these criteria. Because this represents an area of design with few successful precedents and these guidelines are intended to encourage innovative thinking, this discussion will cover the following subject areas: (a) an introduction to the seismic design problem encompassing some of the fundamentals of what is known about earthquakes and their prediction, (b) examples of how structures are affected by mild and medium earthquakes, (c) the controlled base isolation concept, and (d) some of the design principles necessary for successful expansion joint and bearing performance during a typical earthquake. Some of the new tools and concepts that could be useful in seismic design are described together with their performance criteria and the testing accomplished to date to verify their performance along with design parameters for their use.

In the past there was, unfortunately, a lack of serious interest in seismic design by owners of our eastern highway network partly because of attendant costs but primarily because of the belief that earthquakes pose no threat to these structures. Comparatively high levels of ground shaking can be expected in 15 eastern states and Puerto Rico, and this situation is aggravated by the previous lack of emphasis on seismic design. Fortunately certain specific structural details can easily be modified especially at bearings and expansion joints, which have proven extremely vulnerable to damage in earthquakes. This discussion will be useful if it creates an awareness of the potential hazards and the catastrophic effects that can occur to essential lifeline structures that must remain operational at all costs during and after a strong earthquake.

SEISMIC EFFECTS ON BEARINGS

Regardless of their magnitude, intensity, or duration, in all earthquakes extensive damage occurs to bearings. Bolt pullout gives clear evidence of the need for strong uplift resistance to upward jerking vertical pullout stresses, a performance capability that will be described hereafter in the discussion of an improved type of bearing that incorporates a trailer hitch concept of uplift restraint. The embedment strength as well as the width and the length of the bearing seats need to be improved. It is now known that many popular bearing concepts are totally inadequate for seismic design.

SEISMIC DESIGN COMPONENTS AND REFINEMENTS

For the last 3 years, the authors of this report have been meeting regularly as a design task group to study what is known about the effects of earthquakes on structures and what can be done in terms of design concept, whether it be the classical or the controlled base isolation concept, to improve on the seismic performance of bridges and structures.

BONAFY--A STRUCTURAL ELASTOMER

The seismic design components described herein use a material known as "Bonafy." Bonafy is an internationally trademarked name for a specially developed structural elastomer in the polyether urethane family. A 50,000 psi material in compression, it is, however, only being loaded as a bearing component to 5,000 psi, which gives it a 900 percent safety factor. A similar material is used as a draft gear to take end-to-end slamming effects between adjacent cars in railroad operations. Bonafy has tremendous impact toughness and high abrasive resistance. It has been used successfully for the past 13 years without a single failure as the load bearing and rotational element in the shear inhibited disc bearing.

It was therefore believed that no known structural elastomeric material was better suited than Bonafy to resist the dynamic multidirectional impact forces of an earthquake. A new family of hardware and refinements in bearings have been developed for the needs of seismic design. For conventional earthquake design the new requirements for bearing systems, and therefore structural supports, are high horizontal force designs; bearings, which can take rotation during uplift, to accommodate uplift forces; special bearing guiding systems that allow rotation in plan; flexible guides that allow for some degree of self-aligning as well as equalization of forces between bearings during seismic conditions; special limit stop buffers and displacement control devices; and special connector cables that allow movement while absorbing energy during seismic events. The new "controlled base isolation" concept, which involves using bearings and displacement control devices, and the test results on these devices will also be discussed.

Uplift Restraint

Uplift bearings, such as the modified shear restriction mechanism shown in Figure 1, which acts like a vertical trailer hitch coupling to accommodate the forces, have been designed to simultaneously accommodate uplift and rotation during seismic conditions. Early attempts to absorb uplift forces

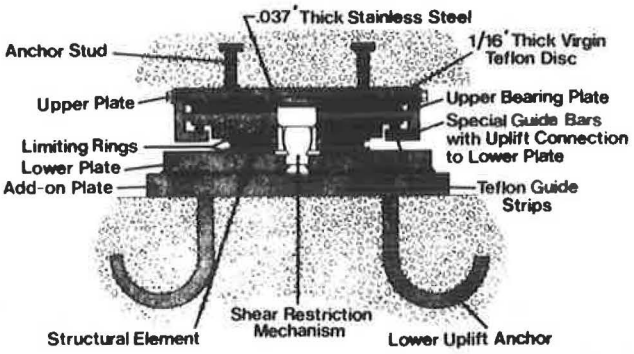

FIGURE 1 Special design bearing for high horizontal and uplift forces.

by simply attaching the bearing to the base plate did not allow rotation with the result that point loaded areas were established that created overload stresses. Simple clamp devices for uplift restraint are also unreliable because of high point stresses that develop during uplift and rotation combinations.

An example of bearing performance that is adequate for seismic needs is the Calgary Coliseum roof, which is shaped like a saddle and uses bearings designed for 400 kips vertical load, 400 kips uplift, 4 percent rotation, 12 in. of movement in all directions, and dynamic uplift--all conditions similar to those of an earthquake situation. Some of the steel plates in the bearings are approximately 8 in. thick. An interesting criterion for these bearings is that all steel was required to meet a notch toughness of 19 ft-lb at -40°F.

Self-Aligning Rotation in Plan

Another new seismic design feature that is also used in nonseismic applications is the self-aligning bearing or the rotation-in-plan concept. For unidirectional or guided bearings (Figure 2), a tetrafluoroethylene stainless steel slide plate is introduced between the disc and the steel plate to allow rotation in plan.

Flexible Guides

Flexible guides provide a way of incorporating Bonafy between the guide and the middle plate. This allows for a small amount of rotation in plan and also results in seismic force distribution between different bearings on the project. With conventional guides, one bearing must be designed to take the total horizontal force. Bearings such as this have been manufactured for the new Bear River Bridge in Nova Scotia, Canada, which is potentially a seismic area.

Limit Stops

Limit stop devices for seismic design vary in concept from a rubber tire to a sophisticated hydraulic ram system. Figure 3 shows a high-quality Bonafy elastomeric limit stop buffer.

Displacement Control Device

A more positive limit stop device is the displacement control device (DCD), shown in Figure 4, that is a single acting unit. This device can be used at both ends of a guided bearing or all four sides of a multidirectional bearing. The device can give simply a three-phase elastic effect or a three-phase elastic effect with energy absorption. The curve shown in Figure 5 illustrates the load deflection characteristics of the device as it becomes semiconfined and then confined like a pot bearing.

A DCD (Figure 6) is a series of Bonafy or other elastomeric discs in combination, a viscous material cell, and energy space all encapsulated in a steel shell riding on a steel rod assembly in a single acting device. Energy is also absorbed in the first seismic cycle.

The same DCD can be double acting. In that case,

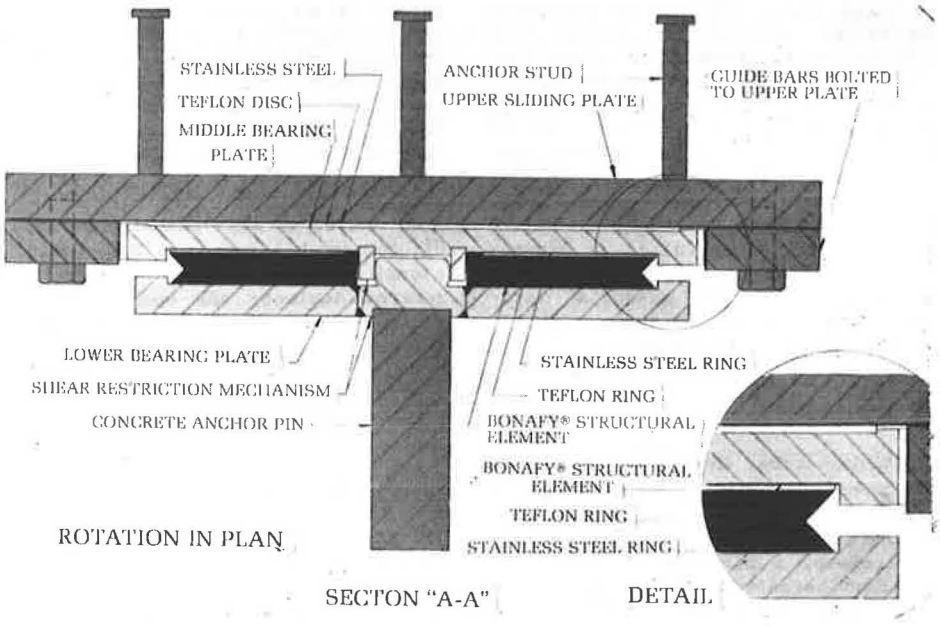

FIGURE 2 Self-aligning bearing.

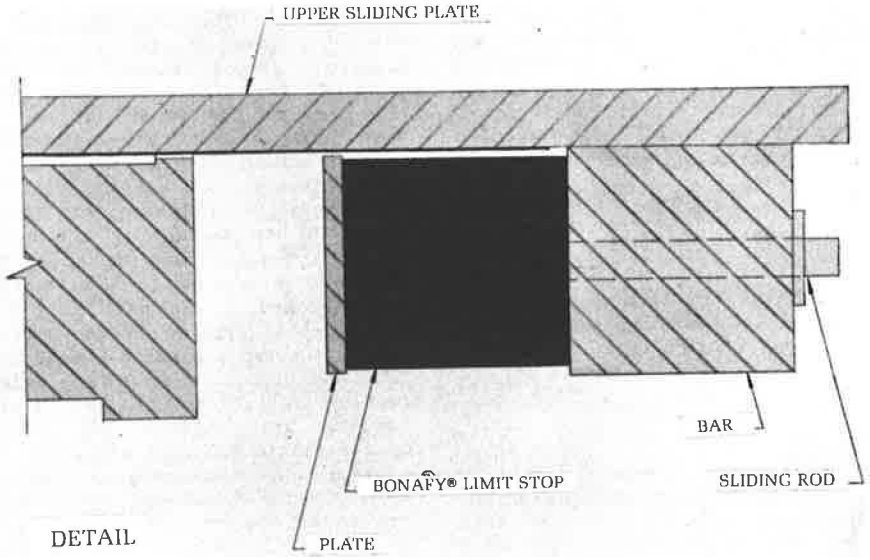

FIGURE 3 Bonafy® elastomer limit stop buffer.

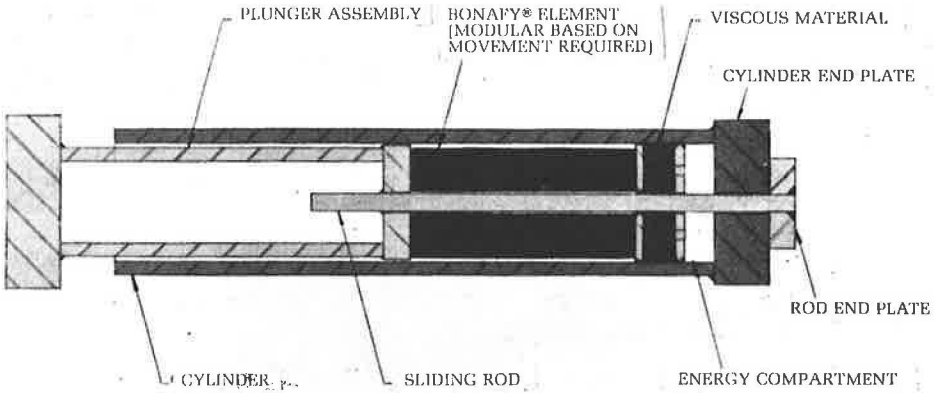

FIGURE 4 Single acting limit stop displacement control device.

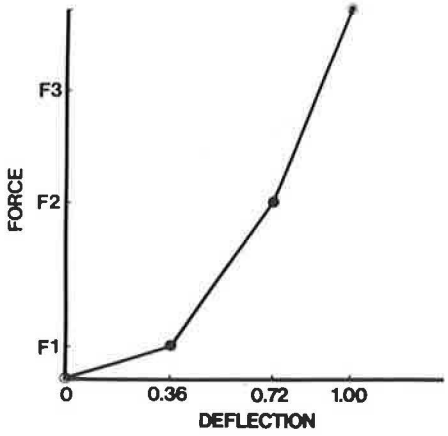

FIGURE 5 Typical load deflection curve.

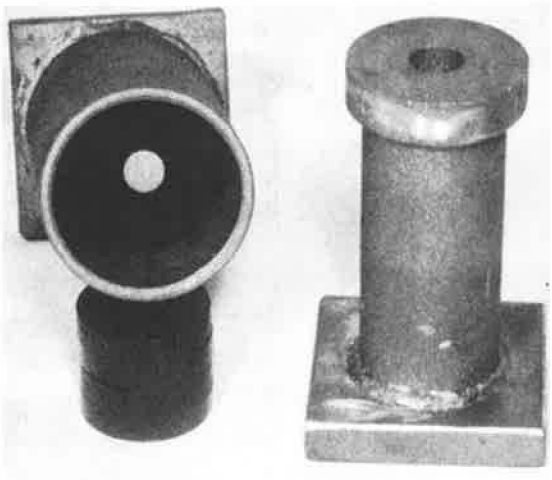

FIGURE 6 Displacement control device.

energy absorption is double acting and continues throughout the seismic forces and reduces movements substantially. This helps keep the seismic expansion joint design and cost minimized. This device functions in the following manner: the Bonafy discs are compressed as the DCD moves in each direction until the discs become fully confined when the energy absorption phase begins.

Restraint

The same DCD can be incorporated like a cable connector between spans or at abutments of new concrete or steel structures. It can also be used in retrofit situations.

Controlled Base Isolation

The controlled base isolation earthquake protection concept involves a conventional disc bearing that sits on a slip plane. The slip plane consists of a stainless steel-to-polytetrafluoroethylene sliding surface at the bearing seat location (Figure 7). A standard shear inhibited disc bearing system is connected to a slip plane by DCDs that are designed to perform at a predetermined earthquake force. Before seismic events, the bearing is independent of the slip plane and functions normally. During earthquake movements, DCDs, which also act as energy dissipators, control the translation of the bridge deck in relation to that of the piers and abutments.

Displacement Control Device

The key element in this earthquake protection concept is the DCD. The principal functions of this device (Figure 8) are to allow movement of the structure during seismic forces, dissipate the energy of those forces, control and reduce the displacement of the structure, and restore the structure to its original pre-earthquake position.

The entire DCD assembly is connected to the superstructure and bearing seat by universal hinge connectors that allow seismic movement in any direction. A key element is the hinge connection that works like a ball and socket system to allow multidirectional movement. Uplift forces can be controlled through the use of a DCD coupled to the bearing seat applied in the vertical direction. The use of the two preloaded DCDs coupled to the bearing seat and structure at 90°F provides earthquake protection regardless of the direction of seismic forces. The residual compression force generation of the elastomers will dissipate the seismic energy, control the displacement, and apply a restoring force to the structure. To conduct further tests on an actual bearing system that uses these displacement control devices, a new test machine has been designed to verify performance. This machine has a 4,000-kip vertical capacity with a 1,200-kip capacity in the horizontal plane.

On the basis of the testing done to date, DCD selection tables have been formalized. Through the use of seismic design criteria the engineer calculates the earthquake force that is anticipated. With this force in mind, the designer can refer to Table 1 and select the outside diameter and area of the DCD cylinder. Along with the forces, the engineer must calculate the anticipated seismic displacement

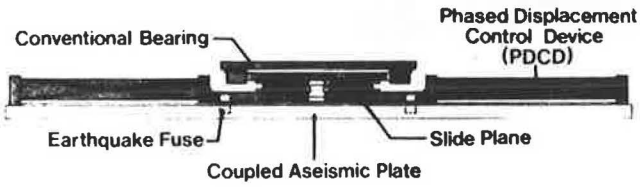

FIGURE 7 Controlled base isolation concept.

TABLE 1 Earthquake Force Versus Outside Diameter and Area of DCD Cylinder

Earthquake Force		Displacement Control Device			
		Outside Diameter		Area	
Kips	kN	in.	mm	in.^{2}	m^2
35	150	4	101	7	0.004
100	440	6	152	20	0.013
250	1110	10	254	51	0.033
550	2440	14	356	114	0.073
1,000	4440	20	508	230	0.148
1,500	6670	24	610	332	0.214
2,000	8890	27	686	410	0.264

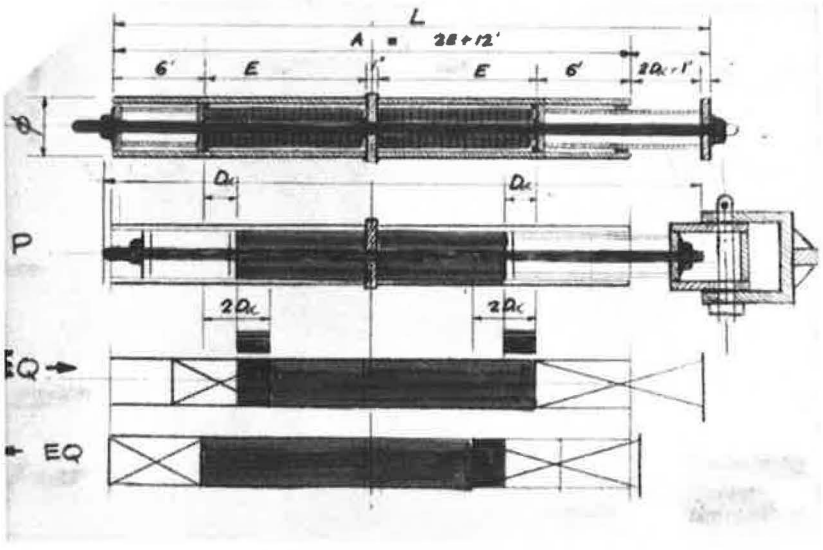

FIGURE 8 Schematic of displacement control device.

TABLE 2 Earthquake Displacement (N) Versus DCD Displacement (d), Length (L), and Elastomer Thickness

		Displacement Control Device									
N		d		L		SK 1		SK 2		SK 3	
in.	mm	in.	mm	in.	mm	KS1/in.	MPa/mm	KS1/in.	MPa/mm	KS1/in.	MPa/mm
2	51	1	25	26	660	0.444	0.121	1.480	0.402	13.90	3.781
4	102	2	51	36	914	0.222	0.060	0.740	0.201	6.95	1.890
6	152	3	76	46	1168	0.148	0.040	0.493	0.134	4.63	1.259
10	254	5	127	66	1676	0.089	0.024	0.296	0.080	2.78	0.756
20	508	10	254	116	2946	0.044	0.012	0.148	0.040	1.39	0.378
30	762	15	381	166	4216	0.030	0.009	0.099	0.027	0.927	0.252
40	1018	20	508	216	5486	0.022	0.006	0.074	0.020	0.695	0.189

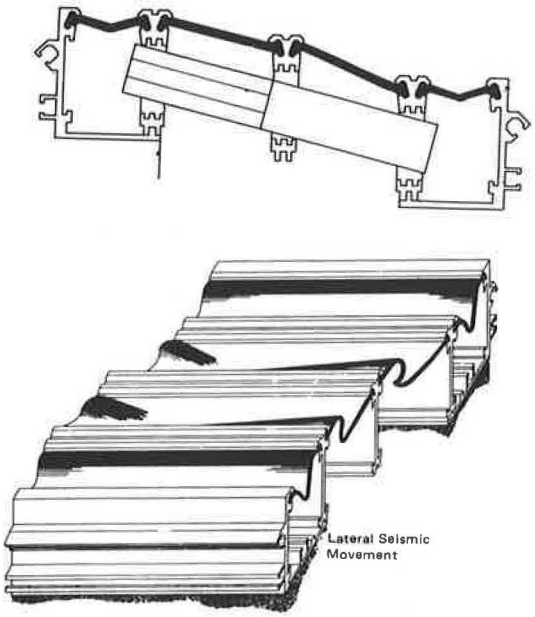

FIGURE 9 Expansion joint.

of the structure. The DCD is designed to reduce the seismic displacement by a factor of 2. Table 2 gives the engineer the new displacement value and the length of the device. This table also gives the three different stiffness stress factors SK 1, 2, and 3. These factors will give the designer the three phases of the force displacement curve. With these steps completed, the engineer has the dimensions of the DCD, and the earthquake protection system can be designed into the structure.

Seismic Expansion Joint

Figure 9 shows an expansion joint, with large movement potential, that has been specially designed to accommodate multidirectional seismic movements from virtually any direction in addition to its normal stroke of thermal dilation.

Publication of this paper sponsored by Committee on General Structures.

Horizontally Curved I-Girder Bridge Analysis: V-Load Method

MICHAEL A. GRUBB

ABSTRACT

The V-load method is a widely used approximate method for the analysis of horizontally curved I-girder highway bridges. Previously, this method had been proven valid only for noncomposite I-girder bridges with radial supports. Thus, a study was made to extend the method to composite I-girder bridges with any general support configuration. V-load-analysis results for noncomposite and composite I-girder bridges under dead load and live load were compared with the corresponding results from three finite-element curved bridge models with different combinations of radial and skewed supports. The dead-load V-load results were extremely accurate. The live-load V-load results were strongly influenced by the lateral distribution factors that were used; specification distribution factors gave acceptable V-load results for exterior girders and conservative results for interior girders. More accurate results were obtained with more realistic factors. It is also shown that the V-load method is not a valid approximation for closed-framed I-girder systems with horizontal lateral wind bracing. Approximate expressions are presented to compute the warping stresses in the girder flanges, an important consideration in curved I-girder bridges.

Horizontally curved composite I-girder bridges are being increasingly used for highway interchanges and river crossings. Curved bridge girders offer several inherent advantages. They are more aesthetically pleasing than a series of straight girders along the chords of a roadway curve, and curved girders allow designers to use longer spans, thus eliminating much of the substructure. Curved bridges may also result in simpler and more uniform construction details because girder spacing and concrete slab overhang are generally constant along the length of the structure. One problem with curved bridge design, however, has been the difficulty in mathematically analyzing curved girders; curvature causes torsional loadings that complicate the stress analysis. Rigorous methods have been available for the structural analysis of curved bridges, but highway engineers generally prefer simplified techniques.

In 1963 a report was published (1) that presented a simplified approximate analysis technique for open-framed curved I-girder bridges [open framing was defined originally in that report as noncomposite I-girders connected by diaphragms (floorbeams) or cross frames (K- or X-bracing) with no horizontal lateral bracing near, or in, the plane of the bottom flanges]. The method was modified and greatly simplified for multigirder systems a few years later (2). Agreement with more complicated analyses was excellent. This approximate method eventually became known as the V-load method because a large percentage of the torsional load on the girders is approximated by sets of vertical shears known as V-loads. The V-load method has been widely used in consulting engineering offices. According to a 1969 survey the method was used for the design of approximately 75 percent of the curved steel I-girder bridges in the United States (3).

One limitation of the V-load method, however, was that it had only been proven valid for noncomposite curved open-framed systems with the bridge piers on a radial alignment. In reality, curved I-girder bridges have a reinforced concrete slab and often depend on composite action to resist the loads. Also, horizontal lateral bracing is sometimes included near, or in, the plane of the bottom flanges to help resist wind loads (a so-called closed-frame system). Furthermore, many curved bridges have foundations on skewed alignments because of geometric restrictions. Thus, for the V-load method to be general, it must be established that the V-load-analysis results are valid approximations for these cases.

Recent efforts to extend the V-load method to composite curved open-framed bridges (no horizontal lateral bracing) with any general support configuration by comparing the V-load-method results to the results from several finite-element bridge models are discussed. Noncomposite and composite bridges, with combinations of radial and skewed supports, were analyzed with both methods under the correct dead and live loadings. The effect of horizontal lateral bracing was also studied for selected cases.

Another important consideration in the design of curved I-girder bridges is the warping stresses (lateral bending stresses) that develop in the girder flanges. These stresses arise from resistance to the out-of-plane warping of an I-girder cross section that is caused by the applied torsional loads. The approximate calculation of these warping stresses is also presented.

V-LOAD THEORY

Conceptually, the V-load method can be considered as a two-step process. First, the curved structure is straightened out so that the applied vertical loads are assumed to induce only longitudinal girder stresses. Next, external forces are applied to the straight structure such that the resulting internal forces are the same as those that exist in the curved structure subjected to only vertical load. To satisfy static constraints, the applied external forces must be determined such that they result in no net vertical, longitudinal, or transverse forces on the total structure. Thus, in the V-load development, the curvature forces on the equivalent straight structure are treated as externally applied loads.

To illustrate this, the curved bridge system shown in Figure 1 consists of two prismatic girders continuous over one interior support with full-depth cross frames spaced a distance d along Girder 1. The cross frames provide the primary resistance to the

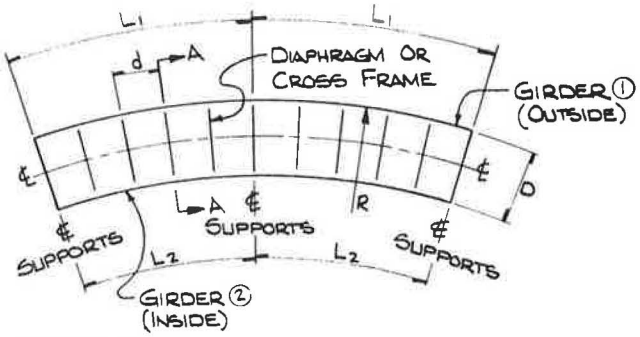

FIGURE 1 Curved bridge—plan view.

torsional loads caused by the bridge curvature. They must, therefore, be designed as primary load-carrying members. Girder 1 has a radius of R, and the distance between the girders is D. In the V-load method, the curved girders are analyzed as isolated straight girders with developed span lengths equal to their respective arc lengths, L_1 and L_2.

Torsional Load

A plan view of the top flange of one of the girders in the example curved bridge is shown in Figure 2.

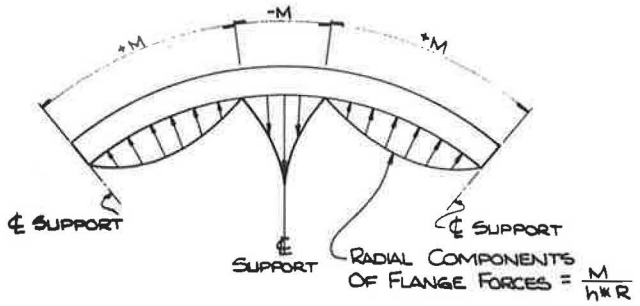

FIGURE 2 Curved top flange—plan view.

When the flanges are assumed to resist the full moment, the axial force in the flange at any point is equal to the bending moment on a transverse section, M, in the girder at that point divided by the depth, h, between the midthickness of the top and bottom flanges. Because of the bridge curvature, these axial forces are not collinear along any given segment of the flange. Thus, to maintain equilibrium, radial components of the internal flange forces are developed. These distributed radial forces have a magnitude of M/(h•R) for small angles. Note that the radial forces are directed outward where the flange is in compression (positive bending), and inward where the flange is in tension (negative bending). The corresponding radial forces in the bottom flange are in the opposite direction. It is these equal opposing forces times the depth, h, that cause twisting of the girders about their longitudinal axes.

Development of V-Loads

Consider a segment of the curved top flange of the outside girder, a distance d/2 on either side of a cross frame. To determine the torsional load resisted internally by the girder at the cross frame, the assumption is made (2) that the distributed radial flange force has a constant value of M/(h•R) over the segment, where M is the bending moment in the curved girder at the cross frame. The force exerted on the flange by the cross frame is, therefore, equal to (M•d)/(h•R) for small angles. Equal and opposite reaction forces are developed in each flange of each curved girder in the system (H_1 and H_2) at every cross frame (it is assumed that no internal reactions are developed in the web). H_1 and H_2 are shown in Figure 3 acting on the flanges of each girder on a free-body diagram of the cross frame at Section A-A of the example curved bridge. These forces create counterclockwise torsional couples at each end of the cross frame and corresponding clockwise resisting couples in each girder.

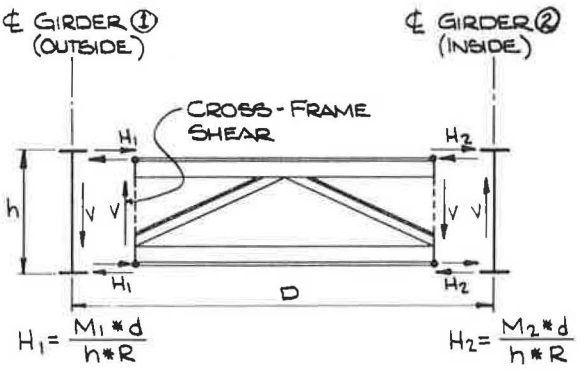

FIGURE 3 Section A-A of curved bridge.

To equilibrate the torsional couples on the cross frame, vertical shear forces, V, develop at each end of the cross frame as a result of cross-frame rigidity and end fixity. These shear forces then react on the girders resulting in a set of self-equilibrating girder shears. The net effect of the shears is to shift the total load on the curved bridge toward the outside girder. These girder shears, which are applied as the external loads to the equivalent straight structure to account for the curvature, are known as the V-loads. Application of the external V-loads ensures that the internal forces in the straight structure will be nearly the same as those that exist in the curved structure under applied vertical loads.

Thus, in a V-load analysis of a system, the bending moments at the cross frames, M_{1p} and M_{2p}, in each of the isolated developed straight girders, caused by applied vertical loads, are first determined by applying those loads to the straight girders. These vertical bending moments will hereafter be referred to as primary moments. The corresponding V-load moments caused by the V-loads, M_{1v} and M_{2v}, are then determined by applying the V-loads, in the proper directions, to the straight girders at the cross frames. The final moments in the curved girders, M_1 and M_2, are then obtained by simply summing the respective straight-girder primary and V-load moments. The shears, reactions, and deflections in the curved girders are also determined in the same manner. First, however, a method is needed to calculate the V-loads.

Calculation of V-Loads

In the calculation of V-loads, the distribution of

cross-frame shears across the section becomes important, and the relative stiffnesses of the adjacent girders must be considered. The problem is simplified if it is assumed that (a) all the girders in the section have nearly the same vertical stiffness, (b) the girder shears across the section are self-equilibrating, and (c) the loading on girders outside the longitudinal centerline of the system is increased, and the loading on girders inside the longitudinal centerline is decreased. An important assumption can then be made about the apportionment of the cross-frame shears to the individual girders. The assumption is that the shear on a girder is proportional to the distance of that girder from the longitudinal centerline of the bridge, which, based on the preceding assumptions, implies a linear distribution of girder shears across the section. This is a reasonable approximation because the assumption that all girders have nearly the same vertical stiffness is good for curved bridges under normal highway loadings. However, for curved bridges under exceptional conditions, which result in girders with large stiffness variations, the girder-shear distribution may be nonlinear and the method would not give a valid approximation of actual behavior. For such cases, a more detailed analysis should be made.

The calculation of the V-loads, based on the previous assumptions, will be illustrated with reference to the four-girder system shown in Figure 4. All girders in the cross section are assumed to be equally spaced. It is assumed that the section is subjected to a net torque from the internal radial forces, H, in each of the girder flanges. These forces (not shown) are in the same direction as the forces in Figure 3. It is also assumed that the cross frames are rigid enough that the torques in the individual girders at the section can be summed.

To equilibrate this net torque, the internal cross-frame shears, V_1, V_2, and V_3, are developed. These shears are shown acting at inflection points in the cross frames, which are assumed to be at distances a, b, and c from the respective girders (arbitrarily shown at the cross-frame midspace in Figure 4). Because these shears develop reactions at the adjacent girders, and the shears, V, on the outside and inside girders are assumed to be equal and opposite, $V = V_1 = V_3$. Invoking the assumption that the girder shears are proportional to the distance of the girders from the longitudinal centerline of the bridge, the shears on the two interior girders are equal to (1/3)V acting in opposite directions. This also means that $V_2 = V_1 + (1/3)V = (4/3)V$. The factor 1/3 is a proportionality factor that is based on the geometry of the bridge cross section. Note that the girder shears add up to zero across the section as assumed. The V-loads, which would be applied to the straight structure, are equivalent to the girder shears in the curved structure and are shown below the section.

Next, moment equilibrium between the inflection points is enforced at the bottom of each girder and results in the following equations:

$$V_1 \cdot a = H_1 \cdot h = (M_1 d)/R \quad (1)$$

$$V_1 \cdot [(D/3) - a] + V_2 \cdot b = (M_2 d)/R \quad (2)$$

$$V_2 \cdot [(D/3) - b] + V_3 \cdot c = (M_3 d)/R \quad (3)$$

$$V_3 \cdot [(D/3) - c] = (M_4 d)/R \quad (4)$$

where M_1, M_2, M_3, and M_4 are the final moments in the respective curved girders at the cross frames. Substituting $V_1 = V_3 = V$ and $V_2 = (4/3)V$, and solving the four equations simultaneously for V gives

$$V = (M_1 + M_2 + M_3 + M_4)/[(10 \cdot R \cdot D)/(9 \cdot d)] \quad (5)$$

Because the V-load moments are generally small compared to the primary moments, the simplifying assumption is made that

$$M_1 + M_2 + M_3 + M_4 = M_{1p} + M_{2p} + M_{3p} + M_{4p} \quad (6)$$

Substituting these terms in Equation 5 gives

$$V = (M_{1p} + M_{2p} + M_{3p} + M_{4p})/[(10 \cdot R \cdot D)/(9 \cdot d)] \quad (7)$$

or the more general relationship

$$V = \Sigma M_p/(C \cdot K) \quad (8)$$

where ΣM_p is the summation of the primary moments in each girder at a particular cross frame, C is a coefficient that depends on the number of girders in the system, and K is equal to (R•D)/d (R and d are for the outside girder). Coefficient C for various multigirder systems assuming equal girder spacing is

No. of Girders in System	Coefficient C
2	1
3	1
4	10/9
5	5/4
6	7/5
7	14/9
8	12/7
9	15/8
10	165/81

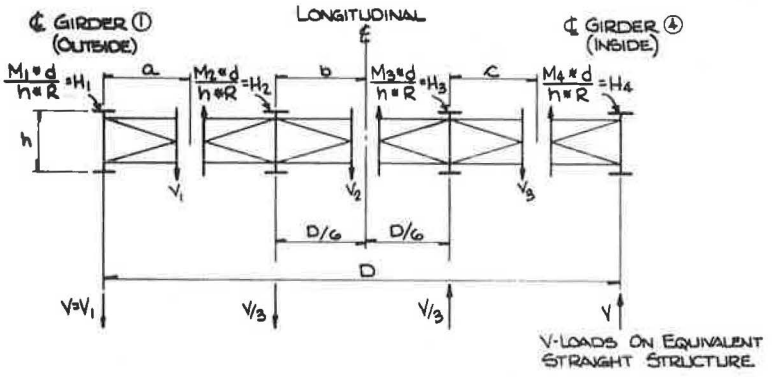

FIGURE 4 Cross section—multigirder curved system.

Equation 8 is, therefore, the general equation for the V-loads on the outside and inside girders of the equivalent straight structure at the cross frames. The proper proportionality factors are applied to these values to obtain the V-loads on the other equivalent straight girders in the section. Special attention must always be given to the direction of the loads.

FINITE-ELEMENT MODELS

Mathematical finite-element models of the preliminary designs of three curved I-girder bridges (noncomposite and composite) with different combinations of radial and skewed supports were developed to check the accuracy of the V-load method. Three curved bridge schemes, representative of common highway structures, were chosen for the study. They will hereafter be referred to as

- Scheme A--radial supports,
- Scheme B--parallel skewed supports, and
- Scheme C--two parallel skewed supports and one radial support.

Plan views of the schemes (noncomposite) are shown in Figure 5.

All three bridges are two-span, continuous, four-girder structures with unequal spans and compound radii. All schemes are initially open framed, that is, with no horizontal lateral bracing. The span lengths are generally different among the three schemes and are shown in Figure 5. The radii, R_1 and R_2, of each girder in each span are the same for all schemes and are also shown. The cross-frame spacings along the outside girder are shown on each bridge. The spacings were chosen to minimize the lateral bending stresses in the flanges caused by warping of the girder cross sections. The skew angle of the supports in Schemes B and C is approximately 41 degrees. All three bridge schemes have the same basic cross section shown at the top of Figure 6. The specified compressive strength of the concrete, f'_c, modular ratio, n, and rebar area, A_s, are shown in Figure 6. A typical cross frame is shown at the bottom of Figure 6. The cross frames are K-braces made up of structural tees (WT5x12.5).

The preliminary designs of the girders were prepared with the bridge-design program SIMON (4). SIMON is a straight-girder design program; therefore, some adjustments had to be made to the program

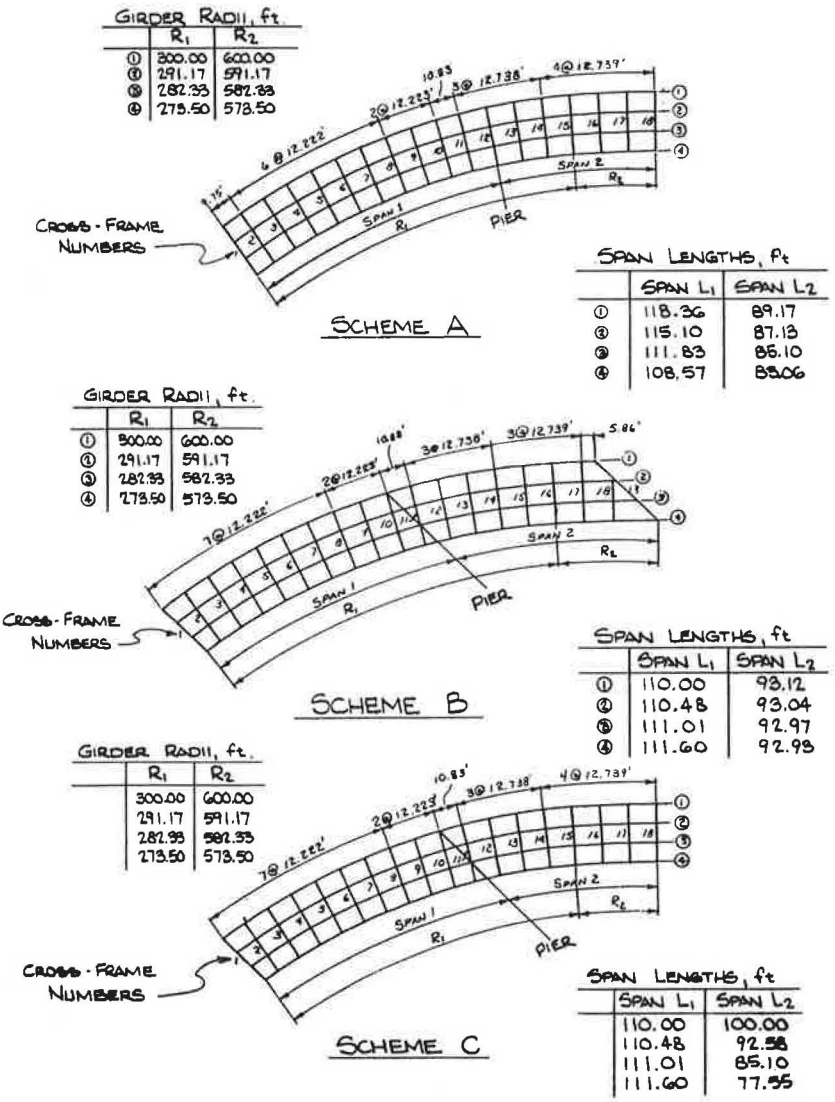

FIGURE 5 Curved-bridge schemes.

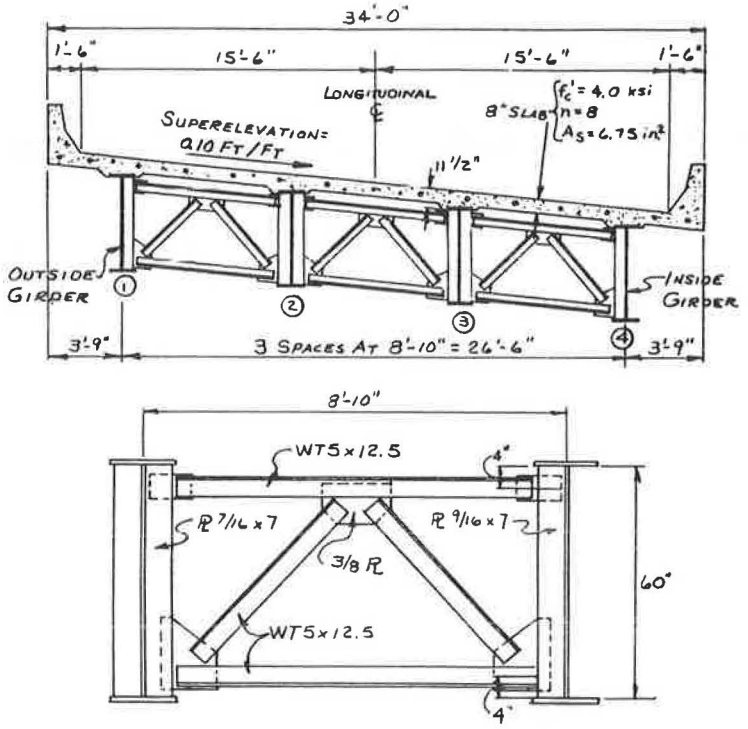

FIGURE 6 Bridge-scheme cross sections.

input to achieve an appropriate design. The girders were designed for noncomposite dead load and composite dead and live loads using 50-ksi yield-point steel and the load factor design method in the AASHTO Standard Specifications for Highway Bridges (5). All girders are nonprismatic with thicker flanges over the interior pier. All webs are 60 in. deep and transversely stiffened. The girder designs for all three schemes are similar--the only difference is minor variations in the flange thicknesses. In regions of negative bending (over the pier), the composite moment of inertia of the girder and rebars only was used in the analysis and design; the concrete was assumed to be ineffective. Computer models of each of the three curved bridge schemes were developed using the finite-element program MSC/NASTRAN (6). Noncomposite models were generated for all three schemes. Composite models, including concrete slab elements, were generated for Schemes A and C only. The bridges were supported vertically and radially at all three supports, and longitudinally at the interior support only.

To account for cross-sectional warping, a modeling technique was used whereby the two flanges and web are modeled as separate BEAM elements (7). Two groups of three straight flange and web BEAM elements along the arc length of the curve were used for each girder between each cross frame to approximate the curved girders. Because the model is three dimensional, the full-depth cross frames can also be modeled using BEAM elements. This is shown for the noncomposite Scheme A model in Figure 7.

In the composite models, QUAD4 plate elements with bending stiffness through the thickness were

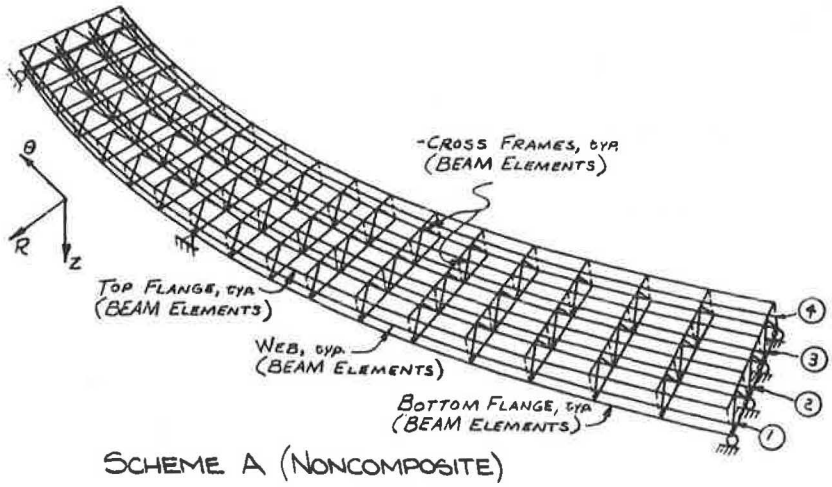

FIGURE 7 MSC/NASTRAN finite-element model.

used to model the concrete slab. The flange and web BEAM elements were offset the proper distances from the slab-element grid points, so each girder actually behaved compositely. For composite dead load, the elastic modulus of the concrete elements was reduced by two-thirds (equivalent to 3n concrete) to account for creep. A Poisson's ratio of 0.15 was assumed for the concrete.

DEAD-LOAD RESULTS

Noncomposite

The noncomposite uniform dead load for all the schemes is 1.210 k-ft on the outside and inside girders, and 1.227 k-ft on the two interior girders. These loads include an assumed weight for the girders and cross frames. The maximum and minimum noncomposite MSC/NASTRAN bending moments, for the four girders in all three noncomposite models, were compared to the corresponding V-load-analysis moments. The results for the girders of Scheme C (the most complicated scheme) are summarized in Table 1. The corresponding primary moments are also presented. The difference between the primary and V-load moments represents the effect of curvature. Note that the curvature generally increases the moments in Girders 1 and 2 and decreases the moments in Girders 3 and 4. All of the V-load noncomposite results for all three schemes were within 7.5 percent of the MSC/NASTRAN results. The skewed supports had little effect on the accuracy of the V-load results.

Composite

The uniform superimposed dead load on all the composite girders for all the schemes is 0.411 k-ft. The maximum and minimum composite MSC/NASTRAN bending moments, for the four girders in the composite Scheme A and C models, were compared to the corresponding V-load-analysis moments. The results for the girders of Scheme C are summarized in Table 2. The corresponding primary moments are also presented. All of the V-load composite dead-load results for both schemes were within 8 percent of the MSC/NASTRAN results. The composite slab had a negligible effect on the accuracy of the V-load results.

LIVE-LOAD RESULTS

For this particular study, it was not practical to develop and compare the full live-load moment envelopes in the girders calculated from influence surfaces in the curved bridge (using MSC/NASTRAN) and influence lines in the developed straight girders (using the V-load method). Therefore, the live-load bending moments at only three locations were investigated: the negative moments at the pier, and at points near the maximum moment in each span. Influ-

TABLE 1 Noncomposite Dead-Load Bending Moments (Scheme C)

Location	Primary Moment, k-ft	MSC/NASTRAN Moment, k-ft	V-Load-Analysis Moment, k-ft
		Girder 1	
Maximum Moment in Span 1	+975.1	+1393.1	+1392.6
Minimum Moment - Pier	-1947.7	-2132.9	-2144.7
Maximum Moment in Span 2	+672.6	+607.7	+617.8
		Girder 2	
Maximum Moment in Span 1	+1060.8	+1205.6	+1196.9
Minimum Moment - Pier	-1819.8	-1945.5	-1894.2
Maximum Moment in Span 2	+552.9	+533.6	+536.8
		Girder 3	
Maximum Moment in Span 1	+1120.0	+1007.2	+990.1
Minimum Moment - Pier	-1706.6	-1687.0	-1633.4
Maximum Moment in Span 2	+412.9	+415.9	+425.6
		Girder 4	
Maximum Moment in Span 1	+1159.3	+770.5	+808.5
Minimum Moment - Pier	-1571.3	-1287.9	-1378.6
Maximum Moment in Span 2	+288.2	+319.6	+302.8

TABLE 2 Composite Dead-Load Bending Moments (Scheme C)

Location	Primary Moment, k-ft	MSC/NASTRAN Moment, k-ft	V-Load-Analysis Moment, k-ft
		Girder 1	
Maximum Moment in Span 1	+369.6	+520.5	+536.8
Minimum Moment - Pier	-571.1	-641.0	-655.9
Maximum Moment in Span 2	+271.2	+247.7	+261.4
		Girder 2	
Maximum Moment in Span 1	+397.0	+459.3	+451.9
Minimum Moment - Pier	-520.1	-565.1	-549.7
Maximum Moment in Span 2	+222.5	+220.9	+219.7
		Girder 3	
Maximum Moment in Span 1	+416.0	+362.8	+362.1
Minimum Moment - Pier	-490.3	-478.7	-460.9
Maximum Moment in Span 2	+172.1	+172.6	+173.1
		Girder 4	
Maximum Moment in Span 1	+436.9	+267.0	+282.6
Minimum Moment - Pier	-459.5	-351.0	-380.0
Maximum Moment in Span 2	+127.9	+129.8	+129.6

ence lines, generated by program SIMON for each girder, were used to determine the approximate position and direction of the loads for the minimum (negative) moment at the pier and the maximum (positive) moment in each span. Because the influence surfaces for the curved bridges were not readily available, it was initially assumed that the three loading positions are the same for the curved-bridge and straight-girder models.

The composite MSC/NASTRAN models were loaded with two AASHTO HS 20 trucks at each of the three loading positions determined from SIMON. The two trucks were placed side by side within their design lanes according to the AASHTO rules. For the V-load analysis, AASHTO straight-girder live-load lateral distribution factors were used to distribute the wheel loads to the individual girders. Applying the AASHTO rules for the calculation of these distribution factors, the values for the girders in Schemes A and C are

- Exterior Girders 1 and 4: 1.423 wheels and
- Interior Girders 2 and 3: 1.606 wheels.

These factors are used to determine the original primary live-load moments in the developed straight girders.

A separate lateral distribution factor is needed to compute the V-load live-load moments. In using the AASHTO distribution factors, it is assumed that a truck (or trucks) will eventually be positioned over each individual girder to cause the maximum possible moment to occur in that girder. However, the V-loads on each girder--for the truck (or trucks) in that loading position--act concurrently; therefore, using the AASHTO distribution factors to compute the V-loads would overestimate the V-loads. Because the V-loads act concurrently, the summation of V-load distribution factors across the section should equal the number of wheels on the structure. Because the lateral placement of the wheels has little effect on the summation of primary moments across a section, a wheel-load lateral distribution factor for V-loads can be simply computed as

$$\text{Distribution Factor}_{V\text{-load}} = (2 \cdot N_L)/N_G \quad (9)$$

where N_L is the number of lanes loaded, and N_G is the number of girders in the section. There is only one V-load distribution factor for all the girders in a particular bridge.

A comparison of the approximate MSC/NASTRAN and V-load maximum and minimum live-load bending moments, for the girders of Scheme A, is given in Table 3. All moments are factored and include impact. These results are typical because in all cases the V-load-analysis live-load moments in the interior girders were anywhere from 20 to 55 percent conservative compared to the MSC/NASTRAN moments. The V-load-analysis moments in the exterior girders were, in most cases, within 15 percent of the MSC/NASTRAN values.

TABLE 3 Live-Load Bending Moments (Scheme A)

Location	Primary Moment, k-ft	MSC/NASTRAN Moment, k-ft	V-Load-Analysis Moment, k-ft
		Girder 1	
Maximum Moment in Span 1	+2681.1	+3648.0	+3562.6
Minimum Moment - Pier	-1032.9	-1525.4	-1335.3
Maximum Moment in Span 2	+2035.5	+2541.6	+2400.0
		Girder 2	
Maximum Moment in Span 1	+2973.7	+2342.2	+3267.8
Minimum Moment - Pier	-1330.6	-1155.6	-1438.3
Maximum Moment in Span 2	+2222.0	+1787.3	+2367.5
		Girder 3	
Maximum Moment in Span 1	+2906.9	+1895.2	+2627.4
Minimum Moment - Pier	-1358.6	-875.3	-1246.3
Maximum Moment in Span 2	+2137.3	+1528.2	+2076.0
		Girder 4	
Maximum Moment in Span 1	+2525.4	+1914.5	+1711.2
Minimum Moment - Pier	-1213.8	-944.9	-866.6
Maximum Moment in Span 2	+1833.0	+1680.7	+1572.6

Therefore, in a further study, the V-load live-load analyses for Schemes A and C were redone using different wheel-load lateral distribution factors to compute the primary moments in the exterior and interior girders. These revised factors were simply calculated from the equilibrium of a straight bridge cross section undergoing a rigid-body rotation. This rotation is due to the torsional moment on the bridge section caused by the eccentricity of the wheel loads (with respect to the longitudinal centerline of the bridge) as the trucks are shifted toward the outside girder. These recalculated distribution factors were

- Exterior Girders 1 and 4: 1.611 wheels and
- Interior Girders 2 and 3: 1.204 wheels.

The percentage errors between the MSC/NASTRAN- and V-load-analysis moments for the interior girders, using these factors, were all reduced from a range of 20 to 55 percent to well within 10 percent. The percentage errors for the majority of the moments in the exterior girders were slightly increased, but almost all errors were on the conservative side.

The V-load live-load moments were approximately the same in all the girders using both sets of factors because the distribution factors for the V-loads in either case must always add up to the number of wheels on the structure. The major difference was in the primary moments. Therefore, the V-load-method results for live load are only as good as the distribution factors that are used to calculate the primary moments. Using the present AASHTO distribution factors, in most cases, gave satisfactory results for the exterior girders and conservative results for the interior girders. More realistic lateral distribution factors have been derived for fatigue design (8), but more research is needed on distribution factors for strength design--particularly for bridges with full-depth cross frames.

CLOSED-FRAMED SYSTEMS

All of the analyses thus far were for open-framed systems, with no horizontal lateral bracing near, or in, the plane of the bottom flanges. Though not presently required (9), bottom lateral bracing (structural tees or angles) is sometimes included in some or all of the bays of curved I-girder bridges to share in the wind-load resistance with the slab. It has also been shown that the addition of this bracing may improve the load distribution to the individual girders in the bridge (10).

To confirm this, lateral-bracing elements were added to the MSC/NASTRAN noncomposite and composite Scheme A models in the plane of the bottom flange elements. Structural tees, WT6x32.5 with a cross-sectional area of 9.54 in.^{2}, were selected. In Table 4, the approximate maximum and minimum factored live-load moments for the Scheme A bridge, with lateral bracing in every other bay and in all

TABLE 4 Closed-Framed System Live-Load Bending Moments (Scheme A)

Location	MSC/NASTRAN Moment, No Bracing, k-ft	MSC/NASTRAN Moment, Bracing in Every Other Bay (Outside Bays), k-ft	MSC/NASTRAN Moment, Bracing in All Bays, k-ft
		Girder 1	
Maximum Moment in Span 1	+3648.0	+2504.7	+2320.6
Minimum Moment - Pier	-1525.4	-1186.3	-913.2
Maximum Moment in Span 2	+2541.6	+1768.2	+1615.6
		Girder 2	
Maximum Moment in Span 1	+2342.2	+2175.7	+1977.4
Minimum Moment - Pier	-1155.6	-1128.0	-959.3
Maximum Moment in Span 2	+1787.3	+1591.5	+1403.4
		Girder 3	
Maximum Moment in Span 1	+1895.2	+1834.1	+1622.0
Minimum Moment - Pier	-875.3	-817.2	-818.3
Maximum Moment in Span 2	+1528.2	+1401.5	+1262.4
		Girder 4	
Maximum Moment in Span 1	+1914.5	+1553.1	+1579.5
Minimum Moment - Pier	-944.9	-809.0	-746.7
Maximum Moment in Span 2	+1680.7	+1331.2	+1321.7

bays, are compared to the original moments for the bridge with no lateral bracing. In almost all cases, there was a significant decrease of the bending moments.

It is apparent from these results that the bridge behaves as a different structure when lateral bracing is added; the V-load-method assumptions are no longer valid. The composite bridge section, in particular, probably behaves more like a multicellular box-girder. Equations are available to calculate an equivalent plate thickness for common configurations of truss-type lateral bracing (11). The section could then be analyzed as a multicellular box-girder under combined bending and torsion. However, this analysis may be more complicated than a V-load analysis. Also, because the lateral bracing members are now primary load-carrying members, it is important that they be carefully designed to safely carry the loads. The many additional connection details for the bracing must also be carefully designed and fabricated. All of these factors must be weighed against the advantages that might be gained from the improved load distribution (e.g., smaller girders).

TORSIONAL STRESSES

The V-load method assumes that the internal torsional load on the bridge is resisted primarily by the shears that develop in the diaphragms or cross frames. Any remaining torque, however, must be resisted internally by the girders. An open section, such as an I-shaped girder, has two basic kinds of torsional stiffness--St. Venant and warping. Together, St. Venant and warping torsion cause additional bending and shear stresses on the girder sections that must be accounted for. The theory behind the development of these torsional stresses in open sections is well documented (12,13). For I-shaped girders, however, the warping stiffness is usually much greater than the St. Venant stiffness. Thus, in the V-load method, the St. Venant torque and corresponding shear stresses are neglected. It is assumed that all of the applied torque, which is resisted internally by the girders, is resisted in warping torsion only. This was also justified in an earlier development of the V-load method (1).

In a curved bridge, the cross frames reduce the lateral bending, and, consequently, the warping stresses in the girder flanges. Thus, the cross frames act as lateral supports for the flanges. The lateral bending is caused by the radial flange forces due to curvature. As before, a conservative assumption is that the lateral distributed force on each flange has a constant value of $M/(h \cdot R)$, where M is the total vertical bending moment in the girder at each cross frame. Because the cross frames are assumed to act as rigid supports for the flanges, the approximate lateral flange warping moment at each cross frame can be calculated from the expression for the fixed-end moment in a straight beam under a uniformly distributed load:

$$M_{fw} = (M \cdot d^2)/(12 \cdot h \cdot R) \quad (10)$$

Again, M is the total vertical bending moment (primary plus V-load) in the girder at the cross frame. The flange warping moments are equal and opposite in the top and bottom flanges.

Flange warping moments computed from Equation 10 were compared to the flange warping moments at each cross frame computed from MSC/NASTRAN flange models. Each flange of Girder 1 in Schemes A and C was isolated and analyzed as a straight flange rigidly supported at every cross frame. The flange models were laterally loaded with the appropriate distributed radial flange force for that girder, M/(h•R). The results were generally well within 10 percent of each other.

The maximum warping normal stress at the flange tip can then be computed as

$$\sigma_w = (M_{fw})/(S_f) \quad (11)$$

where S_f is the section modulus of the flange about its strong axis. This stress may be significant and should not be ignored; it is usually on the order of 5 to 10 ksi. The maximum warping normal stress is combined with the maximum longitudinal bending stress (in the flange) to determine the maximum total normal flange stress. Approximate warping shear stresses could also be similarly determined but these stresses are generally small and may be neglected.

In composite girders, the top flange and concrete slab act together to resist the top lateral warping moment. This warping moment is approximately the same magnitude as the corresponding moment in the bottom flange; however, the lateral-bending section modulus of the top flange and slab together is so large that the top warping stresses are negligible. Detailed equations are available to calculate the warping stresses in composite sections, if desired (14).

CONCLUSIONS

The V-load method is a widely used approximate method for simply analyzing horizontally curved open-framed highway bridges. The V-load method assumes that most of the internal torsional load on the bridge, due to the curvature, is resisted by self-equilibrating sets of diaphragm or cross-frame shears. The results presented in this paper have shown that the method can be extended to composite open-framed bridges with any general support configuration.

The agreement between the V-load and MSC/NASTRAN results (maximum and minimum girder bending moments) was excellent for dead load on three noncomposite and composite bridge schemes with varying combinations of radial and skewed supports. The accuracy of the V-load live-load results, however, was strongly influenced by the lateral distribution factors that were used to determine the primary moments in each of the developed straight girders due to the design truck wheel loads. The results were generally quite conservative; however, research on lateral distribution factors in the near future should greatly improve their accuracy.

Two limitations on the validity of the V-load method are noted. First, the method is only valid for loads such as normal highway loadings. For exceptional loadings, a more detailed analysis is required. Second, the present V-load method is not applicable to a closed-framed system with horizontal lateral bracing near, or in, the plane of the bottom flanges. Closed-framed systems probably should be analyzed as equivalent boxes.

The warping stresses and flange warping moments, due to lateral bending of the girder flanges, can be calculated with approximate formulas in the V-load method. For composite sections, the warping stresses in the top flanges and concrete slab are comparatively small and may be ignored. St. Venant torsional shear stresses in the girders also may be neglected.

ACKNOWLEDGMENTS

The author gratefully acknowledges the contributions of P.S. Carskaddan of the U.S. Steel Technical Center, R.L. Mion of U.S. Steel Construction Services, G. Haaijer of AISC, and W.N. Poellet and W. Till of Richardson, Gordon, and Associates, Pittsburgh, Pennsylvania.

REFERENCES

1. Richardson, Gordon, and Associates. Analysis and Design of Horizontally Curved Steel Bridge Girders. Structural Report ADUSS 88-6003-01. United States Steel Corporation, Pittsburgh, Pa., 1963.
2. Highway Structures Design Handbook. ADUSS 88-1895-01. United States Steel Corporation, Pittsburgh, Pa., 1965, Vol. 1, Chapter 1.
3. Subcommittee on Curved Girders of the Joint AASHTO-ASCE Committee on Flexural Members. Survey of Curved-Girder Bridges. Civil Engineering, Feb. 1973.
4. SIMON--A Computer Program for the Design of Steel Girders. United States Steel Corporation, Pittsburgh, Pa., n.d.
5. Standard Specifications for Highway Bridges, 12th ed. AASHTO, Washington, D.C., 1977.
6. C.W. McCormick, ed. MSC/NASTRAN User's Manual. MacNeal-Schwendler Corporation, Los Angeles, Calif., n.d.
7. G. Haaijer. Discussion of Thin-Walled Curved-Beam Finite Element by S.K. Chandhuri and S. Shore. Journal of the Engineering Mechanics Division of ASCE, Vol. 104, No. EM5, Oct. 1978, pp. 1301-1303.
8. C.G. Schilling. Lateral Distribution Factors for Fatigue Design. Journal of the Structural Division of ASCE, Vol. 108, No. ST9, Sept. 1982, pp. 2034-2044.
9. Guide Specifications for Horizontally Curved Highway Bridges. AASHTO, Washington, D.C., 1980.
10. C.P. Heins and J.O. Jin. Load Distribution of Braced Curved I-Girder Bridges. University of Maryland, College Park, April 1982.
11. C.F. Kolbrunner and K. Basler. Torsion in Structures--An Engineering Approach. Springer-Verlag, New York, 1969.
12. C.G. Salmon and J.E. Johnson. Steel Structures--Design and Behavior. Harper and Rowe, New York, 1980.
13. W. McGuire. Steel Structures. Prentice-Hall, Englewood Cliffs, N.J., 1968.
14. C.P. Heins and J.T.C. Kuo. Torsional Properties of Composite Girders. American Institute of Steel Construction Engineering Journal, Vol. 9, No. 2, April 1972.

Publication of this paper sponsored by Committee on Steel Bridges.

Prestressed Steel Beam-Concrete Slab Composite Bridge Units for County Road Use

THOMAS HENDRICK, CLIFFORD CLOTTEY, and THOMAS M. MURRAY

ABSTRACT

The results of the first three phases of a research project to study the behavior of a prestressed steel beam-concrete slab bridge unit specifically designed for county road use are presented. The units are constructed by steel fabricators in an upside-down position, trucked to the site, and turned over and set in one operation. During fabrication, heavy steel forms are hung from the beams and their weight plus the weight of the concrete provide the prestressing. The advantages of this type of construction are that it requires less structural steel, less reinforcing steel, and less concrete for the deck. In addition, because the units are prefabricated, the labor force and the construction time at the job site are reduced. Data are presented on concrete, reinforcing bar and steel beam strains, and vertical displacements for a 1-year period of observation with the unit under sustained loading. Behavior of the unit when subjected to 500,000 cycles of repeated loading is described. Data from a static 50 percent overload test are also presented. The test unit performed satisfactorily, and county road bridges are currently being constructed in Oklahoma using three or four of the units. An additional 2-year period of sustained load observation followed by static tests to failure is planned.

A research program is being conducted at the Fears Structural Engineering Laboratory, University of Oklahoma, under the sponsorship of the Oklahoma Department of Transportation, to study the strength and stiffness characteristics of a full-scale precast, prestressed steel beam composite bridge unit. Two, three, or four of the units can be used to construct county road bridges for small stream crossings. The test unit is 55 ft long and 6 ft 9.5 in. wide and consists of two W21x50 steel beams and a 7.5-in.-thick reinforced concrete slab and weighs 39,000 lb. The test unit was designed for AASHTO HS 20 loading with a 100,000 cycle fatigue rating.

The objective of the study is to experimentally investigate the behavior of the unit under various types of loading: sustained load, repeated load, and static loading to failure. The research project will take 3.5 years; it began in April 1982 with completion scheduled for December 1985. The project consists of six phases: 1 year of observation under sustained load; 3 months of repeated loading (500,000 cycles); operating rating loading; 2.5 years of observation under sustained dead load; static flexural test to failure; and transverse slab strength tests. As of this date (December 1983), the first three phases of the research project have been completed. Results are summarized herein.

BRIDGE UNIT SPECIMEN

The unit was fabricated by Robberson Steel Company, Oklahoma City, Oklahoma, using design drawings provided by Grossman and Keith Engineering Company, Norman, Oklahoma. The concrete was cast with the beams in an upside-down position using a heavy steel form hung from the beams as shown in Figure 1. When the concrete had been poured and finished, an additional steel weight was placed on the beams. After the concrete had cured, the weight and the forms were removed. The concrete was poured on April 1, 1982, and the forms were removed on April 8, 1982. The unit was moved to the Fears Structural Engineering Laboratory on April 8, 1982, in an upside-down position using a "pole" truck. The unit was turned over on delivery and was placed on small support beams on an existing concrete slab outside the laboratory. Elastomeric bearing pads were placed between the support beams and the unit beams. The bridge unit and the control cylinders were subjected to prevailing weather conditions. Three weeks after the unit was poured, 4 x 8 x 16-in. concrete blocks weighing 33 ± 0.1 lb each were placed on the unit to simulate dead load of 36 psf from an asphalt overlay.

Concrete

An air-entrained concrete with a design strength of

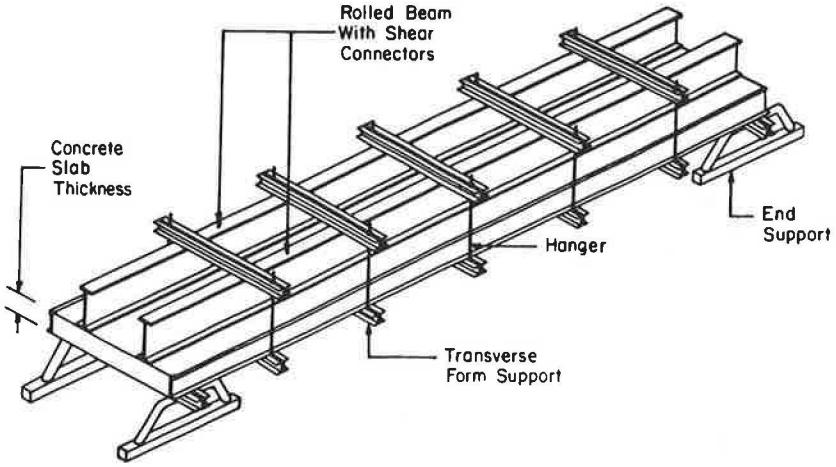

FIGURE 1 Method of fabrication of bridge unit.

5,000 psi and a design slump of 1 to 3 in. was used for the unit. The concrete was obtained from a local ready-mix plant and was manufactured with Type III portland cement and normal weight aggregate having a maximum size of 1 in.

During the pouring of the concrete, a total of 50 control cylinders, 6 in. diameter by 12 in. high, were cast from two mixing trucks. Slump tests were performed before the cylinders were cast. Water was added at that time and additional mixing was done until the appropriate slump was achieved. Then cylinders were cast for approximately each half of each truck designated as Series 1A and 1B for the first truck and Series 2A and 2B for the second truck. Because of high slump obtained for the second half of the second truck, an additional ten cylinders were cast for that half (Series 2C). The amount of entrapped and entrained air was determined using stereo-optical microscope scanning. The slump, air content, age, and strengths of concrete are given in Table 1.

Steel

The two steel beams were standard W21x50 sections of A588 steel. Deformed steel bars of Grade 60 steel were used as reinforcement for the concrete slab deck. Stress-strain curves for the reinforcing bars were obtained from tension tests of coupons supplied by the fabricator.

Fabrication

Shear connectors were welded to the W21x50 beams before the beams were placed in the forms. The shear connectors were standard steel studs. Pairs of studs were welded to the top flange of each beam with variable spacing. The spacing varied from 12 in. at each end to 30 in. at the midspan. In addition, seven C7x9.8 by 6-in. long channels were welded to the top flange of each beam at 9-ft intervals. These channels were used as spacers between the top flange of each beam and the steel form to ensure uniform thickness of the concrete slab deck.

The beam sections were connected together at the ends and third points with a welded diaphragm consisting of 3 x 3 x 0.25 angles. Center-to-center spacing of the beams was 3 ft 9.5 in.

TABLE 1 Concrete Properties—Bridge Unit

Properties	Age (Days)	First Truck		Second Truck		
		First Half (1A)	Second Half (1B)	First Half (2A)	Second Half (2B)	Second Half (2C)
Slump (in)	-	1½	2¼	1 3/4	4¼	4¼
Air Content %	-	5.4	5.4	5.8	5.8	5.8
Entrained Air	-	4.5	4.5	5.0	5.0	5.0
Entrapped Air	-	0.9	0.9	0.8	0.8	0.8
Compressive Strength (Psi)	1	2970	2370	3060	2430	2150
	4	4320	4240	4240	3890	3860
	8	4750	4540	4890	4100	4100
	21	5450	5215	5720	4840	5040
	29	5730	4950	5700	5290	4830

The concrete slab was reinforced with No. 4 bars both longitudinally and transversely. The longitudinal bars were spaced at 9 in. at the top and at 18 in. at the bottom of the slab. The closer spacing at the top was intended primarily to minimize creep strains in the concrete slab. Both top and bottom transverse reinforcement was placed at variable intervals symmetrically about the midspan. Starting from the midspan and going toward each end, the spacings were 5.5 in., 11 in., and 16.5 in. for each one-sixth of the span length. The intention of this variable spacing was to study at a later date the influence of transverse reinforcement on the transverse strength of the concrete slab.

The top and bottom slab reinforcement mats were preassembled and tied using standard practices in a specially constructed layout template. All of the longitudinal reinforcing bars were single length except for those that were strain gauged. The longitudinal bars with strain gauges were lap-spliced at the third points with a splice length of 2 ft 6 in. The reinforcing mats and the beam assembly were then hoisted into a well-oiled steel form in the upside-down position. The formwork, which was simply supported at the ends, was then hung from the steel beams at 9 ft 0 in. intervals with hangers as shown in Figure 1. The concrete was then poured and additional weight (approximately 7,000 lb) was placed on the beams at midspan. Shims were used at midspan to limit vertical deflection to 3.5 in.

The concrete slab and the control cylinders were moist-cured in the formwork for 7 days. The exposed surface of the concrete was covered with wet burlap and polyethylene sheets during the 7-day curing period. On the eighth day, the forms were stripped and the specimen was transferred in the upside-down position from the fabrication shop to the Fears Structural Engineering Laboratory where it was turned over and set on supports as previously described.

Instrumentation

With the exception of the shear connectors, all components of the bridge unit, reinforcing steel, steel beams, and concrete slab were fully instrumented. Ten longitudinal reinforcing bars, five top and five bottom, were strain gauged longitudinally at the midspan with electrical resistance strain gauges having gauge lengths of 0.25 in. Similar gauges were mounted on six transverse reinforcing bars, three top and three bottom. The instrumented transverse bars were located in the different spacing regions discussed previously.

Before placing the steel beams in the concrete form, eight 0.5-in. gauge length strain gauges were installed on the flanges of each beam near midspan. The gauged cross section was 8 in. from midspan to avoid effects induced by a spacer channel located at midspan.

After the bridge unit was removed from the forms but before the unit was turned over, two 10-in. gauge electrical extensometers were mounted on the top and the bottom surface of the concrete slab at midspan and along the longitudinal axis of the unit.

After the bridge unit was turned over, six concrete strain gauges were mounted longitudinally at midspan and on the top surface of the concrete slab. Initially, four strain gauges with 2-in. gauge length were mounted. These were later replaced with two strain gauges with 4-in. gauge length.

When the bridge unit had been set in place at the laboratory, two direct-current differential transformer deflection transducers were positioned to measure the midspan deflections of the slab near the top flange of each beam. To determine the influence of temperature, a thermometer bulb was embedded in the concrete slab.

To accumulate creep data, two switch and balance units and two strain indicator units were permanently wired to the strain gauges to make strain measurements. A DC voltage supply and standard voltmeter were used to monitor the deflection transducers. The entire set of measuring instruments was stored in a refrigerator (set at 70°F) in a temporary building adjacent to the test unit.

SUSTAINED LOADING TEST

Creep Measurements

Before the unit was turned over, initial readings were taken from the two extensometers, the eight strain gauges on the beams, and the ten strain gauges on the longitudinal reinforcing bars. After the bridge unit was turned over, readings from the extensometers and the strain gauges were again taken to determine the strains due to the turning operation. Two weeks after the specimen was turned over, final instrumentation of the specimen was completed. Additional dead load was applied when the specimen was 21 days old.

Daily readings were taken for the first 60 days of the sustained loading tests. Thereafter, readings were taken weekly. Strain data from the ten longitudinal reinforcing bar strain gauges, eight beam strain gauges, two concrete strain gauges, and two extensometers were recorded. In addition, output from the deflection transducers and temperatures were recorded at the same time. Readings were taken between noon and 4 p.m. and weather conditions were recorded each time data were taken.

Test Results

The creep data taken for the first year are presented graphically in Figures 2-6. Stress data were obtained from the strain data using Hooke's law (assuming perfectly elastic material) and an assumed modulus of elasticity of 29 million psi for steel.

The average midspan deflection of the bridge unit and temperature changes are shown in Figure 2. Variations in the concrete strain at midspan along the longitudinal axis of the bridge unit are shown in Figure 3. Stress variations in both the top and bottom reinforcements along the longitudinal axis of the bridge unit are shown in Figure 4. Figure 5

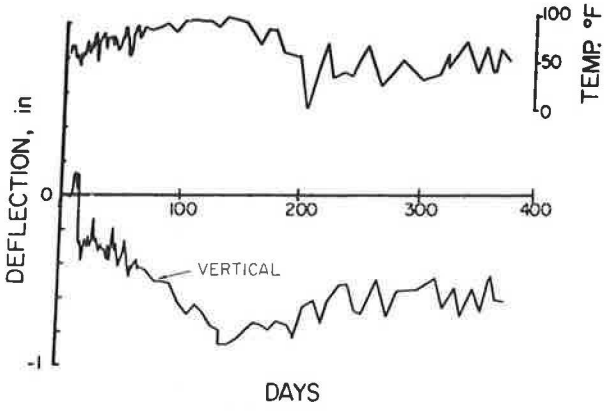

FIGURE 2 Change in deflection versus time.

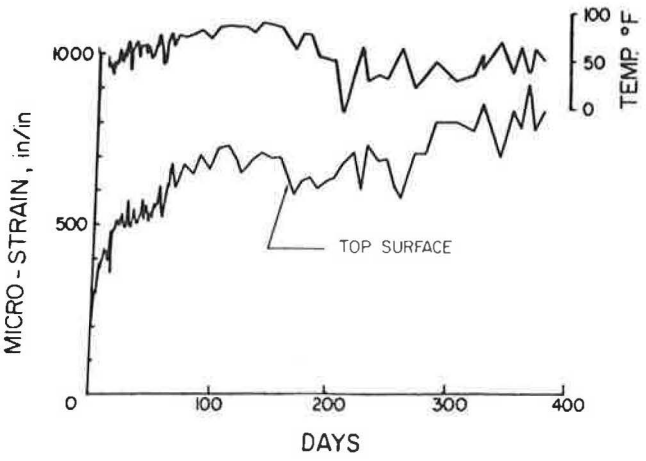

FIGURE 3 Change in strain of concrete surface versus time.

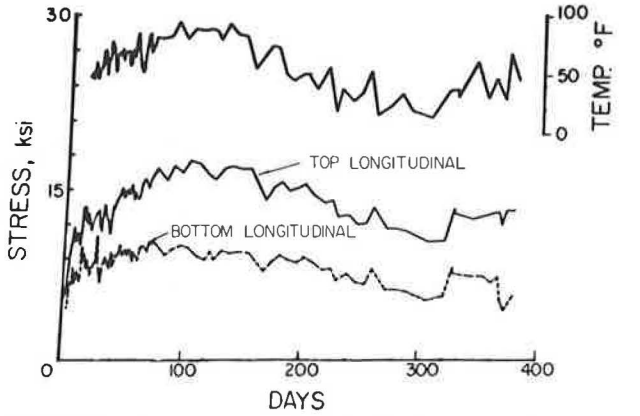

FIGURE 4 Change in stress of reinforcing bars versus time.

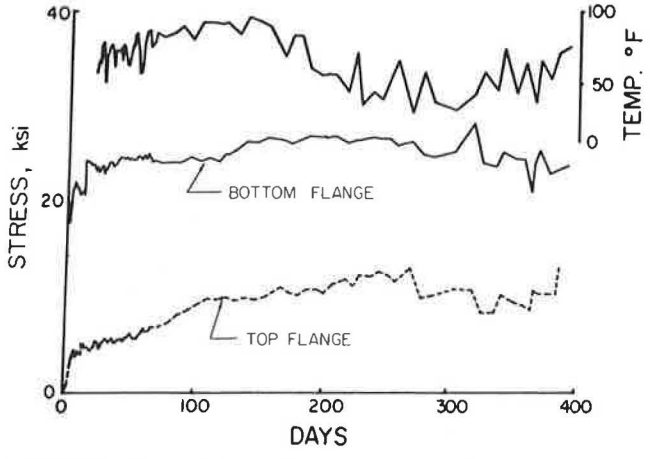

FIGURE 5 Change in beam flange stress versus time.

shows the variations in stresses on the top and bottom flanges of one beam. Changes in the neutral axis location in the steel beam versus time are shown in Figure 6.

Discussion of Results

An examination of Figures 2-5 shows that all the strain values, and consequently all the stress values, along with vertical deflections are sensitive to changes in temperature. Changes in strain on the girder and changes in strain on the rebars appear to be least affected by temperature changes; vertical deflection and changes in strain on the concrete surface are the most sensitive. Thus, the variation in temperature must be considered in any interpretation of results.

Figure 2 shows the variation in vertical downward deflection at midspan. It is evident that variations in temperature caused variations in the vertical downward deflection. Figure 2 also shows that a growth in camber occurred in the bridge unit until the additional sustained dead load was placed on the bridge (approximately the 21st day). The vertical downward deflection then increased substantially as the temperature increased. The maximum change in vertical downward deflection of 0.87 in. was reached near the 150th day (first week of September 1982). Thereafter, the vertical downward deflection decreased (increased upward) as the temperature decreased.

A study of Figure 3 shows that the change in strain at the concrete surface closely followed the change in temperature. As the air temperature increased, the change in strain increased and as the air temperature decreased, the change in strain also decreased. Increases in strain were found to be most rapid during the first few days of observation. The change in concrete strain steadily increased during the warm months (May-August 1982) and fluctuated during the late fall and winter months (December 1982 to February 1983) when the temperature also fluctuated significantly. As Figure 3 indicates, concrete strain values had not yet asymptotically approached a maximum and changes were still occurring at the end of the observation period.

Figure 4 shows the behavior of the strain in the top and the bottom longitudinal reinforcing bars at the centerline of the bridge unit. A comparison of Figures 3 and 4 shows that the change in strain of the concrete surface is similar to the change in strain of the reinforcing steel. The strain (hence the stress) increased and decreased as the temperature increased and decreased. As was the case with the concrete surface strains, the greatest increases in reinforcing steel strains occurred during the first few days of observation. However, the strains on the reinforcing bars did not increase as rapidly as the strains at the concrete surface, nor did they change as rapidly as the temperature increased.

Figure 5 shows the stresses on the bottom and top flanges of one beam. Stresses were calculated from strain data assuming a modulus of elasticity of 29 million psi. A comparison of Figures 3 and 5 shows that temperature has less effect on the change in stress of the beams than it does on the concrete surface strains. A sharp increase in stress in the bottom flange occurred when the bridge unit was turned over and when the additional dead load was applied. Increases also occurred in the top flange but to a lesser degree. After the application of the dead load, the stresses in the top and bottom flanges gradually increased until about the 265th day (January 1, 1983). Subsequently, the stresses in both the top and bottom flanges decreased somewhat. Initially, the stresses in the top flange increased at a slightly faster rate than those of the bottom flange, indicating that the location of the neutral axis was moving away from the top flange toward the bottom flange.

Figure 6 shows the neutral axis location from the top of the beam versus time. The location of the neutral axis was determined using the beam flange strain readings and assuming a linear strain distri-

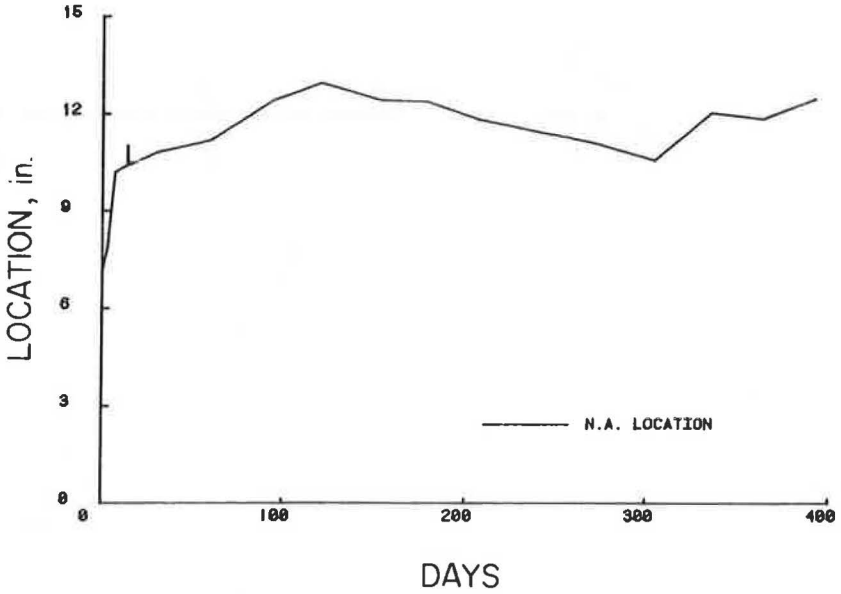

FIGURE 6 Neutral axis location from top of concrete versus time.

bution within the steel section. The location is plotted in Figure 6, with respect to the top concrete surface. Initially the neutral axis moved rapidly toward the bottom flange. The rate of increase subsequently decreased and at the end of the reporting period the neutral axis location appeared to be stationary. The location remained within the steel section throughout the observation period.

Figure 7 shows a comparison of the measured midspan deflection of the bridge unit with the deflections predicted using a method proposed by Branson (1). The predicted total deflection due to creep and shrinkage plus temperature is shown as well as the individual computed deflections due to differential shrinkage and creep and those due to temperature effects. Only the total measured deflection is shown because no distinction could be made between deflections caused by creep and shrinkage and deflections caused by temperature effects.

It can be seen from Figure 7 that the measured and the predicted curves have basically the same shape and are in good agreement considering the complexity of predicting creep, shrinkage, and temperature effects. The measured effects are less than the computed effects even though prestressing effects were not considered in the calculations.

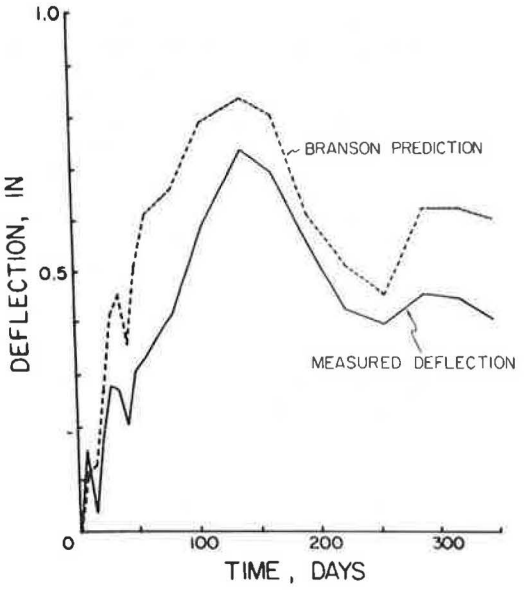

FIGURE 7 Comparison of measured midspan deflection due to shrinkage, creep, and temperature effects with that predicted by Branson method.

REPEATED LOADING TEST

Test Description

At the end of 1 year of sustained loading observation the bridge unit was moved into the laboratory to be subjected to 500,000 cycles of repeated loading to simulate traffic load. The unit was supported on two W10x49 steel beams. The same elastomeric bearing pads used earlier were placed between the support beams and the unit beams.

To simulate traffic load a two-point loading system was used with the load points 14 ft apart and equidistant from the midspan. Spreader beams were used to distribute the loads transversely to the unit at four load points that were directly above the steel beams.

Additional Instrumentation

To determine possible deterioration of composite action during the repeated loading, additional instrumentation was installed. Three displacement transducers were mounted on the soffit of the concrete slab next to the top flanges of one steel beam. The plunger of each transducer rested against an angle spot welded to the top flange of the steel beam. These transducers were placed at sixth points starting from one end and were used to measure differential displacement (slip) between the concrete slab and the steel beam.

In addition to these displacement transducers, piano wires were anchored to the soffit of the concrete slab on the exterior side of the same beam at

48-in. intervals. These piano wires crossed the longitudinal seam between the top flange of the beam and the soffit of the concrete slab. Lines were then marked across the soffit of the concrete slab and the top flange to coincide with the piano wire. Through this means, any residual slip that occurred during the dynamic loading could be detected and measured with a hand-held measuring microscope.

Procedure

The repeated loading was applied with a 55,000-lb closed-loop hydraulic testing system at a frequency of 0.5 Hz for 500,000 cycles. The repeated loading varied between 7,000 and 62,000 lb (including the weight of the loading and the spreader beams) corresponding to a minimum midspan moment of 70,400 ft-lb and a maximum midspan moment of 622,300 ft-lb. The repeated loading was applied 8 hr per day.

The first cycle of loading was applied statically at 5,000-lb intervals. After each load increment, strain readings on the longitudinal reinforcing steel, the steel beams, and the surface of the concrete were taken. In addition, readings of displacement transducers were taken to determine the vertical downward displacement as well as the slip between the steel beam and the concrete. The repeated loading was interrupted after the 1st cycle and after every 50,000th cycle thereafter to determine any deterioration in stiffness of the bridge unit that may have occurred during the repeated loading. In addition, the piano wires and diaphragm welds were visually inspected for any sign of distress at 50,000-cycle intervals.

Results and Discussion

Selected results of the repeated load tests are shown in Figures 8 and 9. Figure 8 shows the change in midspan deflection as measured at each 50,000th static cycle versus number of cycles. Figure 9 shows a change in stress in the top reinforcing steel and bottom beam flange at maximum static load versus number of cycles. From these plots, a very small amount of deterioration is detected between the 450,000th and 500,000th cycles.

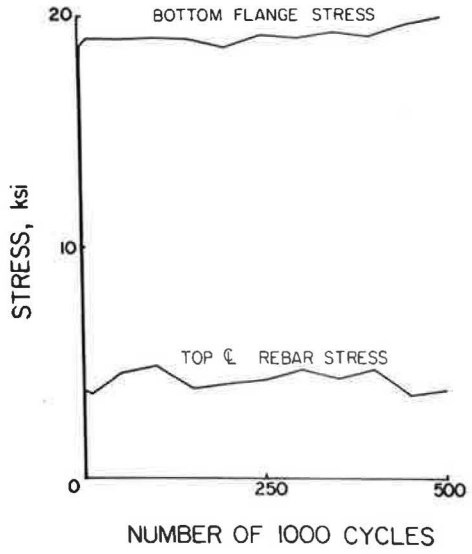

FIGURE 9 Flange and rebar stresses versus number of cycles.

OPERATING RATING LOADING TEST

At completion of the repeated loading test the unit was subjected to loading equivalent to AASHTO HS 30 rating. This loading is 50 percent greater than the design loading (HS 20) and the magnitude was determined based on a tension flange stress of 0.75 of the yield stress of the material (e.g., 37.5 ksi). The same test setup used for the repeated loading test was used. Figure 10 shows the resulting measured vertical load versus centerline vertical deflection relationship. The theoretical deflection based on a modular ratio value, n, of 7.5 is also shown. It is noted that the experimental load-deflection curve is linear and there was no permanent set.

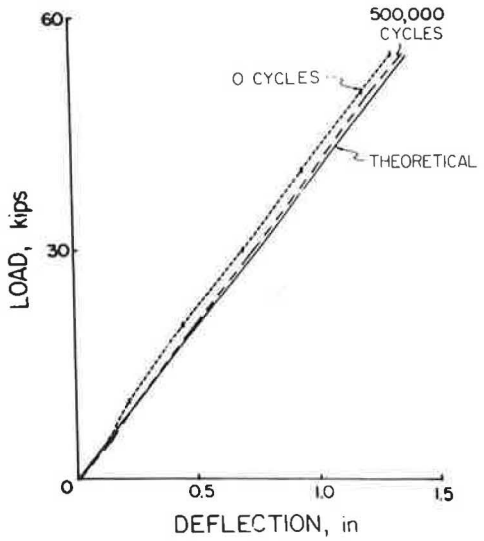

FIGURE 8 Load versus vertical deflection, repeated loading test.

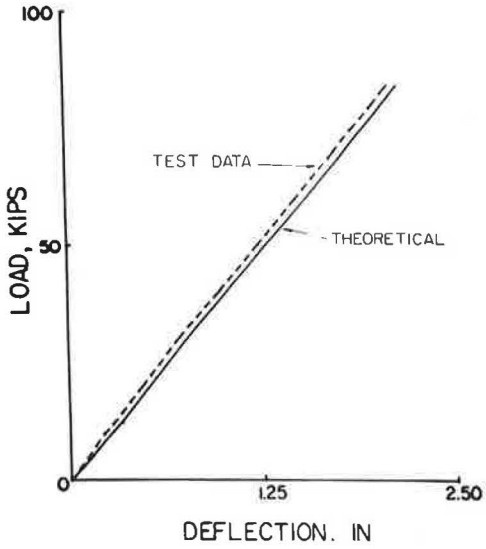

FIGURE 10 Load versus deflection, operating rating loading test.

CONCLUSIONS

Sustained Loading

The strain values in the concrete slab, the reinforcing bars, and the steel beam as well as the downward deflection of the unit were influenced by changes in temperature. The strain values in the concrete slab did not asymptotically approach a maximum. On the other hand, strains (hence stress) in the steel beam and the reinforcing bars appeared to have leveled off to constant values. The neutral axis location also appeared to be stationary and the vertical deflection appeared to have stabilized. As expected, the major portion of the creep deformation occurred during the first 90 days of testing. At the end of 1 year of sustained loading, it appears that although creep deformation continues, the rate of increase of creep is minimal.

Repeated Loading

The results show that the load-displacement curve changed little between the first and last cycles of testing. Insignificant slip was recorded between the concrete slab and steel beams during the static cycles. It is concluded that the strength and stiffness characteristics of the bridge unit are not detrimentally affected by repeated loading for which the unit was designed.

Operating Loading

Results of the operating loading test show that the test unit is able to sustain this loading without permanent set. The behavior of the unit was elastic during the test.

The unit has been placed outside for 2 additional years of sustained loading observation. At the end of that period, the unit will be loaded to flexural failure and the slab will be studied for transverse bending strength.

ACKNOWLEDGMENTS

This paper was developed from a research project sponsored by the Oklahoma Department of Transportation. The authors wish to thank Tim Borg, Jim Schmidt, and Dwight Hixon of the ODOT Research and Development Division and Veldo Goins of the ODOT Bridge Division for their helpful suggestions and assistance.

REFERENCE

1. D.E. Branson. Deformation of Concrete Structures. McGraw Hill, New York, 1977.

Publication of this paper sponsored by Committee on Steel Bridges.

Temperature Problem in a Prestressed Box-Girder Bridge

P. C. HOFFMAN, R. M. McCLURE, and H. H. WEST

ABSTRACT

The temperature effects on an experimental, prestressed concrete, segmental, box-girder bridge were evaluated. Field measurements, including vertical deflections and thermocouple readings for temperature, were collected over a 1-year period under various weather conditions. Critical ambient temperature conditions were gleaned from field observations. With the field observations (surface temperatures) as input, three-, two-, and one-dimensional heat-flow analyses were conducted. The three-dimensional heat-flow analysis was a statistical comparison of temperature readings at various longitudinal locations in the experimental bridge. The two-dimensional analysis involved the collection of hourly temperature readings from 24 thermocouples at the midspan of the test bridge for 18 diurnal cycles within a 1-year period. In addition an alternating-direction implicit finite difference analysis was performed, and the results compared well with the field observations. Finally, a one-dimensional approach was formulated with the application of an initial-value method. This was found to be in agreement with the alternating-direction implicit finite difference model and the collected field data.

In the past, the thermal environment was ignored in the design process except for accounting for the longitudinal movement that could occur and the influence such movement could have on joint integrity. However, relatively recent incidents of bridge distress, including the Newmarket Viaduct in New Zealand (1), the fourth Danube Bridge in Vienna, and the development of a crack 56 ft (17 m) long and 0.20-0.24 in. (5-6 mm) wide in the web of the Jagst Bridge in Untergreisheim (2) have prodded the profession to address the complete structural response to the thermal environment.

A field study was conducted to determine the complexity and magnitude of the temperature problem

in a segmental box girder (3). Then an analytical study was performed to evaluate the severity of the temperature problem with regard to design (4). The significant findings are summarized here.

LOCATION, CONFIGURATION, AND INSTRUMENTATION OF TEST BRIDGE

Field observations were recorded for a segmental, prestressed, box-girder bridge located at the Pennsylvania Transportation Research Facilities, which are adjacent to The Pennsylvania State University's main campus (Figure 1). The test bridge was composed of two curved and superelevated, prestressed box girders, each composed of 17 segments. The complete bridge layout, segment and joint numbers, and cross-sectional dimensions are shown in Figure 2.

FIGURE 1 The Pennsylvania Transportation Research Facilities.

The topography of the site provided an environment that was more severe thermally than the environment to which many bridges are subjected. The terrain at the research facilities consists of gently rolling hills and is completely void of large obstacles. Such topography allows maximum solar radiation to be incident on the bridge surfaces, and such openness maximizes any wind-induced convection. In addition, because the bridge configuration involved a large superelevation and a north-south alignment, the western web exterior surface was subjected to a relatively extreme level of radiation. Normally such radiation on web surfaces would not occur because of the shading provided by the cantilevered flanges.

The temperature measurements were recorded on an Esterline Angus model E1124E multipoint recorder. The field observations of temperature variation proceeded in two stages. The initial portion of the thermal study was concerned with the possibility of a longitudinal temperature variation. This study compared 10 thermocouple (copper versus constantan)

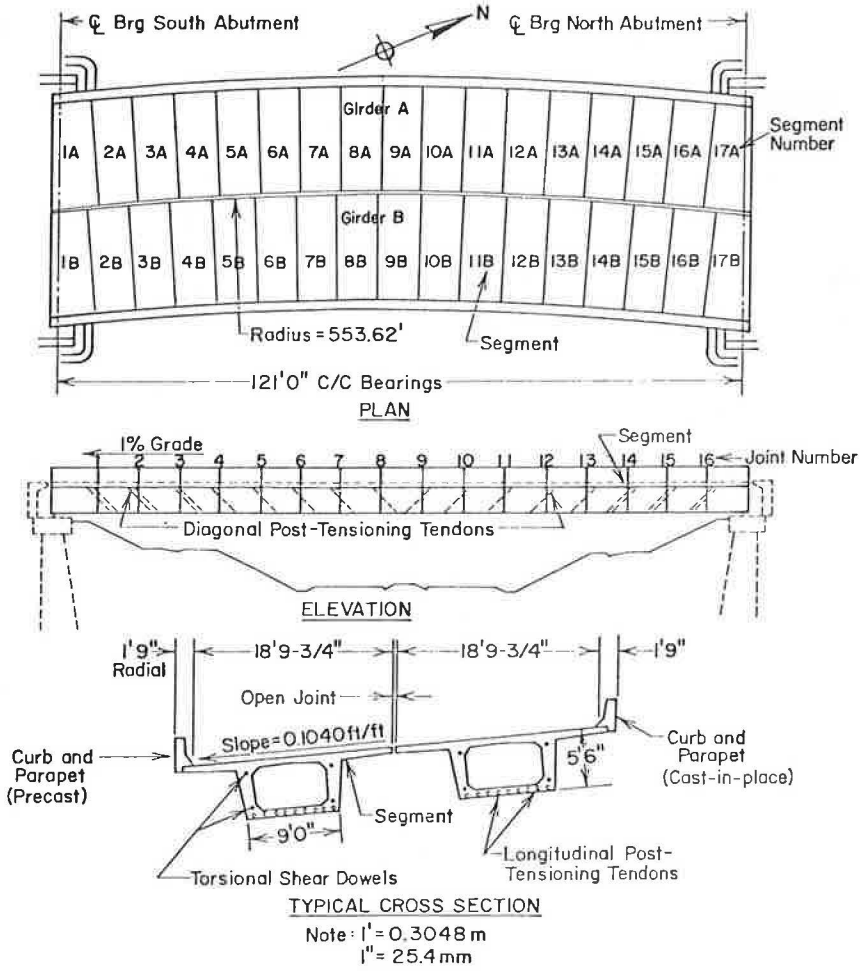

FIGURE 2 Layout and configuration of test bridge.

readings at hourly intervals for three different diurnal cycles between Segments 2A and 5A, and Segments 2A and 9A (Figure 3). When the longitudinal temperature study was concluded, all 24 thermocouples were located at Segment 9A for the transverse temperature study (Figure 4).

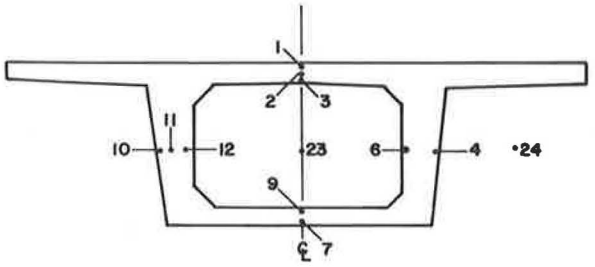

FIGURE 3 Thermocouple locations—longitudinal study.

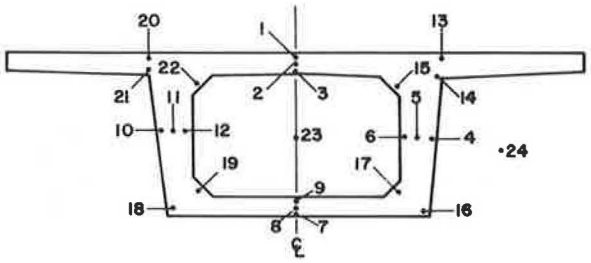

FIGURE 4 Thermocouple locations—transverse study.

The vertical movement of the structure was measured by dial gauges located at both ends and at the midspan of Girder A (Figure 5). The dials had a least count of 0.0001 in. (0.0254 mm). The dials were initially set at the beginning of the readings for the day and left untouched until the termination of the readings at the end of the day. The result of these vertical readings was a set of relative movements from the initial dial readings. Subsequently, the temperature distributions (24 thermocouple readings) were scanned for the set of readings that came closest to a uniform temperature distribution. Then the vertical dial gauge readings were rereferenced to the time of the approximate uniform temperature distribution. The result was the observation of vertical deflections with respect to the equilibrium position under dead load and the prestressing force.

In addition to the data collection at the test site, environmental information was obtained from two other sources. The first source was the Meteorology Observatory at The Pennsylvania State University, which is located approximately 5 miles southeast of the bridge site. The monthly weather summary obtained from the observatory gave the recorded high and low temperatures, the average wind velocity, the sky conditions, and the solar radiation for each day of the month. The second source of meteorological information was the University Park Airport, which is situated approximately 1 mile south of the bridge.

FIELD OBSERVATIONS

The thermal study was initially concerned with the possibility that a significant temperature variation existed in the longitudinal direction of the bridge. To evaluate such a possible variation, temperature readings were taken at Segment 2A and Segment 5A on June 30, 1978, and at Segment 2A and Segment 9A on July 11, 1978, and August 22, 1978, to compare observations for similar thermocouple locations (Figure 3). The ordered pairs of readings were then analyzed both graphically and statistically. From the longitudinal study it was concluded that the heat-flow problem from a practical viewpoint was not three dimensional. Therefore, the complexity of the general heat-flow problem required a two-dimensional study.

In the absence of a longitudinal temperature variation, the vertical deflection measurements can be converted to curvature. Because each transverse section was found to be subjected to the same temperature distribution at any point in time, each transverse section must physically respond in the same manner. In other words, for identical temperature distributions, the induced curvatures must be identical. Therefore, the curvature (M/EI diagram) must be constant. This fact, in turn, means that if the midspan deflection is known, the curvature can be readily determined by appropriate application of the moment area theorems. First, the division of the midspan deflection by a quarter of the bridge span is the angle change between the midspan and the endpoints. Second, the division of the angle change by half of the bridge span equals the curvature at each section. Hence, the vertical deflection measurements in conjunction with the internal thermo-

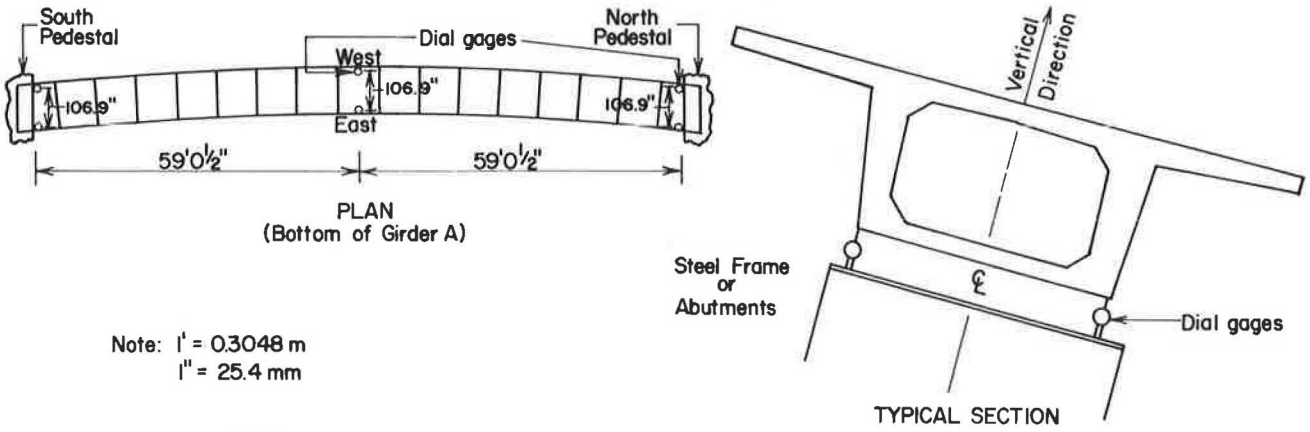

FIGURE 5 Locations of dial gauges.

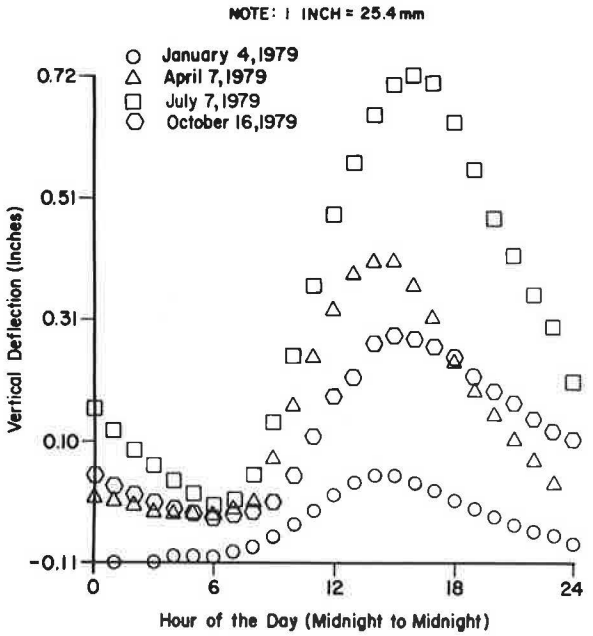

FIGURE 6 Vertical deflections using uniform temperature distribution as reference.

couple readings provided excellent supporting data for the analytic studies.

A graphic display of the seasonal observations of deflections immediately indicated that the extremes occur in winter and summer (Figure 6). The deflections when multiplied by $8/L^2$ (L = span length) are the observed curvatures. The magnitude of the deflections was found to exceed substantially that of the deflections due to live loading (5). Consequently, an effort was undertaken to identify and quantify the inputs that caused the vertical deflections.

The first area of investigation was the effects of ambient air temperature and solar radiation. These thermal inputs could be reasonably measured. With data from the Meteorological Observatory and field readings, comparisons of thermocouple readings, solar radiation, vertical deflections, and ambient air temperature were analyzed for each set of diurnal observations (a total of 18 diurnal cycles). For illustrative purposes, the normalized values of Thermocouple 1, ambient air temperature (Thermocouple 24), solar radiation, and vertical deflection versus time for July 7, 1979, are shown in Figure 7. This figure indicates a relatively large temperature variation for Thermocouple 1 in comparison with the ambient air temperature. The peak values for Thermocouple 1 and for vertical deflection occurred during the same hour, which was 4 hours after the maximum hourly solar radiation. A complete statistical analysis focused on ambient air temperature and solar radiation.

The investigation concluded that exterior surfaces not subjected to direct solar radiation could reasonably be expected to maintain a surface temperature equivalent to the ambient air temperature. For surfaces exposed to direct solar radiation, the temperature was modeled as the sum of the ambient air temperature, a coefficient times the cumulative solar radiation for the previous 4 hours, and a coefficient times the cumulative solar radiation. The coefficient of determination (R^2) indicated a high degree of interrelationship. However, because the data base was limited, a definitive statement about the values of each of the coefficients could not be formulated. The statistical analysis did verify the fact that ambient air temperature and solar radiation were the two major inputs to the thermal problem. In other words, heat convection and reradiation were present but were not observed to cause any significant problems.

TWO-DIMENSIONAL ANALYTICAL STUDY

The findings from the field observations indicated that the temperature problem was, in its most complex form, a two-dimensional problem. From a practical viewpoint, temperature-induced bridge movements were defined as the critical design concerns. To evaluate the magnitudes of deflection in both the horizontal and vertical directions, a two-part analytical scheme was developed. The first, numerical

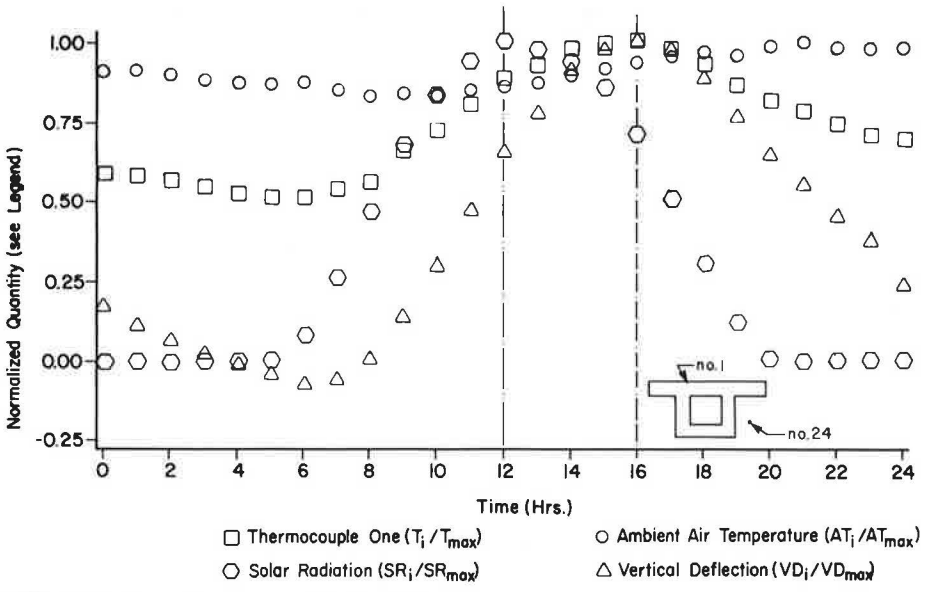

FIGURE 7 Normalized curves, July 7, 1979.

part was a two-dimensional analysis of the transient heat-flow process to determine temperature distributions. The second part used the temperature distributions as input for the computations of curvatures about the x and y axes.

The determination of the temperature distribution of the transient heat-flow problem for an isotropic material required a numerical solution to the parabolic differential equation

$$\partial^2 T/\partial x^2 + \partial^2 T/\partial y^2 = 1/\alpha\, \partial T/\partial t \quad (1)$$

where

T = temperature at point (x,y),
x,y = coordinate axes,
t = time, and
α = thermal diffusivity.

The alternating-direction implicit finite difference method was used as the numerical technique. The observed surface temperatures (field study) were used as the boundary conditions, and the observed internal temperature readings were used to validate the numerical technique.

The computation of curvatures consisted of a double summation (6) as follows:

$$\phi_y = \alpha/I_x \sum_{i=1}^{n} \sum_{j=1}^{m} t(x_i y_j) \cdot y_j \cdot \Delta x \Delta y \quad (2)$$

$$\phi_x = \alpha/I_y \sum_{i=1}^{n} \sum_{j=1}^{m} t(x_i y_j) \cdot x_i \cdot \Delta x \Delta y \quad (3)$$

where

ϕ_y = curvature due to bending about x axis,
ϕ_x = curvature due to bending about y axis,
α = coefficient of thermal expansion,
I_x = second moment of area about the x axis,
I_y = second moment of area about the y axis, and
t(x,y) = temperature variation as a function of x and y.

Such formulation of the temperature effect is valid because the temperature does not vary longitudinally. Therefore, the curvature would be invariant, which leads to the conclusion that bending deformations must also be constant. With constant curvatures corresponding to bending about each of the two principal axes, twisting is nonexistent, and the thermal response can be viewed as the superposition of these two curvatures.

Several observed surface temperature cycles were applied to the numerical model, and the resulting curvatures were computed (Figure 8). The conclusion was that the bending action about the major axis for box sections with overhanging flanges was very small. The small rise in the major-axis curvature plot (from 20 to 23) was probably due to the sudden jump in the exterior surface temperature of the western web, resulting from the setting sun (Figure 9). However, the interior temperatures showed little change with the sudden rise in surface temperature. Therefore, it was concluded that the existence of major-axis bending was negligible. Consequently, a one-dimensional analysis was feasible for the determination of significant bridge movement.

ONE-DIMENSIONAL ANALYTICAL STUDY

The one-dimensional heat-flow analysis emphasized evaluating structural movement under the thermal environment. In addition, the residual stresses (the equilibrating stresses that remain after the development of curvature and expansion) due to the nonlinear temperature distributions were computed. The analysis consisted of applying the initial-value method to determine the temperature variation with depth (4). Then a single summation simplification of Equation 3 was used to find curvatures.

The initial-value method is a numerical method that discretizes the one-dimensional heat conduction equation

$$\partial^2 T/\partial y^2 = 1/\alpha\, \partial T/\partial/t \quad (4)$$

and is applied to a nodal pattern (Figure 10). In the field study, the surface temperatures, which were taken as the known boundary conditions for Equation 4, were measured on the hour. Also, the rate of change of temperature at the top surface (Node 1) was linearly approximated as

$$(\partial T/\partial t)_1 \approx (T_1^{k+1} - T_1^k)/60 \quad (5)$$

where T_1^k is the observed surface temperature at Node 1 at the kth hour.

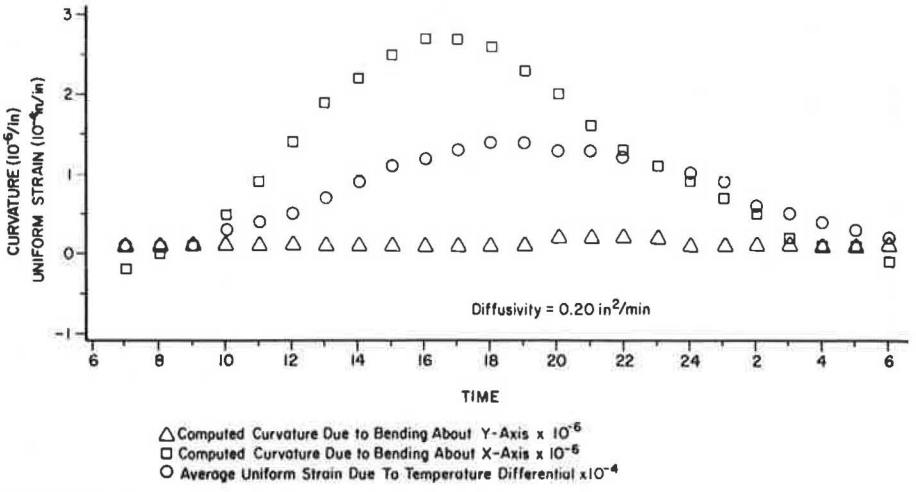

FIGURE 8 Computed numerical results for July 7, 1979.

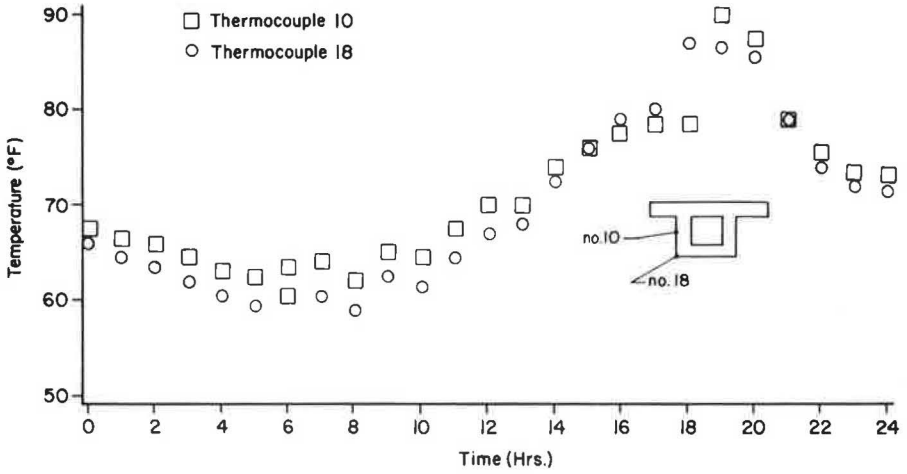

FIGURE 9 Exterior web temperatures, July 7, 1979.

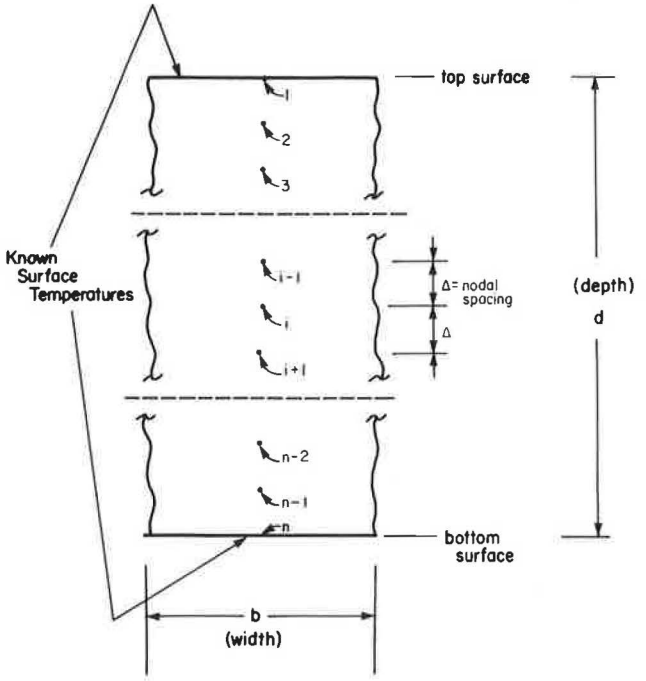

FIGURE 10 Nodal formulation.

If the first partial derivative of temperature with respect to depth ($\partial T/\partial y$) were known at the top surface, then a simple numerical integration from the first node (top surface) to the second node could be conducted. Consequently, the procedure would terminate at the nth node (bottom surface), with the results being the nodal temperature distribution. However, the correct value for the first partial derivative of temperature with respect to depth is an unknown. If an assumed value for the first partial derivative is used in the integration, then the particular temperature at the nth node $(T_n)_p$ would in all likelihood differ from the observed value. Any error is due solely to the error in the assumed first partial derivative at the top surface. Therefore, a separate homogeneous solution vector could be developed from an assumed first partial derivative with respect to depth (any value other than zero) and a top surface temperature of zero degrees. The second solution vector (nodal temperatures) consists of numerical partial derivatives; that is, the ith element gives the rate of change of temperature at Node i with respect to a change in the first partial derivative with respect to depth at Node 1. Hence, a linear combination of the two numerical solutions for the nth node (bottom surface) can be formulated such that the sum equals the observed temperature:

$$(T_n)_p^{p+1} + C \cdot (T_n)_h^{p+1} = (T_n)_o^{p+1} \tag{6}$$

where

$(T_n)^{p+1}$ = temperature at nth node at time period p + 1,
p = subscript for particular solution,
h = subscript for homogeneous solution, and
o = subscript for observed value.

When the coefficient (C) has been determined from Equation 6, the interior nodal temperatures are readily computed from

$$(T_i)_c^{p+1} = (T_i)_p^{p+1} + C \cdot (T_i)_h^{p+1} \tag{7}$$

where $(T_i)_c^{p+1}$ is the computed temperature at Node i. From the computed nodal temperatures, the curvature can be determined by a simplified version (single summation) of Equation 3.

To apply the one-dimensional analysis, the box section was divided into sections and a heat-flow analysis was performed on each section (Figure 11). The vertical temperature distribution was assumed to

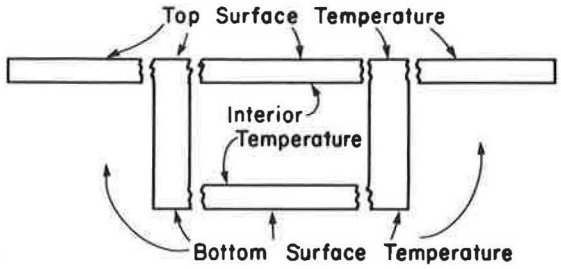

FIGURE 11 Sectional subdivision of box sections for one-dimensional heat-flow analysis.

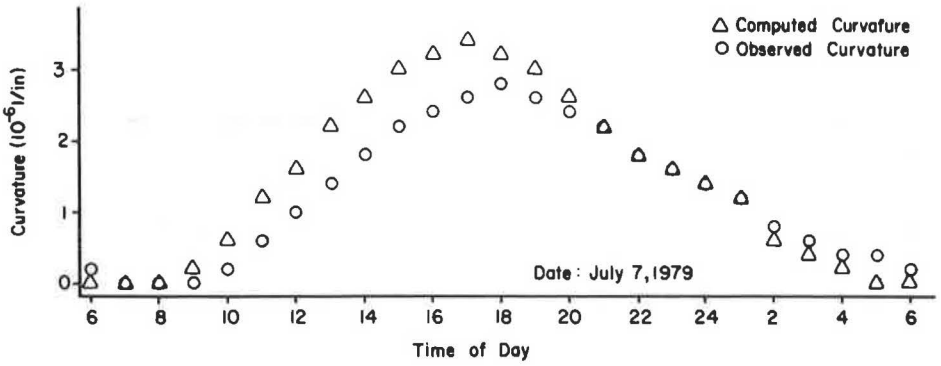

FIGURE 12 Observed curvature versus computed curvature.

be constant across the width of each section: webs, flange, and soffit. This approach has some degree of error because it allows discontinuities at the intersection of the members. However, the error is localized at specific points, and comparisons between the observed values and the numerical values displayed good agreement (Figure 12). It was noted that the computed curvatures disagreed with the observed values by approximately 20 percent. However, the same discrepancy was experienced in static load testing of the bridge (5). Therefore, it was concluded that the end conditions of the bridge developed a rotational restraint of 20 percent fixity. Hence, the one-dimensional approach seemed applicable for the evaluation of deflections.

As a final investigation, the residual stresses in the bridge structure were analyzed. When a bridge is subjected to a nonlinear temperature differential, t(y), the bridge will respond by elongating (due to the incremental change in the mean temperature) and hogging or sagging (due to the difference in temperature). Hence, a uniform strain from the longitudinal change in length ($\epsilon = \Delta L/L$) and a curvature strain ($\phi \cdot y$) develop. These two strains occur at the same time that a thermal strain, $\alpha \cdot t(y)$, would develop if the end conditions were fully restrained. Therefore, the combination of strain developments multiplied by Young's modulus (E) determines the magnitude of the residual stress (f_r):

$$f_r = E[\phi \cdot y + \epsilon - \alpha t(y)] \quad (8)$$

The temperature distribution that caused the maximum curvature development for July 7, 1979, was determined by the initial-value method (Figure 13). Then, by applying Equation 8, the residual stress distribution was computed (Figure 14). The tempera-

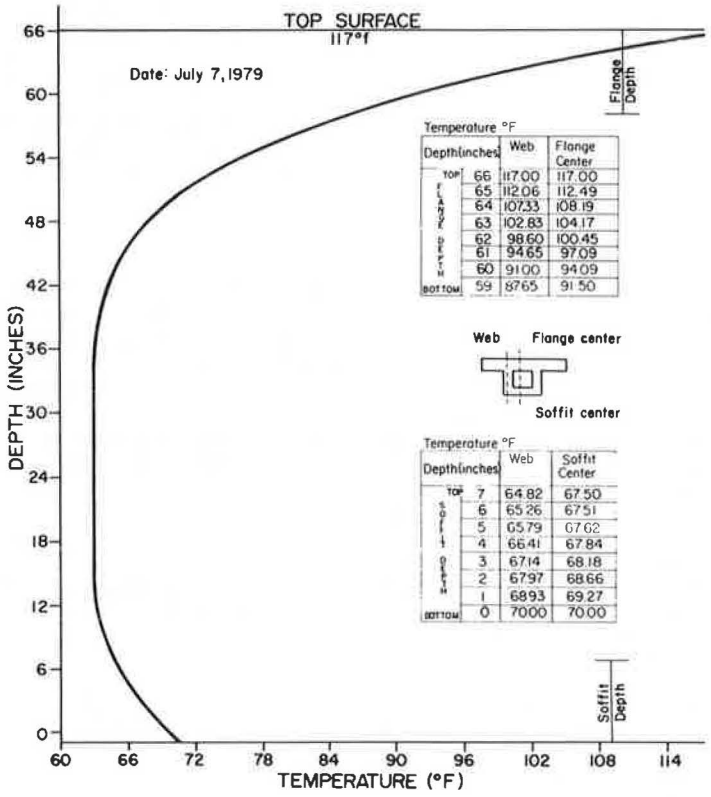

FIGURE 13 Web temperature with depth as computed by the initial-value approach (5:00 p.m.).

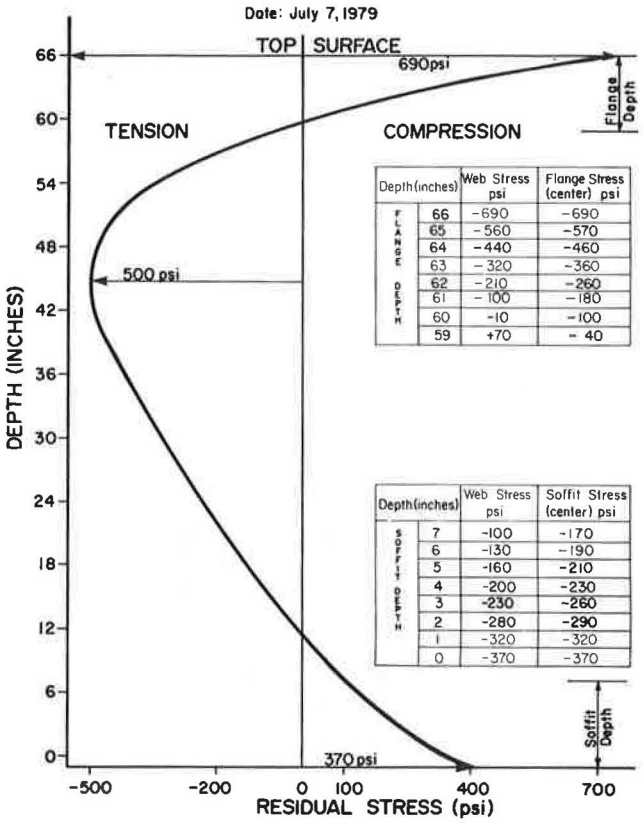

FIGURE 14 Residual stresses (5:00 p.m.).

ture distribution (and so, the residual stress plot) is conservative due to the computational initialization. From the field data, 6:00 a.m. appeared to be the best approximation to a uniform temperature distribution. Thus numerical integration started at 6:00 a.m. with a uniform temperature of 63°F, and the temperature distribution and the subsequent curvature were calculated for each hour in the 24-hour diurnal cycle. The maximum curvature was computed to have occurred at 5:00 p.m., and therefore the temperature and residual stress distributions were displayed.

The conservative aspect lies in the fact that only one diurnal cycle was studied. If the process had evaluated continuously three or four diurnal cycles, the initial mean uniform temperature would have been higher than 63°F and the temperature curve would have had greater depth. Consequently, the maximum residual stress distributions would have been different.

The conclusion of the analytical study was that a one-dimensional heat-flow analysis would render a reasonable estimate for curvature. Also, a nonlinear residual stress pattern developed with an upper limit of 690 psi. It was also evident that other residual stress patterns (temperature distributions) developed in which the maximum stress did not occur at the top surface. However, no other temperature distribution caused a maximum value of 690 psi.

DESIGN CONSIDERATIONS--SOPHISTICATION VERSUS SIMPLICITY

The field study indicated that a longitudinal variation was insignificant, and therefore the maximum complexity of the thermal problem required a two-dimensional transient heat-flow analysis. It was also found that a one-dimensional transient heat-flow analysis would give reasonable results. Hence, the question arises of the level of sophistication necessary in a design. The question must be answered in terms of the possible thermal boundary conditions for a given structure.

If the exterior surfaces of the webs and soffit are subjected only to the ambient air temperature, and the deck surface is subjected to the ambient air temperature and solar radiation, then the vertical heat-flow process will be the dominant variation. This dominance was evident both in the field study and in the analytical studies. Hence, with temperature variation dominant in one direction, a one-dimen- sional heat-flow analysis is applicable and will reasonably predict the maximum curvature. However, the accuracy of the predicted stress pattern is questionable when even a slight horizontal tempera- ture variation (approximately 20°F) can occur. In other words, a symmetrical set of thermal boundary conditions justifies the use of the one-dimensional analysis of curvature computation, but is question- able for residual stress analysis. In addition, the thermal problem becomes more complex with the occur- rence of unsymmetrical thermal boundary conditions.

The field measurements indicated that the exterior of the western web was exposed to some solar radiation in addition to the ambient air temperature. The follow-up, two-dimensional study determined that the curvature development about the major axis (with respect to the vertical axis) was negligible. However, if the major-axis curvature is neglected, then the horizontal temperature difference multiplied by the coefficient of thermal expansion ($\alpha = 6 \times 10^{-6}/°F$) and the modulus of elasticity ($E = 5 \times 10^{6}$ psi) can be considered a horizontal residual stress distribution. In the field study, an exterior web surface-temperature differential of 20°F was observed relative to the interior of the web. Hence, without the allowance of any major-axis curvature, a residual stress equaling 600 psi (compression) developed. The residual stress problem as defined by a one- or two-dimensional analysis reaches an intensity at about 600 psi, but the location of the extremes within the cross section differs depending on the analysis used.

SERVICE DESIGN APPROACH

In general, curvature development is the critical concern based on the continuity requirement in a statically indeterminate structure. Therefore, a one-dimensional approach will produce sufficient results. The critical temperature distribution can be determined for the box section in question as in the test case (Figure 13). However, because most of the temperature differential exists in the flange, an equivalent uniform flange temperature differential can be computed that will accurately predict curvature (7). The use of such a uniform flange temperature difference is a relatively simple procedure but does not compromise accuracy. For design purposes, a graph of equivalent uniform flange temperature versus flange thickness can be developed by the application of the one-dimensional analysis. Then, for a given box section, the appropriate uniform flange temperature difference can be taken from the graph, and the curvature can be readily determined.

With regard to the residual stress problem, the formulation of an accurate simplified analysis requires further study. In the research reported here, it was evident that the temperature distribution in the box section was continually changing. Hence the residual stresses were continually varying. Both

the one- and the two-dimensional analyses gave the same magnitude for the residual stress problem, but occurrence in the cross section differed. With the presence of unsymmetrical thermal boundary conditions, therefore, a one-dimensional approach (Figure 11) could be misleading with respect to a residual stress distribution.

Therefore, because of the multitude of possible thermal surface conditions, a simple analytical model is not feasible at this time. However, most design specifications account for the possible combinations of loading extremes by allowing a percentage increase (usually 33 1/3 percent) above the specified working stress limitation. Therefore, it should prove adequate to specify a 600 psi increase in the actual working stress, considering the percentage increase in the allowable working stress. Until more extensive work is performed, such a simplified approach seems prudent.

REFERENCES

1. M.J.N. Priestley. Thermal Gradients in Bridges: Some Design Considerations. New Zealand Engineering, Vol. 27, No. 7, July 1972, pp. 228-233.
2. W.J. Price. Introductory Note, Bridge Temperatures. TRRL Report SR442. Transport and Road Research Laboratory, Crowthorne, Berkshire, England, 1978.
3. P.C. Hoffman, R.M. McClure, and H.H. West. Temperature Studies for an Experimental Segmental Bridge. Research Project 75-3, Report PTI 8010. Pennsylvania Transportation Institute, Pennsylvania State University, University Park, 1980.
4. P.C. Hoffman. Thermal Design Considerations for an Experimental Prestressed Segmental Box Girder. Ph.D. dissertation. Pennsylvania State University, University Park, 1982.
5. R.M. McClure and H.H. West. Field Testing of an Experimental Segmental Bridge. Research Project No. 75-3, Report PTI 8009. Pennsylvania Transportation Institute, Pennsylvania State University, University Park, 1980.
6. M.J.N. Priestley and I.G. Buckle. Ambient Thermal Response of Concrete Bridges. Bulletin 42. Roads Research Unit, National Roads Board, New Zealand, 1979, pp. 26-27.
7. P.C. Hoffman, R.M. McClure, and H.H. West. Temperature: A Service Design Problem. Proc., National Bridge Conference, Pittsburgh, Pa., June 1983.

This study covers only a portion of a major 6-year investigation of an experimental segmental bridge that was conducted at The Pennsylvania Transportation Institute of The Pennsylvania State University. This study was sponsored and funded by the Pennsylvania Department of Transportation and the FHWA. The contents of this paper reflect the views of the authors, who are responsible for the facts and the accuracy of the data. The contents do not necessarily reflect the official views or policies of the sponsors.

Publication of this paper sponsored by Committee on Concrete Bridges.

Seasonal and Diurnal Behavior of Concrete Box-Girder Bridges

K. NAM SHIU

ABSTRACT

Measurements from three instrumented bridges in different parts of the United States were used to assess seasonal and diurnal behavior of concrete box-girder bridges. Effective bridge temperatures were used to evaluate seasonal thermal changes in bridges. Effective bridge temperature is defined as the temperature that governs longitudinal bridge movements. The effective bridge temperatures followed the same seasonal fluctuation as monthly average air temperature at the bridge site. Measured temperature differentials from top to bottom slabs for the three box-girder bridges were between +20°F and -10°F (+11.1°C and -5.6°C) regardless of geographic location. Temperature differentials were calculated by subtracting temperatures of the bottom slab from those of the top slab. Diurnal behavior of one bridge was continuously monitored for 24 hours during each of the four seasons. Longitudinal strains and temperatures were used to evaluate effects of nonlinear temperature gradient on bridge behavior. Internal thermal stresses at the instrumented bridge sections are reported.

Most materials expand with a rise in temperature and contract with a fall in temperature. In the past designers have assumed that structures respond lin-

early to temperature changes. Recent measurements on box-girder bridges (1-5) indicate that thermal response of structures is highly nonlinear and complex. Therefore, design provisions for thermal effects based on assumed linear behavior may be misleading.

Overseas researchers have conducted extensive investigations on thermal behavior of bridges (1,3-5). As a result, thermal provisions based on nonlinear behavior have been incorporated into design codes in Great Britain and New Zealand. However, no similar provisions exist in the AASHTO specifications (6).

Although no major structural distress has been attributed to temperature alone, temperature effects have contributed to structural distress reported in recent years (3,5). As more and more bridges are built with longer spans and complex sections, thermal response of bridges becomes an increasingly important factor to consider in design.

THERMAL BEHAVIOR OF CONCRETE BRIDGES

The thermal response of bridges is discussed in terms of two deformation categories: (a) overall longitudinal movements and (b) temperature-induced curvatures.

Overall Longitudinal Movements

Bridges respond primarily in the longitudinal direction to gradual seasonal temperature variations. Overall longitudinal expansion of a simply supported beam is shown in Figures 1a and 1b. With a gradual temperature rise, the beam expands uniformly in the longitudinal direction by ΔL. The temperature distribution causing this thermal movement is a uniform temperature distribution, ΔT, across the bridge section, as shown in Figure 1b.

If longitudinal movement of the beam is fully restrained, internal stresses will be induced in the beam and no thermal strains will occur. If partial longitudinal restraint is provided, a combination of thermal strains and thermal stresses will occur.

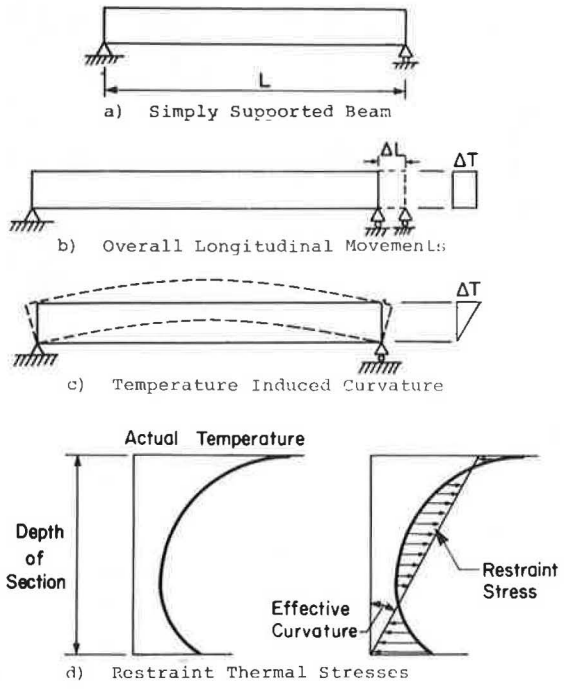

FIGURE 1 Thermal behavior of a simply supported beam.

Temperature-Induced Curvature

In addition to seasonal temperature variations, bridges experience daily temperature variations. As the sun shines on a bridge, the deck heats up. The deck generally responds much faster than the rest of the bridge section. Consequently, temperature gradients exist between the top and the bottom of the bridge superstructure. In the case of a simply supported beam, the beam cambers as shown in Figure 1c. It is generally assumed that the temperature distribution effecting such thermal movement is a linear gradient across the beam section.

However, actual temperature distributions across bridge sections are nonlinear (1-5). Investigations (1,3) have shown that temperature distribution can be more realistically represented by a fifth-order parabola.

For a given nonlinear temperature gradient, the bridge deforms to attain an effective curvature. Because plane sections are assumed to remain plane according to beam theory, the resulting strain has to vary linearly across the bridge section. However, concrete tends to expand or contract according to the coefficient of thermal expansion; consequently, internal restraint stresses are induced, as shown in Figure 1d. Restraint stresses occur in all sections with nonlinear temperature distributions. Some researchers (2,3) have indicated that restraint stresses can be substantial.

FIELD MEASUREMENTS

To understand the actual thermal behavior of bridges, three long-span box-girder bridges were instrumented during construction by the Construction Technology Laboratories. They are Kishwaukee River Bridge (7) in Illinois, Denny Creek Bridge (8) in Washington, and Linn Cove Viaduct (9) in North Carolina. A summary of the characteristics of the three bridges is given in Table 1.

Kishwaukee River Bridge, shown in Figure 2, was instrumented to investigate time-dependent behavior of segmental box-girder bridges. Three sections of a selected span were instrumented. The sections were located next to the pier, at quarter span, and near midspan. Measurements included longitudinal concrete strains, air and concrete temperatures, and deflections. Locations of temperature and strain measurements at a section are shown in Figure 3. Detailed description of the instrumentation program is given elsewhere (7). Readings were taken seasonally for a period of 5 years. In addition, four sets of 24-hour continuous readings on the bridge were taken to monitor diurnal bridge behavior in different seasons.

Denny Creek Bridge, shown in Figure 4, was instrumented to determine time-dependent behavior of a cast-in-place, stage-constructed, box-girder bridge. The instrumentation layout was similar to that used in the Kishwaukee River Bridge. Bridge sections located next to the pier, at quarter span, and near midspan were instrumented. Details of the instrumented span are reported elsewhere (8). Locations of the temperature and strain measurements on each section are shown in Figure 5. Readings were taken periodically during 2 years.

Linn Cove Viaduct in North Carolina is a continuous, precast, box-girder bridge with a highly unusual geometric configuration as shown in Figure 6. The objective of instrumentation was to measure

TABLE 1 Instrumented Bridges

Bridge	Region	Length of Instrumented Span (ft)	Bridge Type	Span Lengths (ft)
Kishwaukee River Bridge	Midwest	250	5 span continuous, precast segmental box section.	170 to 250
Denny Creek Bridge	Northwest	188	16 span continuous, stage construction, cast-in-place box section	143 to 188
Linn Cove Viaduct	Southeast	180	8 span continuous, precast segmental box section	98 to 180

Metric Equivalent: 1 ft = 0.31 m

FIGURE 2 Kishwaukee River Bridge.

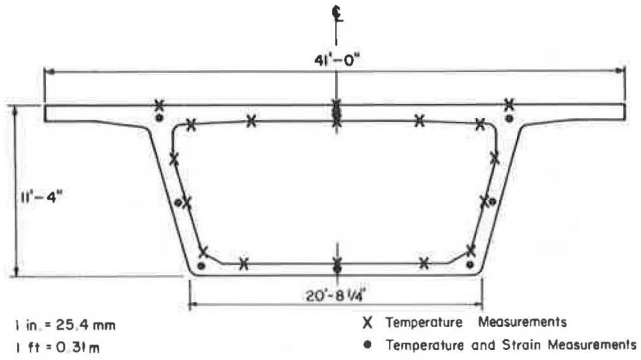

FIGURE 3 Locations of temperature and strain measurements in Kishwaukee River Bridge.

FIGURE 4 Denny Creek Bridge.

and evaluate temperature differentials, thermal and torsional strains, and prestress losses (9). The instrumentation scheme was similar to that used at the Kishwaukee River Bridge. Bridge sections next to the pier, at quarter span, and near midspan of one span were instrumented. Locations of the temperature and strain measurements on each section are shown in Figure 7. A detailed description of the instrumentation program on Linn Cove Viaduct is given elsewhere (9). Readings were collected for approximately 500 days during and after construction.

SEASONAL BEHAVIOR

Effective bridge temperature was used to evaluate seasonal behavior for each instrumented bridge. Effective bridge temperature is defined as the temperature that governs the longitudinal movements of the superstructure. A method of calculating effective bridge temperatures is described elsewhere (4). In this paper, averages of temperatures measured in the top slab, in the web, and in the bottom slab of the box girder were used to calculate the effective bridge temperatures.

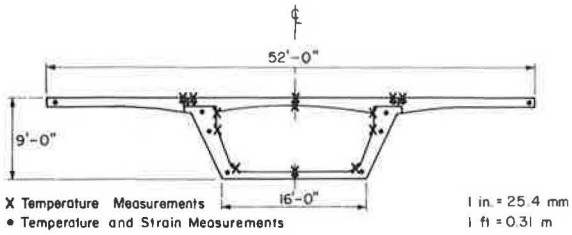

FIGURE 5 Locations of temperature and strain measurements in Denny Creek Bridge.

FIGURE 6 Linn Cove Viaduct.

A comparison of the calculated effective bridge temperatures of the Kishwaukee River Bridge and the monthly average air temperature near the bridge site (10) is shown in Figure 8. Monthly average air temperatures are based on temperature records since 1945. The effective bridge temperature follows the monthly average air temperature fluctuation. Overall

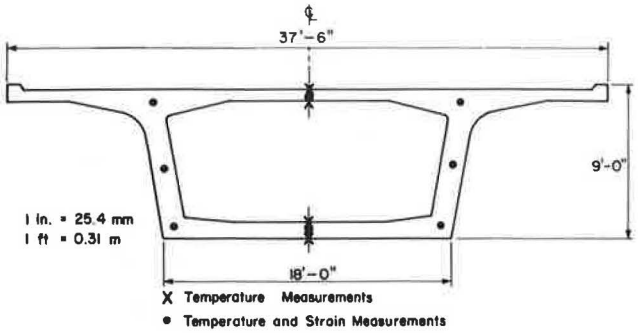

FIGURE 7 Locations of temperature and strain measurements in Linn Cove Viaduct.

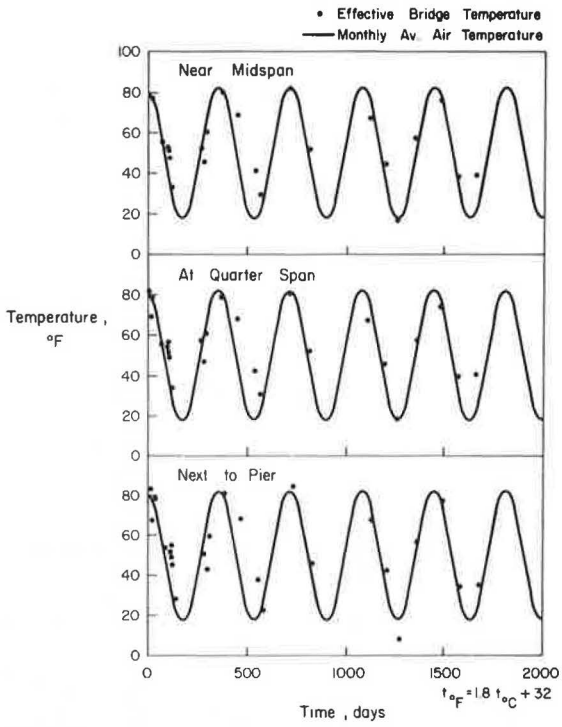

FIGURE 8 Comparison of effective bridge temperature of Kishwaukee River Bridge with monthly average air temperature near bridge site.

longitudinal movements of the Kishwaukee River Bridge are proportional to variations in monthly average air temperature near the bridge site.

A similar observation was made for the Denny Creek Bridge in Washington as shown in Figure 9. No comparison was performed for the Linn Cove Viaduct

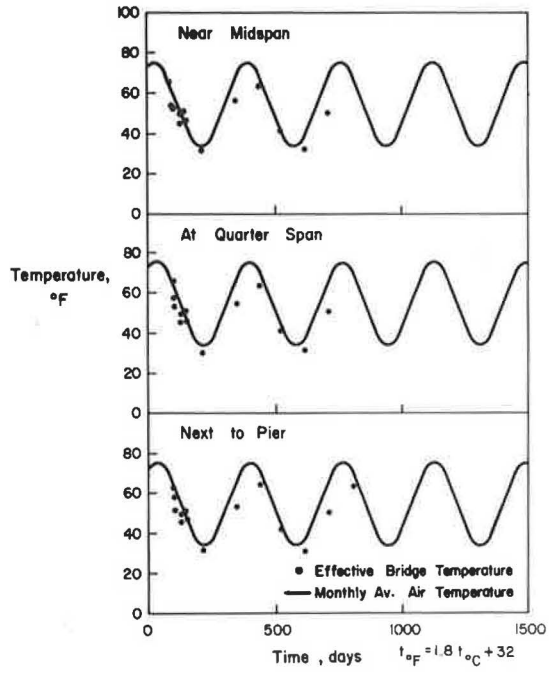

FIGURE 9 Comparison of effective bridge temperature of Denny Creek Bridge with monthly average air temperature near bridge site.

because the collected data were very limited. At Linn Cove readings were taken over a period of 1 year with collected data points clustered in two seasons only. Consequently, comparison of effective bridge temperatures with monthly air temperatures can be misleading.

On the basis of these comparisons, it is concluded that longitudinal thermal movements of concrete box-girder bridges can be estimated by using the average air temperature at the bridge site.

The ranges of temperature specified in the AASHTO specifications (6) for designing concrete structures are a temperature rise of 30°F (17°C) and a temperature fall of 40°F (22°C) in moderate climates, and a temperature rise of 35°F (19°C) and a temperature fall of 45°F (25°C) in cold climates. However, if the average monthly air temperature (10) were used, Kishwaukee River Bridge would have to accommodate a temperature rise of 32°F (18°C) and a temperature fall of 32°F (18°C) relative to the annual mean temperature at the bridge site. For the Denny Creek Bridge, the temperature range would only be a temperature rise of 24°F (13°C) and a temperature fall of 18°F (10°C). It is therefore suggested that monthly average air temperature at bridge sites may be used as a guide for determining the overall longitudinal behavior of bridges as an alternative to the ranges given in the AASHTO specifications (6).

Variation of measured differentials between the temperature of the top and of the bottom slabs of the three instrumented bridges with time is plotted in Figure 10. Temperature differentials were calculated by subtracting temperatures of the bottom slab from those of the top slab. As shown in Figure 10, temperature differentials for the three bridges were within the range of +20°F and -10°F (+11°C and -6°C) regardless of their geographic location. This implies that concrete temperature differentials in box girders are independent of air temperature variations due to change in geographic location. However, it is noted that the observation was based on a limited data sample. More data are needed to confirm this observation. Further investigations on temperature differentials of box girders are recommended.

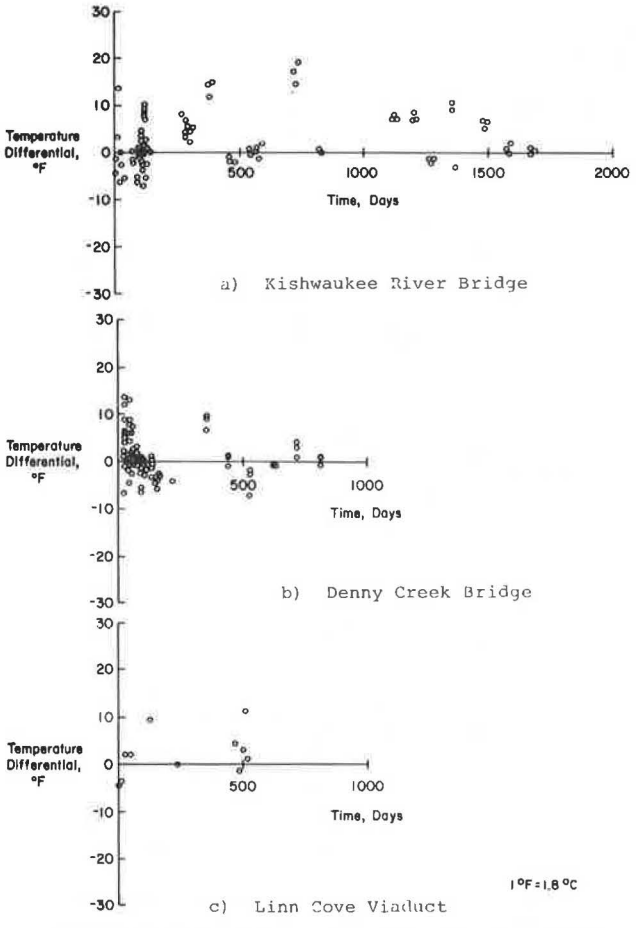

FIGURE 10 Variation of temperature differentials between top slab and bottom slab with time.

DIURNAL BEHAVIOR

Four sets of 24-hour measurements were made on Kishwaukee River Bridge. Measurements included air temperature inside and outside the box girder, concrete temperature, and longitudinal concrete strains. Daily variations in the measured air temperatures for four seasons are shown in Figure 11. Air temperature outside the box girder fluctuated more than air temperature inside.

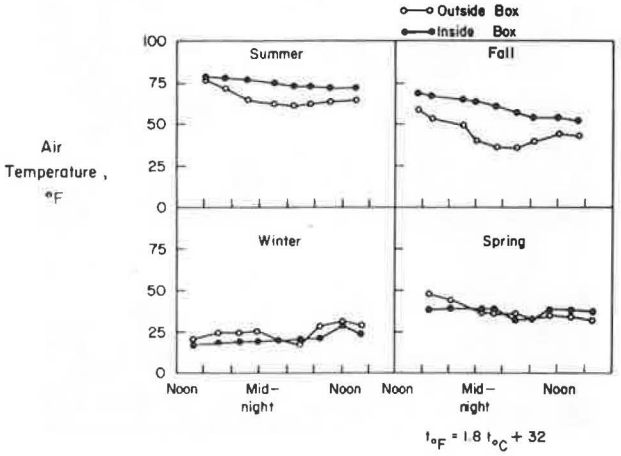

FIGURE 11 Daily variation of air temperatures inside and outside the box girder for four seasons at the Kishwaukee River Bridge.

Temperature distributions in the top and in the bottom slabs of the segment next to the pier in the summer and winter of 1979 are plotted in Figure 12. Values shown at the bottom of the slab are the ambient air temperature. Because of the delayed response of concrete to outside air temperature, temperature distributions across the box section were nonlinear.

Longitudinal strains and temperatures measured during the 24-hour periods were used to evaluate effects of diurnal temperature changes on bridge behavior. Two procedures were used to adjust measured strains for thermal expansion or contraction of both concrete and strain gauges to a standard temperature of 73°F (23°C).

In the first procedure, concrete and strain gauges were assumed to expand or contract proportionally to their respective coefficient of thermal expansion. This simple procedure assumes unrestrained movement of concrete and strain gauges.

In the second procedure, effects of nonlinear temperature gradient were included. The following steps were used to adjust strain readings to the standard temperature of 73°F (23°C):

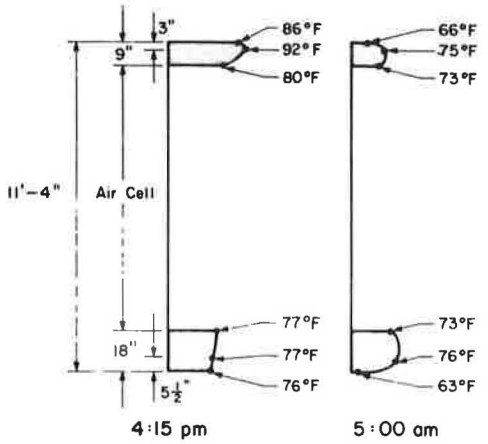

(a) Summer of 1979

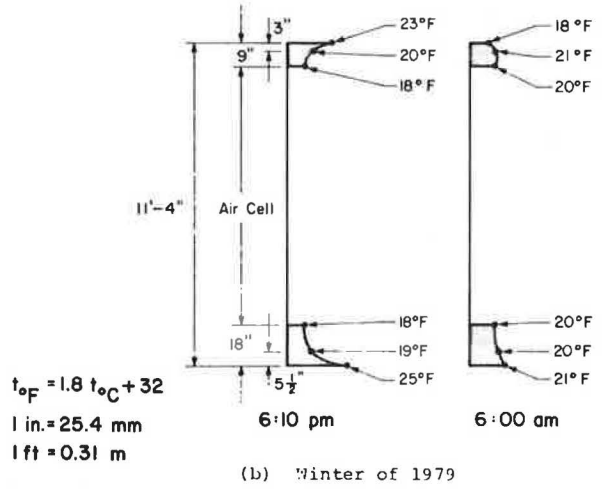

(b) Winter of 1979

FIGURE 12 Temperature distribution in the top and bottom slabs of the segment next to the pier for the Kishwaukee River Bridge.

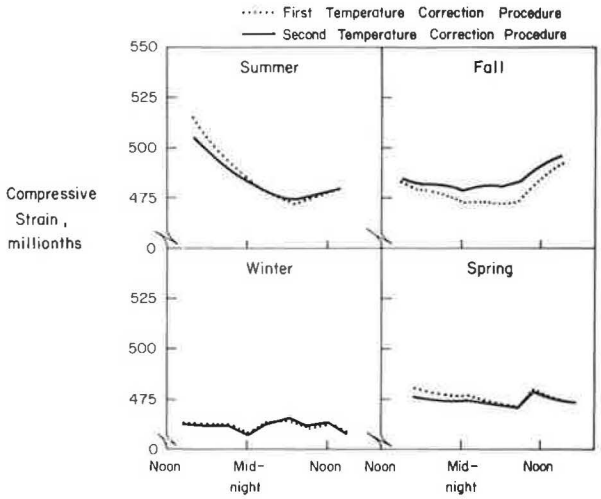

FIGURE 13 Comparison of the daily strain variation in the top slab of the Kishwaukee River Bridge.

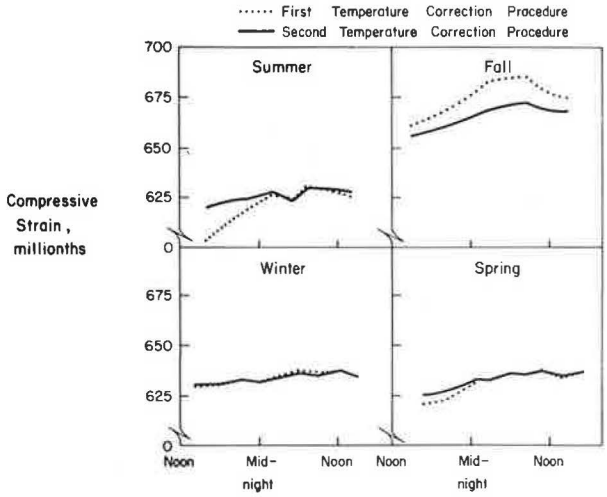

FIGURE 14 Comparison of the daily strain variation in the web of the Kishwaukee River Bridge.

1. Measured temperature data were fitted to a fifth-order parabola to determine temperature distribution across the box girder;
2. Curvature of the section resulting from the calculated parabolic temperature distribution was calculated;
3. From the computed curvature, an equivalent linear temperature distribution to cause the same curvature was determined;
4. Using the equivalent temperature distribution, effective temperatures at the location of the strain gauges were calculated; and
5. Because effective temperatures corresponded to thermal movements across the section, strain readings were adjusted from the calculated effective temperatures to 73°F (23°C).

Comparisons of strains calculated according to the two temperature correction procedures are shown in Figures 13 and 14. Dotted lines in the figures represent reduced strain data using the first temperature correction procedure. Solid lines represent reduced strain data using the second temperature correction procedure. Figure 13 shows daily variation of strains measured in the top slab and Figure 14 represents daily variation of strains measured in the web of the box girder. The difference between strains obtained from the two temperature correction procedures is the restraint thermal strain corresponding to the induced thermal stress.

When the modified compressive strains at each location were less than the strains calculated with the assumption of free expansion and contraction, tension restraint stresses were induced. Likewise, when the modified compressive strains were larger than the strains calculated using the free thermal movement assumption, compressive stresses were induced in the section.

In Figures 13 and 14, maximum restraint strains ranged from 20 millionths in compression to 20 millionths in tension. Measured concrete modulus of elasticity was between 4,190 ksi (28.9 GPa) and 4,760 ksi (32.8 GPa). For simplicity, a modulus of 5,000 ksi (34.5 GPa) was used to calculate the equivalent restraint stresses. Calculated restraint stresses ranged from 100 psi (689 kPa) in tension to 100 psi (689 kPa) in compression. The restraint stress range is based on a limited number of field measurements. Therefore, reported stress range should not be treated as the range of maximum anticipated restraint stress levels.

The calculated restraint stresses of 100 psi (689

kPa) in magnitude is substantially less than stresses predicted from the modified New Zealand temperature distribution. Restraint stresses calculated for the Pennsylvania box-girder bridge (2) using the modified New Zealand temperature distribution (1,3) were reported to range from 488 psi (3362 kPa) in tension to 577 psi (3976 kPa) in compression.

In addition, restraint stresses were quite transient. Internal restraint stresses increase and decrease within hours. Although restraint stresses are present only for a short time, some consideration should be given to these stresses in design.

CONCLUSIONS

On the basis of the preceding discussion, the following conclusions are drawn:

1. Annual variation in the effective bridge temperature was found to be quite similar to the variation in monthly average air temperature at the bridge site.
2. Measured temperature differentials between the top and the bottom slabs of three box-girder bridges ranged between +20°F and -10°F (+11°C and -6°C). Measured temperature differentials seem to be independent of geographic location. Further investigations of temperature differentials in box girders are needed.
3. For the Kishwaukee River Bridge, internal restraint stresses from nonlinear temperature distribution varied between 100 psi (689 kPa) in tension to 100 psi (689 kPa) in compression. The calculated restraint stresses were substantially less than stresses computed using the temperature provision of the New Zealand Code (2).
4. Internal restraint stresses were transient in nature.

ACKNOWLEDGMENT

Data used in this paper were obtained from three investigations conducted by the Structural Experimental Section of the Construction Technology Laboratories, a division of Portland Cement Association, under the direction of D.M. Schultz, Manager, H.G. Russell, Director, and W.G. Corley, Divisional Director. Sponsors of the investigations were the Illinois Department of Transportation, the Washington State Department of Transportation, and the FHWA.

REFERENCES

1. A. Churchward and Y. Sokal. Prediction of Temperatures in Concrete Bridges. Journal of the Structural Division of ASCE, Vol. 107, No. ST11, Nov. 1981, pp. 2163-2175.
2. P.C. Hoffman, R.M. McClure, and H.H. West. Temperature Study of an Experimental Segmental Concrete Bridge. Journal of Prestressed Concrete Institute, Vol. 28, No. 2, March-April 1983, pp. 79-97.
3. M.J.N. Priestley. Design of Concrete Bridges for Temperature Gradients. Journal of the American Concrete Institute, Vol. 75, No. 5, May 1978, pp. 209-217.
4. M. Emerson. Temperature Differences in Bridges: Basis of Design Requirements. TRRL Report LR765. Transport and Road Research Laboratory, Crowthorne, Berkshire, England, 1977.
5. W.J. Price. Introductory Note. In Bridge Temperatures, TRRL Report SR442, Transport and Road Research Laboratory, Crowthorne, Berkshire, England, 1978.
6. Standard Specifications for Highway Bridges, 12th ed. American Association of State Highway and Transportation Officials, Washington, D.C., 1977 and Interim 1978.
7. K.N. Shiu, J.I. Daniel, and H.G. Russell. Time-Dependent Behavior of Segmental Cantilever Concrete Bridges. Illinois Department of Transportation, Springfield; Construction Technology Laboratories, Skokie, Ill., March 1983.
8. K.N. Shiu, J.D. Aristizabal-Ochoa, and H.G. Russell. Instrumentation of Denny Creek Bridge. Confidential Report. Washington State Department of Transportation, Olympia; Construction Technology Laboratories, Skokie, Ill., Aug. 1981.
9. K.N. Shiu and H.G. Russell. Instrumentation of Linn Cove Viaduct. Confidential Interim Report to Teng and Associates, Inc. Construction Technology Laboratories, Skokie, Ill., May 1981.
10. Weather of U.S. Cities, Vols. 1 and 2. Gale Research Company, Detroit, Mich., 1982.

Publication of this paper sponsored by Committee on Concrete Bridges.

Foundation Design: West Seattle Bridge

JOHN H. CLARK

ABSTRACT

Development of foundation design for the West Seattle Freeway Bridge required extensive geotechnical investigations including a seismic intensity determination. This bridge is one of the first major structures to be designed in accordance with the guidelines developed by the Applied Technology Council (ATC-06). Design constraints, procedures, solutions, and details are described.

The West Seattle Bridge is a 1700 m (5,580 ft) long structure carrying a major arterial over an important ship channel (Figure 1). The 32 m (105 ft) wide deck carries six lanes of highway traffic and will serve an estimated daily volume of 80,000 vehicles by the year 2000. Navigation clearance over the ship channel (West Waterway) required a 180 m (590 ft) main span with 43 m (140 ft) vertical clearance. The structure chosen for construction is a twin, single-cell, concrete, box-girder main span unit of three spans--114, 180, and 114 m (375, 590, and 375 ft). Structure depth varies from 3.7 m (12 ft) at midspan to 9.1 m (30 ft) over the piers. The principal dimensions of the main span unit are shown in Figure 2. Typical piers are shown in Figures 3 and 4.

The superstructure was built segmentally in free cantilever and the deck was transversely posttensioned to provide a monolithic unit. Approaches on either end are composed of precast prestressed girder spans of 49 m (160 ft) maximum. The roadway slab casting sequence for these approach spans provides continuity for live load and part of the dead load. Longitudinal frame units are typically five spans in length. The pier cap beams were cast around the erected precast girders to provide a monolithic frame. The choice of the structural scheme was strongly influenced by seismic design considerations.

The structure is founded on vertical precast prestressed concrete piles of 60 cm (24 in.) diameter except for the two main span piers adjacent to the West Waterway, which are carried by 91 cm (36 in.) diameter steel pipe piles (Figure 5). Pile capacities used for design were 1800 kN (200 tons) for the concrete piles and 5300 kN (600 tons) for the steel piles under static loads. Maximum design conditions under seismic loads were limited to twice the static capacity.

The bridge site was dictated by the existing development and arterial street pattern. Existing viaducts fixed the end points and valuable industrial properties limited alternate routes. Subsurface site conditions were a significant design problem particularly when coupled with the seismicity of the area. The area traversed by the project is a buried glacial valley filled with recent alluvial deposits and man-made fill as shown in Figure 5. Surface deposits are generally 3-6 m (10-20 ft) of hydraulic fill (loose to medium dense silty sand). This fill is underlain by alluvial soils consisting of medium to dense silty sand and sandy silts with loose silt pockets. Underlying the alluvial soils at depths of 10-70 m (30-250 ft) below the ground surface are glacially consolidated sediments consisting of hard to very dense clays, sands, and fill. These consolidated deposits are estimated to be several hundred meters thick. On the west bank of the West Waterway the strong glacial till deposits are found at a depth of approximately 50 m (160 ft), and under the east bank and the entire east approach area the depth to this material is from 60 to 80 m (200 to 250 ft). Shear wave velocities in these materials are 170-300 mps (550-1,000 fps) in the alluvial sands and silts and about 600 mps (2,000 fps) in the glacial till.

Seattle is located in the central part of the Puget Lowland seismotectonic province (1). The Puget Lowland is a major, elongated topographic and structural depression separating the Olympic Mountains on the west from the Cascade Range on the east. Quaternary sediments overlie the bedrock complex consisting of interbedded Tertiary volcanics and sediments. These sediments were consolidated under Pleistocene glaciers one or more times.

Correlation of regional seismicity with specific faults is difficult or impossible due to this sedimentary cover. The region has experienced moderate seismic activity within historical times (1827 to present). Approximately 140 earthquakes with epicentral intensities of IV [Modified Mercalli (MM)

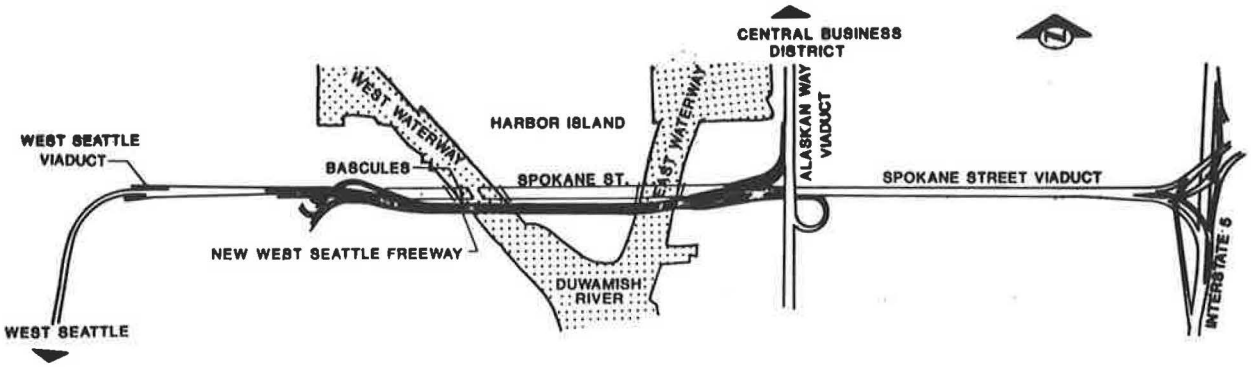

FIGURE 1 Vicinity map.

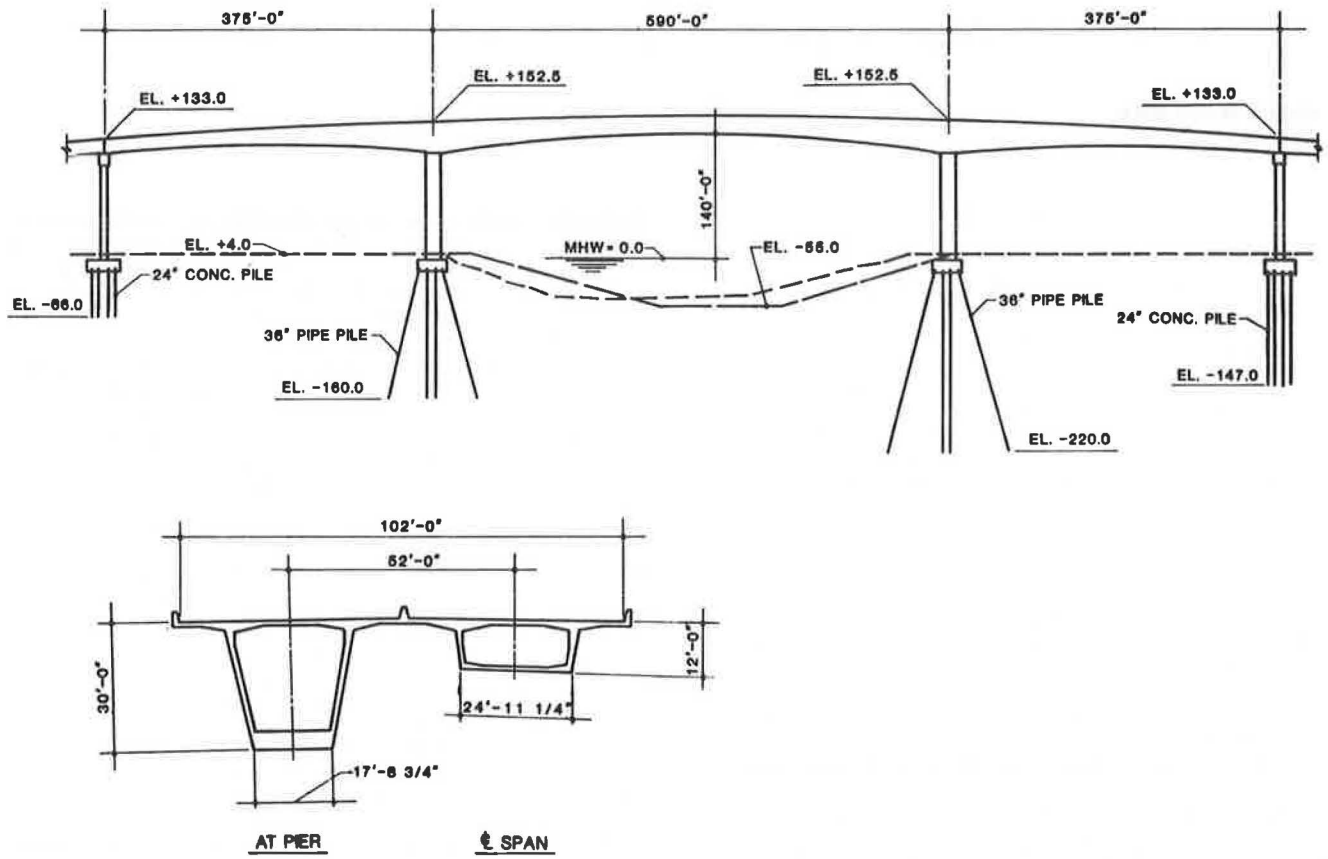

FIGURE 2 Elevation and cross sections.

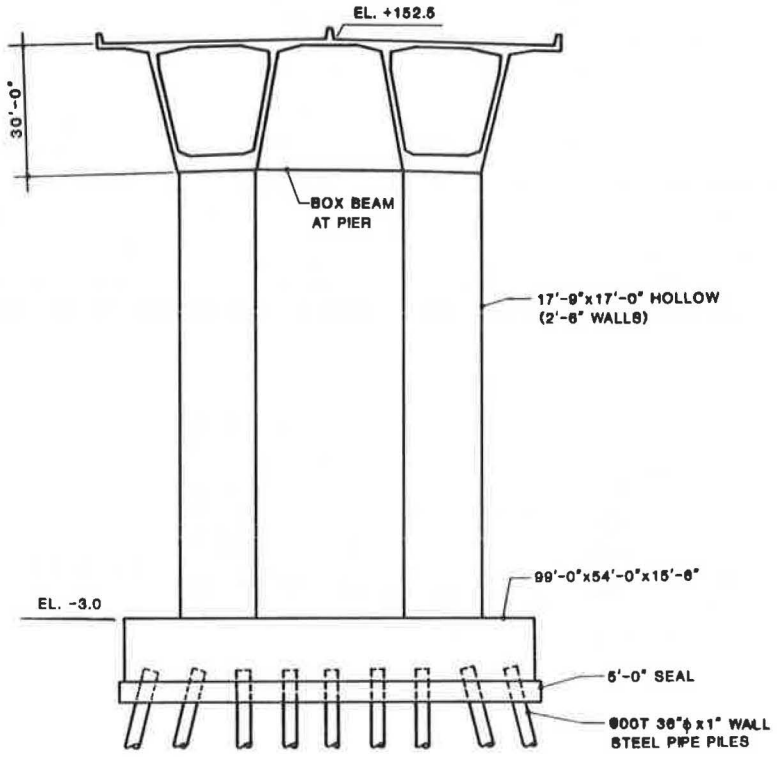

FIGURE 3 Section at main pier.

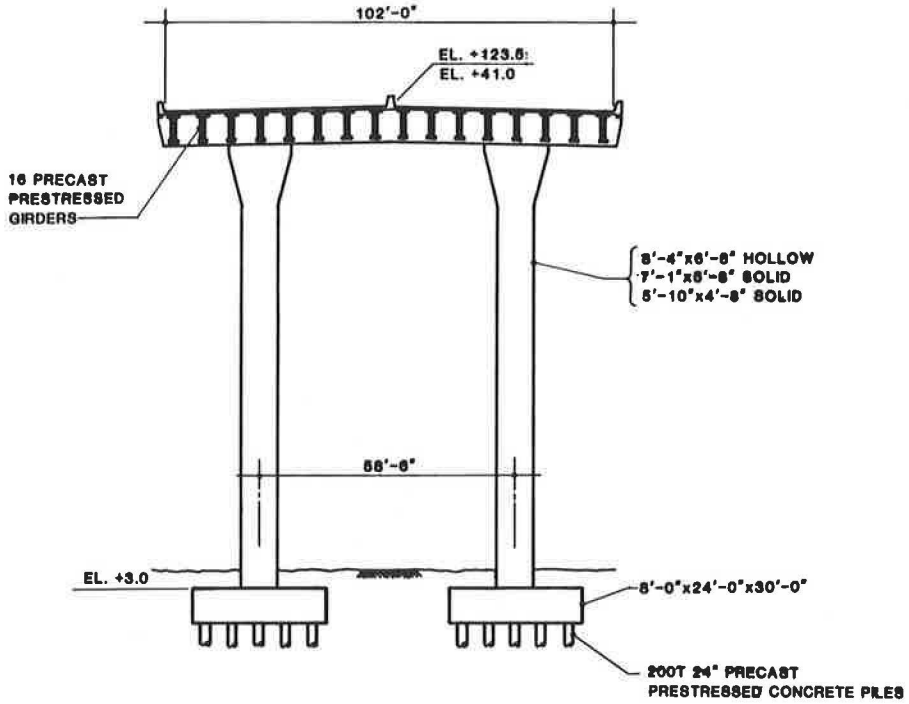

FIGURE 4 Section at pier, approach spans.

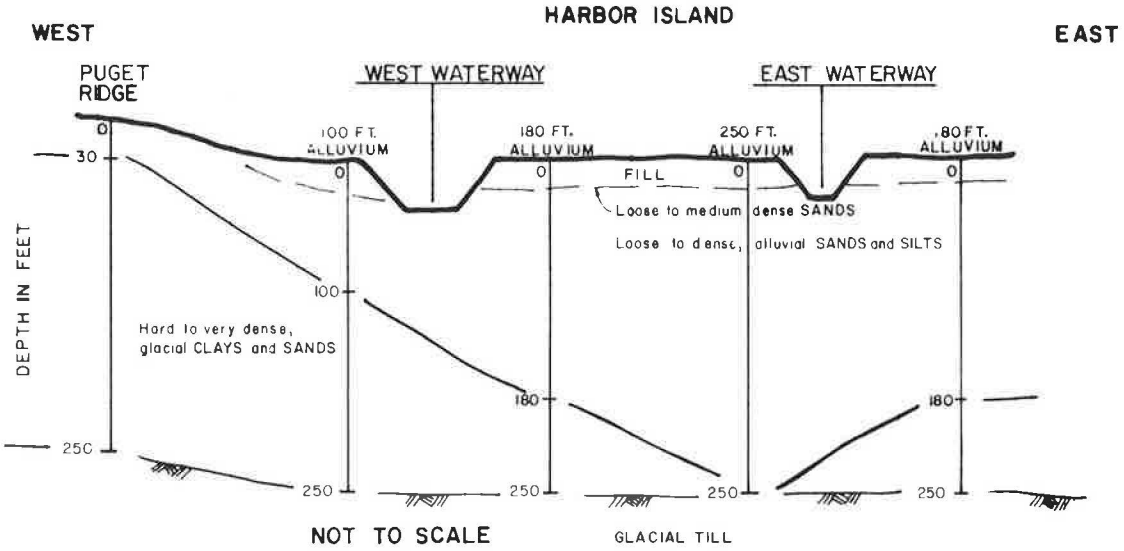

FIGURE 5 Schematic soils profile.

scale] or larger including two with epicentral intensity VIII have been recorded within a 90-km (55-mile) radius of the site. Data on these earthquakes follow.

Earthquake Epicentral Intensity (MM)	Cumulative No. of Earthquakes
VIII	2
VII	7
VI	32
V	86
IV	143

The area is classified by the Uniform Building Code as Zone III (compared to Zone IV of the Los Angeles area of Southern California). The results of the seismicity study indicated that the design earthquake, corresponding to a return period of approximately 500 years, would produce ground shaking of intensity high VIII to low IV at the site. The shock would be approximately 7.5 Richter magnitude occurring at a focal depth of 60 km.

Liquefaction of the loose sands near the surface was indicated as a possibility by the blow counts recorded in the soil sampling operations and by the grain size distributions. Some minor liquefaction has been noted in the vicinity during past earthquakes.

The designers were thus faced with accommodating the design of a relatively heavy and high structure to a site offering poor foundation conditions under the threat of strong seismic action and potential

liquefaction of near-surface layers. In the balance of this paper, the investigations and design analyses undertaken to solve these problems are emphasized and the principal results are described. Discussion is focused on the foundations for the main span unit. Similar techniques were used for the approaches.

SOILS INVESTIGATIONS

Geotechnical field investigations included an extensive program of test borings, samplings, and Dutch cone probes. The site had been the subject of several previous design studies and thus a comparative wealth of subsurface data was on hand. The natural variability of conditions at the site limited the validity of extrapolation from this previous data. The final design soils program thus included one or more test borings at each pier. Dutch cone probes were used principally to verify design pile lengths and identify areas where liquefaction potential appeared to be significant.

In situ measurements of the coefficient of "at rest" lateral earth pressure, k_o, were made using a self-boring pressuremeter. Soil resistance to lateral displacement of piles (p-y curves) was derived from these tests.

Pile load tests were carried out at five sites over the length of the project including one test at each main channel pier location. Real-time dynamic pile analyzers (Goble) were used during driving of test piles and reaction piles to determine pile ultimate capacity, load distribution, and hammer performance. Load-tested piles were instrumented with both mechanical telltales and resistance strain gauges over their lengths to determine the distribution of load-carrying capacity between side friction and point bearing. A lateral load test was performed at one site on a steel pipe pile. Settlement studies were made to estimate potential settlement under groups of piles in the deep alluvium areas. Details of the pile load tests for the main piers adjacent to the West Waterway are given in Table 1.

The extensive pile test program carried out during the design phase of the project enabled the designers to use ultimate pile axial loads for resistance to seismic motions. The results of the tests allowed a significant savings in the number and lengths required by the final design. The savings were many times the cost of the tests.

Analytic geotechnical studies included empirical site matching studies to estimate the spectral shape corresponding to the design earthquake and analytic ground response studies to account for site-specific

TABLE 1 Pile Load Test Program—West Seattle Freeway Bridge Replacement

	Main Span Substructure	
	Site C	Site D
Site location	East bank of west waterway	West bank of west waterway
Load test pile	24 x 1¼ in. wall steel pipe, open-ended and concrete filled to 184 ft	24 x 1¼ in. wall steel pipe, open-ended and concrete filled to 134 ft
Driving test piles (anchor piles)	One open-ended 36 x ¾ in. wall and one closed and one open-ended 24 x ¾ or 1 in. wall steel pipe piles	
Site conditions		
Approximate ground surface elevation (ft)	2	4
Top elevation of bearing layer (ft)	-186	-81
Type of bearing material	Glacial gravelly, sandy, silty clay	Interbedded glacial clayey silt, silt, and sand
Load test pile embedment length (ft)	212	144
Nearest test boring and depth (ft)	WS-11, 215	WS-7, 180
Driving test pile embedment lengths (ft) (most used as anchor piles)	207-208	117-148
No. of load test and driving test piles	4	4
Test performed		
No. of dynamic pile testing measurements	3	3
Compression load test	1	1
Tension load test	1	1
Lateral load test	1	
Loading procedures	Modified quick test	Modified standard test and modified quick test
Pile-driving hammers		
Make and model	Delmag D62-12	Delmag D62-12
Ram weight (lb)	14,000	14,000
Range of hammer energy for last 5 ft of penetration (ft-lb)	112,000-140,000	147,000-156,300
Measured test loads (tons)		
Compression test	750[a]	1050[b]
Tension test	800[b]	1000[b]
Lateral test	80	

[a]Weld on reaction pile failed at 750 tons.
[b]Pile did not fail at this load.

NOTE:
Soil boring was accomplished at each test site location.

Closed-end steel pipe piles were fitted with flush butt-welded 60 degree Associated Pile & Fitting Corp. P-13006 conical points. Open-end steel pipe piles were reinforced with a welded inner ring.

Dynamic pile testing was accomplished by Goble & Associates, Inc.

Load transfer instrumentation was installed in all load test piles and consisted of telltales and strain gauges attached to an inclinometer casing.

soil conditions. Results of the empirical studies yielded the limiting ground surface motions:

Acceleration = 0.32 g,
Velocity = 32 cm/sec, and
Displacement = 14 cm.

Dynamic analyses of representative soil columns over the site then yielded the design values of spectral amplification factors (2,p.35) for this site:

Acceleration = 2.2,
Velocity = 1.8, and
Displacement = 1.8.

The results of these studies were then combined to produce the design response spectrum (elastic) used for the project (Figure 6).

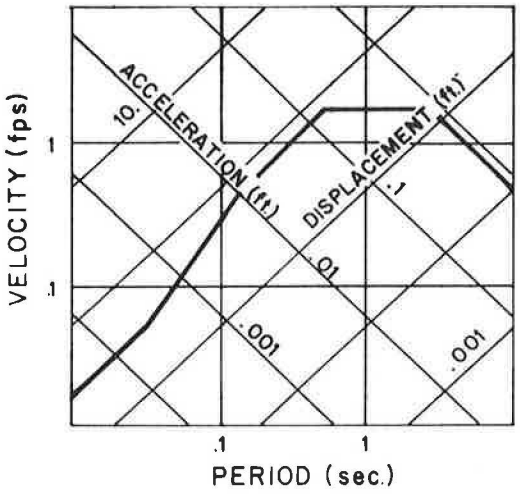

FIGURE 6 Response spectrum.

Analytic procedures used for predicting areas of potential liquefaction were to determine the cyclic stress ratio induced by the design earthquakes, to convert this stress ratio into minimum N-values to resist liquefaction, and to compare this minimum N-value curve with SPT-N-valves obtained from the borings to determine potential problem areas and depths of liquefaction.

FOUNDATION DESIGN

Design for resistance to seismic events was predicated on a philosophy similar to that used in New Zealand Codes (3) and advocated by the Applied Technology Council (ATC) (4). The structure was to remain stable and confine significant damage to areas accessible for repair under the design earthquake--chosen in this case as an earthquake having a return period of 500 years. Inelastic action was to be confined to hinging at the top and bottom of the columns. Response to an earthquake with an estimated 50-year return period was required to cause no significant damage (i.e., stresses to remain within the elastic range).

The design criteria adopted were adapted from the draft version of ATC recommendations and available information on the New Zealand approach to seismic design of highway bridges as reported by Chapman in the ATC workshop, January 1979 (5). The differences between the criteria used for this project and these two sources were minor, principal differences being return period of design earthquake and safety factors. The criteria for this project viewed the design earthquake as a "maximum credible" event and, consequently, some strength safety factors were reduced. In particular, pile loads under seismic action were taken to ultimate pile resistance as established by the pile load tests. An explicit check of column ductility capacity consistent with predicted displacements was made to verify the response modification factor used.

The design procedure is predicated on the approximate equality of maximum deflection for simple elastic and elastoplastic systems subjected to seismic input (6). This principle has been well established by many researchers and has formed the basis for most of the current seismic design codes. This principle allows prediction of maximum structure displacements to be made using modal superposition analyses in the frequency domain as opposed to time-consuming inelastic time history analyses. Past design codes have adjusted the force levels as shown in Figure 7 by using a reduced or inelastic input spectrum.

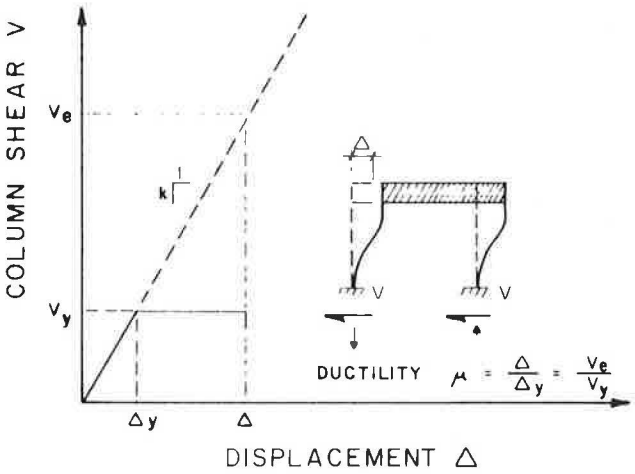

FIGURE 7 Elastic versus inelastic response to ground motion.

The ATC-recommended procedure is to perform the dynamic analysis using the unreduced ground motion spectrum as the input to the elastic response spectrum analyses and then to reduce the forces obtained by the assumed ductility factor. The ductility factor is defined as the ratio of maximum displacement to displacement at first yield. The ductility factor for a real structural system is different for each normal mode; however, for most bridge structures of reasonably regular geometry, the first mode dominates the response. The design forces for determining the required strength in the columns are then the maximum forces obtained from the elastic dynamic analysis divided by the response modification (i.e., ductility) factor (see Equation 1 hereafter).

The additional (compared to ATC 6) step used in the West Seattle Bridge design procedure was to examine the maximum displacements and to analyze

1. The capability of the inelastic system to support the gravity loads in the maximum displacement configuration;
2. The curvature ductility required at the plas-

tic hinges compared to curvature capability of the members; and

3. The capability of the other portions of the structure to force the plastic hinges to form at the assumed locations; response reduction factors used were

Column Section Type	Structural Type	
	Cantilever	Rigid Frame
Hollow	2.5	4.0
Solid	3.5	6.0

Two basic structural models were used for dynamic analysis: A local model of the main span unit expressed the mass distribution quite closely, considering both three-dimensional aspects and plate stiffness of the deck elements (Figure 8). End conditions accounted for the mass and stiffness of adjacent approach units. A second, global, model incorporated the column frames and line elements representing the deck. This model represented the main span and both approach structures from end to end. One portion of the global model is shown in Figure 9.

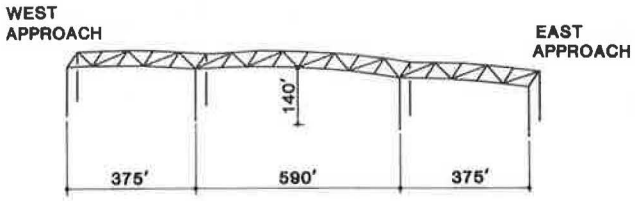

FIGURE 8 Local analytic model, main span.

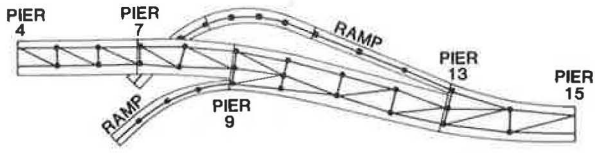

FIGURE 9 Global analytic model, west approach.

The principal difficulty with this global model was a proper representation of the restrainer units used at expansion joints. Two values of stiffness were assumed for the restrainer elements that bounded the likely values, a "material" stiffness calculated from actual Young's modulus, area, and length of the units; and a "secant" stiffness that approximated the effect of the initial slack and some assumed yielding.

The local model was analyzed to exhibit the effects of deck stiffness in relation to first-mode stiffness of the pier frames and higher modes in the columns. The global model was used to study the interaction of the various structural units and to account for the variation in column height. The global model required careful evaluation of results because there were several modes of vibration of unrelated units with nearly identical periods. Thus combination of modal results required careful study and engineering judgment. Modal results were combined in both the root mean square (rms) and the peak plus root mean square (prms) of remaining modes procedures. If the two procedures yielded results that differed by more than 10 percent, a detailed study was made of the individual modal contributions to confirm the applicability of the procedure.

Soil-structure interaction was handled by investigating the sensitivity of the dynamic models to flexible foundations. Foundation flexibility was varied from fully rigid foundations to a liberal estimate of soil flexibility. Flexibility of the pile-footing-soil structure was determined from a conservative (reduced) estimate of soil pressure against the footing versus deformation and from an elastic analysis of pile-to-soil interaction. An iterative procedure was employed to arrive at compatible values of deflection and pressure. Soil modulus variation with depth, n_h, was estimated at 4300 kN/m (16 pci) from static lateral load tests, in situ pressure tests, and other data. This value was reduced by 50 percent to account for group action and by an additional 50 percent to account for the cyclical nature of the loading. The two main pier foundation flexibilities were established using nonlinear p-y curves.

Column exterior dimensions were established in part on architectural criteria with wall thickness determined by minimum load requirements for nonseismic loadings or minimum seismic design resistance as determined by the normal strength design relationship:

$$\phi M_n = [(\gamma M_E \delta)/R] \text{ or } M_L \quad (1)$$

where

ϕ = capacity reduction factor (0.7),
M_n = nominal section strength (corresponding to the axial load present in each case),
γ = load uncertainty factor (taken as 1.0 for seismic case),
δ = slenderness effect,
R = response reduction factor,
M_E = elastic seismic moment, and
M_L = various combinations of nonseismic moments.

The seismic moment in each principal direction was increased by 30 percent of the orthogonal seismic moment to account for shocks occurring in any direction.

Nominal section capacity was calculated by an explicit strain compatibility analysis. Maximum concrete strain of 0.003 was assumed and the distance from the compressive face to the line of zero strain was iterated to produce interaction diagrams. In general, minimum longitudinal reinforcement ratios of 1 percent satisfied strength requirements. A variation of this procedure was also used to develop moment curvature relationships that were used to check the ductility requirements. A Kent-Park-type concrete stress-strain curve was used in this analysis (7).

After column strengths were established, the required pile layouts were determined so as to reliably develop the plastic hinge in the columns. An overstrength factor of 10 percent rather than 25 percent was used for the following reasons:

- Required ductilities yielded steel strains well below the strain level required for onset of hardening;
- Column strengths were in all cases governed by the tensile yield of the steel; and
- Piles had an additional structural capacity beyond that established by the soil strength that had been conservatively established.

Pile flexural strengths were assessed by the ability to resist the shear associated with plastic

hinging in the columns. This analysis accounted for partial passive resistance against the pile cap as described previously. Vertical piles were used throughout except under the two main piers immediately adjacent to the ship channel. Future channel widening will result in a significant length, 10 m (32 ft), of exposed pile. Battered piles were thus used for lateral resistance in these two piers. Steel pipe piles were selected for these elements to provide greater ductility than would be available from concrete piles. This was felt to be necessary to partly offset the less predictable behavior of the batter pile system.

Soil densification was used to mitigate the effects of potential liquefaction. An area extending twice the estimated depth of potential liquefaction beyond the outlines of each footing was densified using the Vibro-flotation technique. Vibro-flotation probe spacing was determined by densification results checked by Dutch cone probes. Soil densification was also used to stabilize the east bank of the West Waterway against slope failure during the design earthquake.

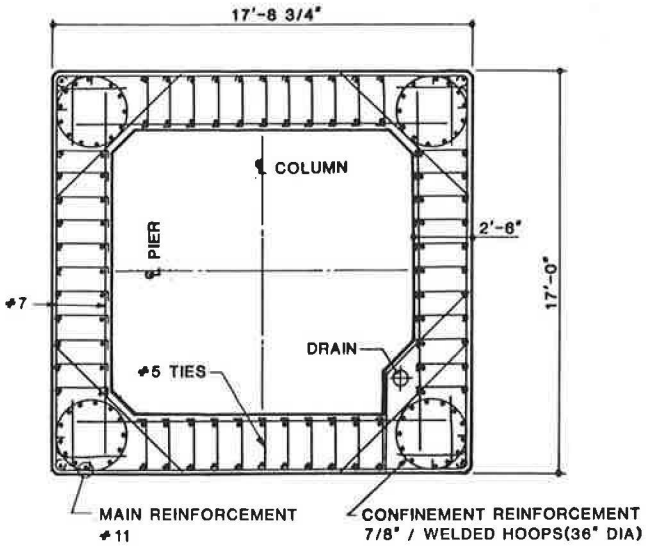

FIGURE 10 Column section, main pier.

DETAILING

Careful attention was given to detailing required to achieve the desired level of seismic performance in order to ensure the ability of the structure to form the plastic hinges in the assumed locations and to sustain the inelastic rotations required without loss of stability. Points of particular concern were the connection of piles into the footings, footing reinforcing, confinement reinforcing in the columns, splicing of the longitudinal reinforcing in the columns, and cap beam and superstructure reinforcing required to force the plastic hinges into the columns.

Piles were extended into the footing 76 cm (30 in.) for concrete piles and 122 cm (48 in.) for steel piles. A mild steel reinforcing cage was extended an additional 152 cm (60 in.) beyond the end of the pile. The bottom layer of reinforcing was placed between piles and a top mat of reinforcing and a face mat on footing sides was used to completely knit together the footing block. Exterior piles were provided with "hairpin" reinforcing to prevent the cracking out of a corner of the footing by pile moment.

Column reinforcing was arranged in two systems. The major portion of the longitudinal steel was arranged in four groups, one in each corner of the column (Figure 10). These groups were confined by tightly spaced, 100 mm (4 in.), heavy, 22 mm (7/8 in.) diameter closed welded hoops in the hinge zones. Outside the hinge zones spacing was increased. The faces of the hollow box sections were provided with a minimum of 0.5 percent (on a local basis) longitudinal reinforcing, horizontal shear reinforcing in each face, and through thickness ties in the hinge regions. Detailed reinforcing layouts were developed, including models, to assure that the intended patterns could be placed and that space was available for concreting.

Expansion joints were located at the ends of the 408-m (1,340-ft) main span unit and at 240-m (800-ft) spacing in the approaches. Gaps at expansion joints were sized to provide for creep, shrinkage, and normal thermal expansion plus two-thirds of the estimated relative motion under design earthquake. It was felt that this would provide for nominal seismic movement without incurring an inordinate cost penalty for the expansion joint unit. A calculated risk philosophy was thus adopted for these elements. Seat lengths for girders at the expansion joints were set in accordance with the empirical recommendations of the ATC. Cable-type restrainers were provided between units at the expansion joints.

SUMMARY

Seismic design of the West Seattle Bridge presented significant challenges requiring extensive investigations and use of the latest concepts for evaluation of seismic response to provide a safe yet economical design for a major bridge at a difficult site. Key elements in the design process contributing to this successful project were

- Detailed geotechnical investigations including pile load tests and studies to carefully define the design earthquake,
- Extensive dynamic analyses with both upper and lower bounds of boundary conditions, and
- Explicit consideration of inelasticity and careful detailing to provide controlled inelastic response.

It should be noted that these studies and analyses were carried out within a compressed design time frame without delay to the overall schedule. Final design began in January 1980 and construction bids were opened in October of the same year for the main span unit. All portions of the improvement are now under construction with final completion scheduled for late 1984.

The project sponsor is the city of Seattle with funding assistance under the FHWA Bridge Replacement Program. The West Seattle Bridge design team is a joint venture of the firms of Andersen-Bjornstad-Kane-Jacobs, Inc.; Parsons, Brinckerhoff, Quade & Douglas; Tudor Engineering; and Kramer, Chin & Mayo of Seattle. Main span superstructure design was provided by Contech, Inc., and the geotechnical consultant was Shannon & Wilson, Inc. The seismicity studies and design spectrum were performed by Shannon and Wilson under the direction of George Yamane. Paul Grant and M.J. Wu developed the pile test program and recommendations developed from the tests. Dynamic analyses, seismic design criteria, and foundation design were performed by Andersen-Bjornstad-Kane-Jacobs under the direction of Thomas Mahoney. Construction contracts totaling $87 million

have been awarded to Kiewit-Grice and Moseman Construction.

It is estimated that the cost impact of the more refined seismic design is limited almost entirely to a small increase in design effort. This additional design effort is a small price to pay for the increased ability of this major structure to survive a major seismic event.

REFERENCES

1. S.T. Algermissen and S.T. Harding. The Puget Sound Earthquake of April 29, 1965. Preliminary Seismological Report. U.S. Coast and Geodetic Survey, Washington, D.C., 1965.
2. N.M. Newmark and W.J. Hall. Earthquake Spectra and Design Engineering. Earthquake Engineering Research Institute, Berkeley, Calif., 1982.
3. Highway Bridge Design Brief. MWD Publication CDP 7-02/D. New Zealand Ministry of Works and Development, Wellington, 1978.
4. Seismic Design Guidelines for Highway Bridges. ATC-6. Applied Technology Council, Berkeley, Calif., 1981.
5. H.E. Chapman. An Overview of the State of Practice in Earthquake Resistant Design of Bridges in New Zealand. Proc., Workshop on Earthquake Resistance of Highway Bridges, Report ATC-6-1, Applied Technology Council, Palo Alto, Calif., 1979.
6. A.S. Veletsos and N.M. Newmark. Effect of Inelastic Behavior on the Response of Simple Systems to Earthquake Motions. Proc., Second World Conference on Earthquake Engineering, Tokyo and Kyoto, Japan, 1960.
7. R. Park and T. Paulay. Reinforced Concrete Structures. Wiley, New York, 1975.

Publication of this paper sponsored by Committee on Dynamics and Field Testing of Bridges.

Prestressed Concrete Highway Bridges in the Federal Republic of Germany—Construction Methods and Experiences

KURT RAHLWES

ABSTRACT

Approximately 63 percent of all bridge surfaces on federal highways in the Federal Republic of Germany consist of prestressed concrete built since 1950. In a short period of time a large volume of work has been accomplished using a new method of construction. Most of the structures meet fully all serviceability, durability, and functional standards with an acceptable maintenance outlay. A few negative experiences could, however, not be avoided. Their causes were faults in design and construction, as well as weak points in the technical regulations, which formed the basis for the design. This report describes the construction principles used in prestressed road bridges, the faults and damage that occurred, and the measures taken to avoid them.

In 1980 approximately 30 percent of the 27,000 bridges in the federal highway and freeway system of West Germany were prestressed concrete bridges (1). This constitutes about 63 percent of the total bridge surface area. Almost all of these prestressed concrete bridges have been built since 1950.

TENDER AND BIDDING PROCEDURE

The client, generally a government agency, works out a design that comprises the technical boundary conditions. The required services and quantities are established on the basis of a preliminary analysis. When the contract is awarded, the contractor, in addition to the actual construction, has to supply and take responsibility for the final structural analysis and the shop drawings. All design documents are checked to the last digit and approved by a federally licensed independent engineer. Construction is continuously supervised by staff of the transportation department. Payment is generally based on unit prices.

In addition to bidding on the original design, the contractor generally has the option of submitting an alternative design. He is responsible for submitting complete and binding quantities and services with the design. When a contract is awarded for a design, payments are made based on unit prices and required material quantities but only up to the total sum submitted in the bid. Approximately 75

percent of all bridges are built according to alternative designs.

CONSTRUCTION METHODS

Precast girders, either pretensioned in casting beds or posttensioned with subsequent bonding, are used primarily with cast-in-place top slabs for bridges over existing roadways. This system is also used for multispan bridges. Maximum spans of up to 160 ft (∿50 m) can be accomplished with this method.

The girders are placed in position by mobile cranes or specially designed launching gantries. They can also be manufactured in situ, for example, by the Schreck method with transverse movable self-supporting scaffolding or by means of traveling falsework. In the latter case, the formwork is stationary during the construction of a particular span and the girders are placed sideways in their final position by movable portal cranes at the bents (Figure 1).

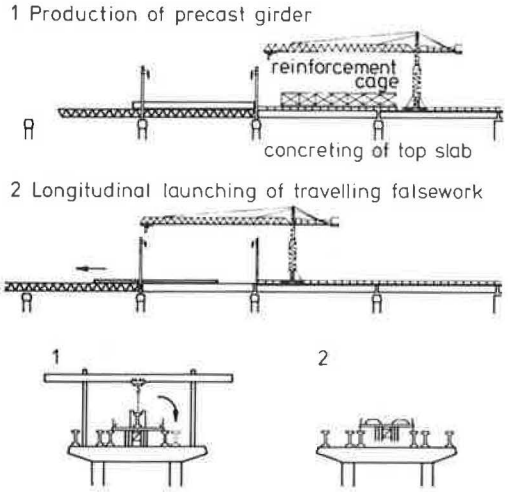

FIGURE 1 Precast girder bridges erected with traveling falsework.

For small girder spacings the upper flanges of the precast girders are used as formwork for the cast-in-place top slab, and for more widely spaced girders additional precast concrete panels or movable formwork are employed. The difference in age between the precast girders and the cast-in-place top has to be considered in the design.

Statically determinate spans are used for up to 130 ft (∿40 m) where the joint between the individual spans is generally covered by a continuous top slab (Figure 2). To allow for sufficient flexibility in this continuous top slab, a soft intermediate layer between the precast girders and the top slab is provided in the vicinity of the joint. This flexible slab has to be designed for all external loads as well as all deformations in the adjacent spans. A main design criterion is the control of crack width. This construction method is very economical in this form; however, piers or bents reaching over the entire width of the bridge section with a large number of individual bearings are required.

Continuous bridge structures can be built with precast girders by joining them monolithically by diaphragms cast in place with the top slab (Figure 3). The top slab reinforcement, using either rebars

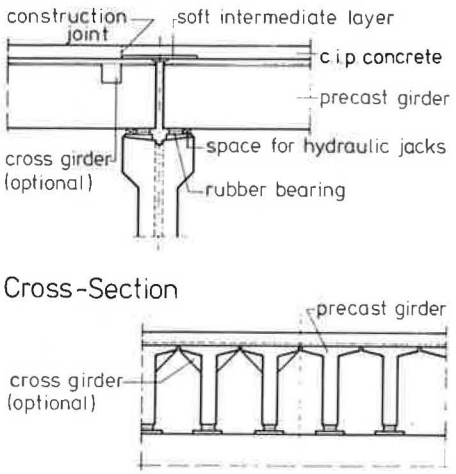

FIGURE 2 Reinforced concrete slab over joint between two spans.

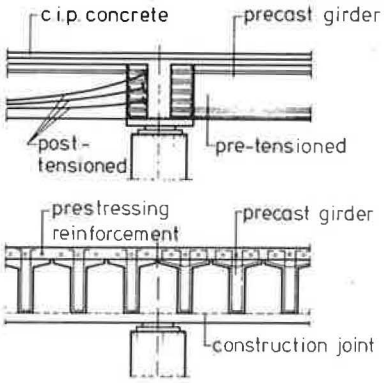

FIGURE 3 Span-by-span construction with precast girders—section through main girder and cross girder.

or prestressing, is designed for negative support moments at the bents.

Both alternatives of this construction method with precast girders feature relatively small main girder spacings in order to minimize or to eliminate the formwork for the cast-in-place top slab and to reduce self-weight. This last objective is achieved in many cases by reducing the web thickness and providing bottom flanges for the precast girders. This results in complex cross sections with large surface areas and edges exposed to potentially aggressive environmental conditions.

A majority of prestressed concrete bridges are built as statically indeterminate, continuous, monolithic, cast-in-place structures. For spans of up to 100 ft (∿30 m), solid or voided slabs are most common. For spans longer than 100 ft (∿30 m), T-girder or box-girder sections are generally used. Total monolithic lengths of more than 3,300 ft (∿1000 m) have been achieved.

There are a number of advantages to these continuous bridge structures over simple-span structures. First, they feature higher structural safety due to internal force redistribution capabilities. Their deformations are smaller and continuous, which improves the dynamic aspects and driving condition of the road surface. Fewer though heavier bearings are required and can be installed with good accessi-

bility for easy maintenance. The number of construction joints and expansion joints that require servicing and maintenance is smaller. Continuous monolithic structures adapt more easily to complex geometric and aesthetic forms. Finally, large spans can only be bridged satisfactorily with continuous structures. The disadvantage of continuous structures lies in their higher sensitivity to temperature effects and support settlements, which have to be accounted for by an appropriate design.

Bridges of only a few spans and short overall length are generally concreted in one pour on falsework and posttensioned with tendons that are subsequently grouted. Longer bridge structures and multispan structures are concreted in sections (Figure 4). The postbonded tendons are connected with cou-

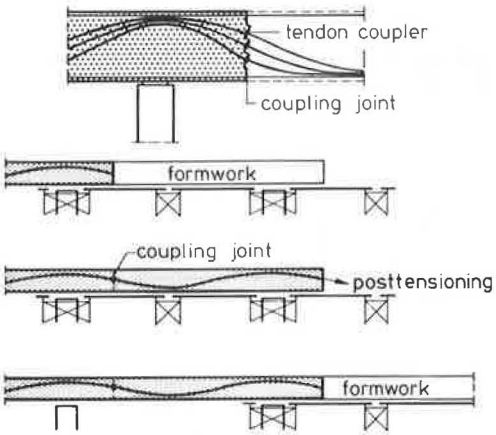

FIGURE 4 Sectional construction of continuous posttensioned concrete bridges.

plers at the construction joints (Figure 5). The present level of development of monolithic sectional construction with scaffolding was reached with the introduction of traveling falsework. The formwork and metal scaffolding travel, supported by special shoring piers, as a unit from one construction sec-

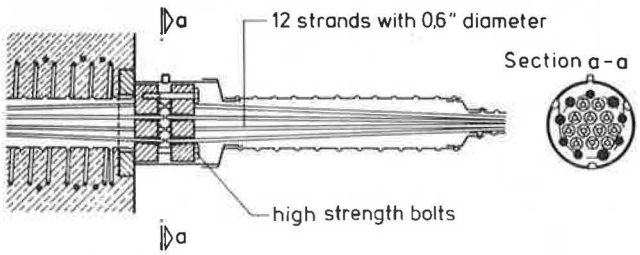

FIGURE 5 Coupling of prestressing tendons with 12 x 0.6 in. strands.

tion to the next (Figures 6 and 7). The economical use of this traveling falsework requires special cross sections that should be uniform over the entire bridge length.

The double webbed T-girder without diaphragms supported by individual piers meets this requirement best. The formwork and the metal scaffolding units can be removed and can travel to the next construction section quite easily. Another advantage of this type of cross section is that the main girder rein-

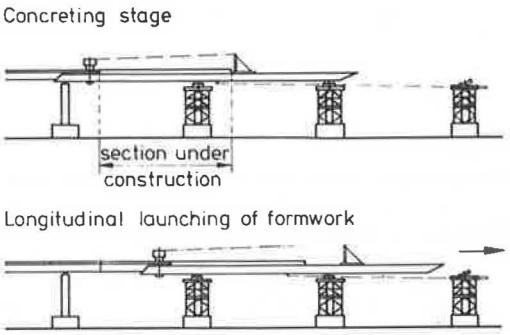

FIGURE 6 Traveling falsework without intermediate supports.

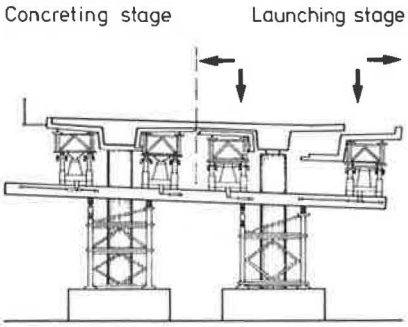

FIGURE 7 Traveling falsework for double T-girder sections.

forcement can be prefabricated and placed as a large reinforcement cage. Box-girders can also be built with traveling falsework with some additional effort for formwork and concreting. Box-girders offer the advantage of readily providing space for service and inspection. The disadvantages of box-girder sections, in addition to increased difficulties in concreting, are the larger changes in internal forces, due to cracking of the concrete, that do not occur to the same extent in T-girder sections. The influences of temperature, differential creep, and shrinkage are more complex and, in some cases, more severe.

The incremental launching method developed by F. Leonhardt is a shoring-free construction method for multiple-span prestressed concrete superstructures. The principle is based on the segmental fabrication of the superstructure in a stationary construction pit located behind one of the abutments and the incremental longitudinal launching of the superstructure by means of hydraulic jacks as each segment is completed. During launching, the superstructure slides on temporary sliding bearings that are installed on the piers or, for large spans, on auxiliary steel or concrete piers (Figure 8). The superstructure is centrically prestressed with tendons distributed uniformly over the cross section and coupled at the construction joints to account for the variation of internal forces during launching. A light steel launching nose tensioned to the front end of the superstructure is used to reduce cantilever bending moments. In addition to the centrical prestressing for the launching stages, tendons are placed in embedded ducts following the moment distribution of the finished bridge structure. They are tensioned when the superstructure has reached its final position. At that stage the temporary sliding bearings are removed and the permanent bearings in-

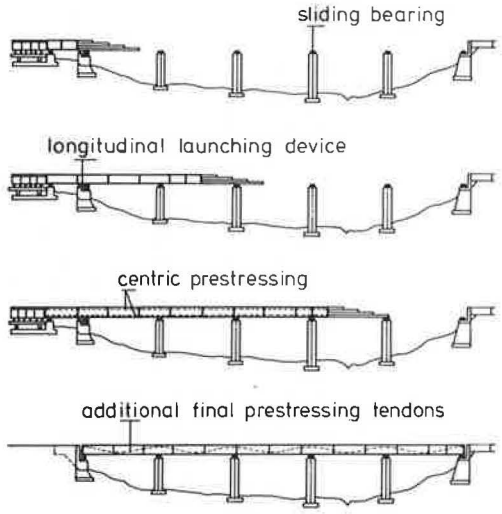

FIGURE 8 Principle of incremental launching method.

stalled while the superstructure is jacked up hydraulically.

The first bridges built with the incremental launching method were of the box-girder type. Since then, however, the double webbed T-girder has proved to be competitive because of the simple construction process. Another advantage of the T-girder is its small torsional stiffness. The T-girder can adapt easily to the forced deformations caused by inaccuracies in the level of the sliding bearings and the bottom of the superstructure, which are encountered during the launching process.

The incremental launching method can also be adapted for curved bridges as long as the radii of curvature in plan and in elevation are constant or nearly constant.

Another shoring-free construction method for continuous, prestressed, concrete bridges is the cast-in-place cantilever construction method that was developed by Finsterwalder and that is primarily used for large-span, beam-type bridges. To date, the bridge with the longest span built this way is the Koror Bridge that connects two smaller islands near the island of Guam. The span is 790 ft (241 m) long. The most important recent application of this method in West Germany was the construction of the Kochertal Bridge with spans of up to 452 ft (138 m) and a total monolithic length of 3,700 ft (1128 m). The box-type center of the cross section (Figure 9) was erected using the cast-in-place cantilever method, and subsequently the cantilevering portions of the top slab were cast up to a total deck width of 100 ft (30.5 m) by traveling formwork and supported by inclined struts.

Extensive experience with the cantilever construction method using precast segments does not exist in West Germany. However, a few bridges of this type have been erected by German contractors abroad.

EXPERIENCES

To point out mistakes that have been made and how they can be avoided it is necessary to elaborate on the negative experiences. It must, however, be emphasized beforehand that most prestressed concrete bridges in West Germany meet fully all serviceability, durability, and functional standards. When the proper servicing and maintenance are provided for these bridges, no serious doubts exist about the life expectancy, which ranges from 50 to 80 years, of these structures. Wearing parts such as surfacing, curbs, and sidewalks as well as expansion joints inevitably have to be repaired at shorter intervals. It is also important to note that so far there have been no deaths or injuries caused by failure in service of prestressed concrete bridges.

GENERAL INFORMATION

The concrete grade normally used is B 45, which means a minimum 28-day cube strength of 45 MN/m² that corresponds to more than 5,000 psi 28-day cylinder strength. The reinforcing steel generally consists of deformed bars of grade BSt 420/500, which corresponds to a grade 60 steel.

There has been no long-term experience with epoxy-coated rebars or with other corrosion protection for the reinforcement in West Germany.

Typically prestressing steels used during the last 10 years have been high-strength alloy bars with a maximum diameter of 1.40 in. (36 mm) and an ultimate strength of 154 ksi (1080 N/mm²) or 0.6-in.-diameter strands with a minimum strength of 250 ksi (1770 N/mm²). Most bridges incorporate transversely prestressed top slabs and diaphragms.

By far the larger number of bridge structures was provided with asphalt surfacing (Figure 10) 1.5-2.5 in. (4-6 cm) thick, which consisted of protection and wearing layers on top of a waterproofing layer covering the entire bridge surface. This waterproofing used to consist of glued aluminum or copper foils, but it is now made up of a 0.4 in. (1 cm) thick asphalt mastic layer on top of a glassfleece sheet for vapor pressure ventilation. The waterproofing is directly connected to the drain inlets

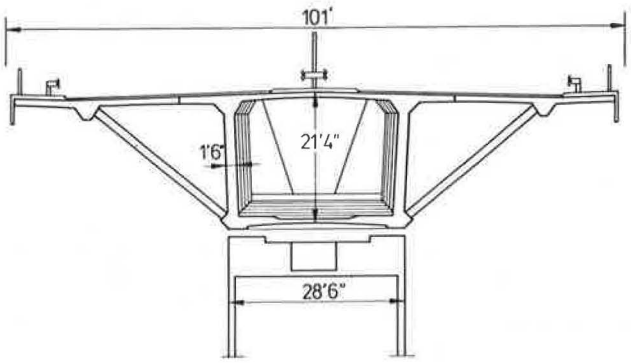

FIGURE 9 Cross section of Kochertal bridge.

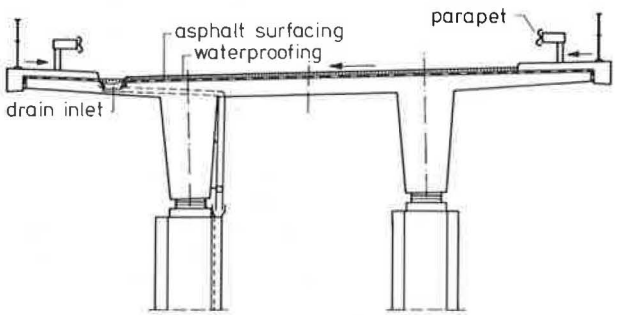

FIGURE 10 Typical cross section of road bridge.

to allow drainage of seepage water. Recently the concrete surface under the waterproofing has been treated with an epoxy-based sealant as an additional barrier to prevent penetration of chlorides from deicing salts. The heavy use of deicing salts also led to the construction of curbs, sidewalks, and facia beams in one unit using air-entrained concrete.

DEFECTS AND DAMAGE

There are two reasons for the defects and damage that have been encountered: the violation of commonly known technical rules in design and execution at the time of construction and weak points in these rules at the time.

Bridges were constructed with not enough or even completely missing concrete covers over the reinforcement as a result of insufficient or inadequate bar supports and the presence of pockets or porous concrete areas caused by inadequate concrete mixtures and insufficient vibration consolidation and curing. Because of both deficiencies, the carbonation of the concrete can reach the reinforcement in only a few years, which results in the destruction of the thin alkaline-based protective oxide film on the reinforcement (Figure 11). The formation of rust, which follows the destruction of the corrosion protective layer, reduces the effective cross section and the fatigue strength of the reinforcement. The expansive properties of rust also lead to fracture planes and spalling of the concrete cover. Damage of this sort is the most frequent and extensive. Repair requires chiseling off the concrete cover, derusting, and applying new corrosion protection for the reinforcement and a new concrete cover.

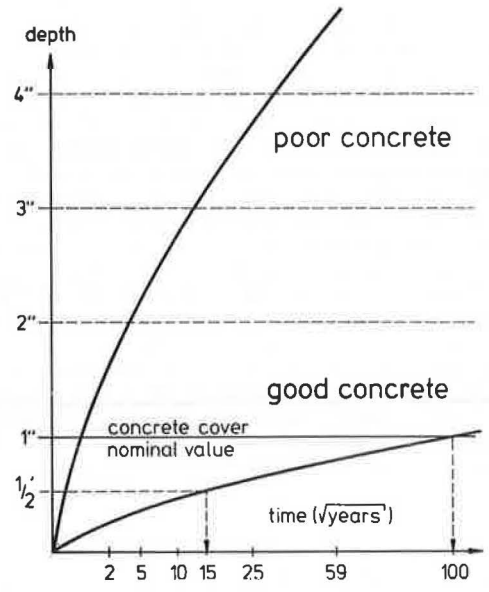

FIGURE 11 Carbonation, chloride penetration (3).

An example of severe damage of this kind is two large viaducts with statically determinate precast concrete girders and expansion joints between spans. These viaducts had to undergo substantial repair work after only 12 years in order to assure unrestricted durability (2).

In addition to the previously mentioned causes of damage, deficiencies and damage resulted from

- Leakage of the bridge deck waterproofing,
- Leakage at the drain inlets,
- Leakage at the expansion joints,
- Clogging of drain pipes, and
- Intensive use of deicing salts on the road surface.

Another construction deficiency of prestressed concrete bridges is prestressing ducts that are not completely or not at all grouted. The partly or completely missing bond and protection against corrosion and stress-crack corrosion constitutes a severe deficiency. The problem was discovered about 10 years ago when, for a short time, a prestressing steel with high sensitivity to stress-crack corrosion was marketed. Some prestressing tendons were forcefully catapulted from ungrouted ducts after rapid stress-crack corrosion led to prestressing steel rupture. The subsequent investigations showed that, much more frequently than expected, tendons were only partly or not at all grouted. Defects, however, could only be found where records of the grouting process showed that, at the end of the grouting of a duct, there was doubt that the flow-out of grout mix at the far end was of the proper consistency.

In the meantime, practical methods of radiographic examination, for example, with Cobalt 60, have been developed to detect these deficiencies. Subsequent grouting by means of a special vacuum process, in which the evacuated amount of air and the injected quantity of grout mix can be checked, is possible. Subsequent grouting is possible provided that the prestressing steel is not severely damaged, which is generally the case for dry and airtight ducts. For the subsequent grouting, holes are drilled into the duct with a special drill that automatically switches off when approaching steel.

Another mistake that was made during construction is missing or inadequate treatment of the concrete during the initial curing phase. All concrete surfaces have to be kept moist. In addition, loss of heat before prestressing has to be prevented by means of an insulating cover over the top slab. When the top slab is not insulated, the heat of hydration of the curing concrete can create large temperature differences. While these temperature differences are compensated, the previously warmer portions of the cross section, such as the section interior, will exhibit tensile stresses. If this happens before prestressing, cracks with large widths can open up in these areas due to the low initial tensile strength of the concrete and the relatively small percentage of mild reinforcement in prestressed concrete structures.

The stresses created by temperature differences during the curing of the concrete are reduced to about 10 percent by creep. However, during the prestressing operation these stresses are present in full magnitude. They can also lead to cracks in the prestressed structural member when additional unintentional tensile stresses, caused by a rebounding effect of the formwork, are superimposed. It is now common practice to consider these effects in analysis and design and to avoid these tensile stresses by a systematic lowering of the shoring during the prestressing operation.

Cracks can also occur when the nominal design prestressing force is not reached at all points. This can be due to deficiencies in design or in construction (Figure 12). Correct prestressing depends on complete determination of all tendon curvatures to calculate friction losses and the exact and systematic installation of the prestressing ducts and tendons. Tendon curvatures should be kept as small as possible to minimize the influence of deviations

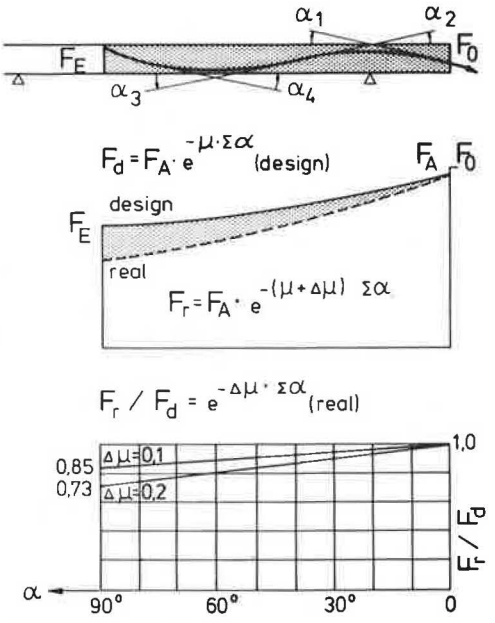

FIGURE 12 Friction losses.

in the friction coefficients. Corrosion of the prestressing steel, especially smooth high-strength wires and strands, and of the prestressing ducts can significantly increase the friction coefficients. Corrosion damage to the prestressing steel can lower its fatigue strength and can be the origin of stress-crack corrosion in the tensioned but ungrouted state. Prestressing steel and ducts should, therefore, be kept protected against corrosion and installed quickly.

One of the most frequent violations of the common rules of technical knowledge in design is cross section dimensions that are too small. They result in reinforcement and prestressing steel concentrations that complicate the placing of the concrete, which in turn leads to the formation of pockets and inadequately vibrated concrete zones. Similar consequences can result from complex cross sections and poor detailing. Another design mistake is not making stress checks at all relevant sections. Areas in the vicinity of the supports of continuous girders can be critical especially when temperature effects are neglected.

In general, however, it should be noted that the system of using federally licensed independent engineers to check the complete design eliminates, to a large extent, mistakes in the design. One of the unfortunate exceptions is a bridge in Berlin-Schmargendorf that was built in 1960 with an overall length of 754 ft (230 m). The bridge was extensively repaired in 1970 but had ultimately to be removed due to the overall lack of safety of the structure (2). The damage resulted from construction deficiencies (about 1/5 of the tendons were not properly grouted); from weak points in the construction and building codes valid at that time; and especially from severe mistakes in the structural analysis, particularly in the shear design. In addition, the cross section caused difficulties in concreting.

The second category of reasons for deficiencies in prestressed concrete bridges is weak points in the building and construction code provisions valid at the time of application. For a better understanding, a short history of the development of the most important code provisions for prestressed concrete bridges in West Germany is useful. The first German building code for prestressed concrete was introduced in 1953. Since 1953 the allowable service stress in prestressing steel has been retained at the low level of 75 percent of the yield strength or 55 percent of the ultimate strength. This generally leads to certain reserves in the theoretical ultimate load state and the possibility of correcting unexpectedly high friction losses during the prestressing operation by means of overstressing, for example, up to 90 percent of the yield strength.

The code provisions for permissible concrete tensile stresses using limited prestressing, which has been used for most of the road bridges, were also retained. The code provision stipulates that no flexural tension due to dead load and 1/2 x live load may occur. Under full live load and dead load, flexural tensile stresses of the magnitude of the tensile strength of the concrete are permitted. It should be noted here that the check on concrete tensile stresses can be very sensitive for slender, large-span bridges because of inaccuracies resulting from differences of large numbers.

The German prestressed concrete code of 1953 allowed the control of crack width by means of a stress check in the mild reinforcement assuming a cracked section. Under service loads, the reinforcement stresses were limited to the usual service stress criteria, and under loads factored by 1.35 the limit was set by the yield stress. Yielding of the prestressing reinforcement was not permitted. In design practice, however, reinforcement was often provided to cover the nominal concrete tensile forces. Only since 1979 have additional crack width control provisions been required. Because the load safety factor of 1.35 is meaningless in the vicinity of the point of contraflexure, this criterion will be replaced by an additive safety term. Even now the analytic check on crack width is questionable. The formulas for the prediction of crack width used in different countries can yield very different results. Reality is not always predicted satisfac-satisfactorily.

Requirements for minimum reinforcement ratios did not change until 1973 (Figure 13). For example, grade 60 deformed bars in the longitudinal direction of a girder web had to be provided to at least 0.15 percent of the concrete area. Later this ratio was raised to 0.4 percent for approximately 5,000 psi (grade B 45) concrete. In addition, the minimum re-

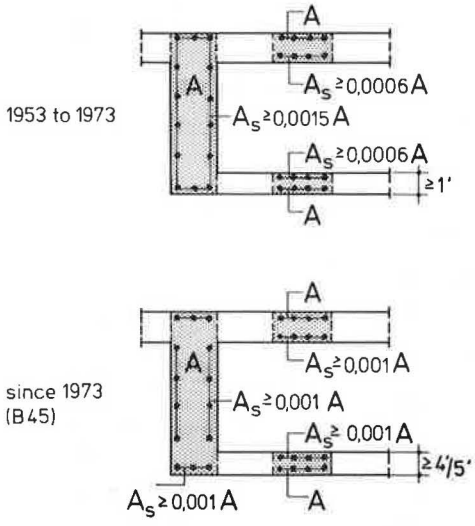

FIGURE 13 Minimum reinforcement requirements.

inforcement ratios are now linked to the concrete grade.

Before 1966 no minimum reinforcement requirement for shear existed. Nominal shear reinforcement was to be provided in all areas where theoretical principal tensile stresses under factored ultimate loads did not exceed the tensile strength of the concrete. Frequently this rule was misinterpreted leading to cross-sectional dimensions that barely met this requirement and, thus, resulted in an underreinforced shear design.

The minimum reinforcement cover was increased in several steps from 0.8 in. (2 cm) in 1953 to 1.4-1.6 in. (3.5-4 cm) now, depending on environmental conditions.

Temperature differences between the top and the bottom face of a structural member were generally not taken into account before 1979. Now superstructures with asphalt surfacing have to be analyzed for a temperature difference of 9°F (5°C) superimposed on the most unfavorable condition caused by live loads.

Significant changes in the design for coupling joints of sectionally erected prestressed concrete bridges were introduced in 1977. Reasons for doing so were the frequent occurrence of cracks in the vicinity of coupling joints and especially the rupture of tendons in the bottom flange of a box-girder bridge near Duesseldorf. The overall stability and safety of the structure were no longer guaranteed and could only be restored with auxiliary supports and reduced allowable traffic loadings (2). Now the bridge has been repaired and reopened to regular traffic (Figure 14).

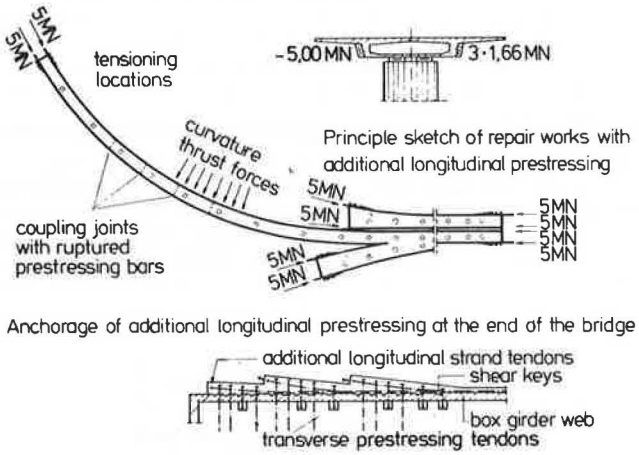

FIGURE 14 Repair of bridge near Duesseldorf (2).

An investigation of all other bridges with coupling joints showed that by the end of 1980 about 21 percent of all structures with T-girder cross sections and 41 percent of the structures with box-girder cross sections exhibited cracks with widths of more than 0.008 in. (0.2 mm) in the vicinity of coupling joints. It had to be decided if sufficient corrosion protection would be maintained by simply injecting the cracks with epoxy resin or if other measures would have to be taken because the cracks led to high cyclic wear on the couplers of the tendons, whose fatigue strength is lower than the fatigue strength of the tendons themselves.

These incidents stirred up considerable public attention and gave rise to critical considerations of the durability and safety of these types of bridge structures. Intensive investigations of the Duesseldorf bridge showed that cracks of up to 0.08 in. (2 mm) had formed in the bottom flange due to the fact that the design concrete compression stress level was not reached. This resulted in higher fatigue loadings and corrosion of the tendons, which led to their subsequent rupture. It became obvious that a number of causes can trigger such a phenomenon. The most important ones are

- Temperature differences, which were not considered in the design, between the top and bottom face of a structural member;
- Inaccuracies in determining bending moments due to dead load and prestressing in the vicinity of the points of contraflexure where coupling joints are usually located; these can also be caused by inexactly known moment redistributions due to creep;
- Increased loss of prestressing force in the area of coupling joints caused by creep and larger steel cross sections of the tendon couplers;
- Nonlinear stress distributions due to tendon anchorages in the coupling joints; and
- Inadequate tendon forces at the coupling joints due to unfavorable friction conditions.

Certainly this does not conclude the list of encountered defects, damage, and deficiencies. Alkali-reactive expansive aggregates, unsuitable concrete additives, the already mentioned oversensitive prestressing steel, and other problems should be pointed out. However, they constitute special phenomena that, when understood, should not be repeated.

EFFECTS OF CRACKS

It is generally agreed that, because of the wide spread of concrete tensile strengths and the various temperature effects starting at construction, prestressed concrete bridges cannot be built completely without cracks. The risk potential of cracks in prestressed concrete bridges is twofold. Where cracks can propagate through the concrete section, the cyclic wear in mild and prestressed reinforcement increases (Figure 15). In the area of prestressing

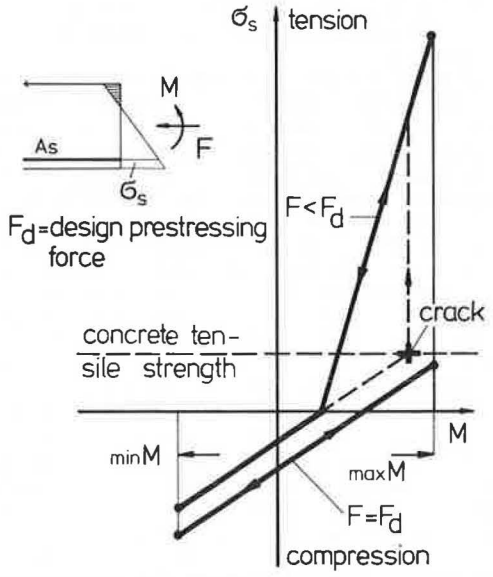

FIGURE 15 Stress deviations in the reinforcement due to live loads.

tendon couplings, which are sensitive to cyclic loading, an appropriate design, especially by means of increased mild reinforcement, has to reduce the effects of cracks to an acceptable level. The investigations of the damage to coupling joints have also shown that not all cracks visible at the concrete surface have led to higher cyclic wear in the reinforcement. Cracks that do not propagate deep into the cross section hardly change the cyclic load characteristics with respect to the uncracked stage. The condition of existing structures can only be determined by measuring the changes in crack width under varying loadings.

The second risk, originating from cracks, is the danger of corrosion. All design rules have in common the avoidance of few and large cracks in favor of more cracks with smaller crack widths. Cracks up to 0.008 in. (0.2 mm) wide are considered harmless under conditions prevailing with bridges. However, Soretz claimed in 1967 that crack width does not have the assumed effect on corrosion of the reinforcement as long as the concrete cover has sufficient depth and the concrete is properly mixed and consolidated. He based his findings on extensive investigations of reinforced concrete bridges in several European countries. Recent investigations by Schiessl (3) based on long-term outdoor experiments and a report by Rostam (4) on more than 2,000 partially prestressed bridges in Denmark seem to substantiate this opinion. Finally, day-to-day experience with reinforced concrete structures has also shown that not so much the crack width, as long as 0.02 in. (0.5 mm) is not exceeded, but rather the depth and quality of the concrete cover determine the susceptibility to corrosion.

Especially under the influence of deicing salts, a proper design, a flawless construction, and a continuous maintenance of the waterproofing and drainage installations are fundamental.

RESULTS

So far, no comprehensive report on the condition of the prestressed concrete bridges in West Germany exists. The yearly costs for maintenance, rehabilitation, and renewal are estimated at between 1.5 and 2.5 percent of the updated initial construction costs. These costs depend directly on traffic development, on environmental conditions, and especially on future use of deicing salts.

A statistical risk analysis (5) based on 76 prestressed concrete bridges built between 1960 and 1980 concludes that 6.6 percent of the bridges show moderate damage and 3.7 percent show severe damage. This investigation will be continued and supplemented by studies on weak points.

An investigation of 281 prestressed concrete bridges in the state of Lower Saxony in 1978 and 1979 (6) indicates a decrease in structural quality with time. In addition, it is shown that of the bridges built between 1950 and 1960, 67 percent are lightly damaged, 44 percent are moderately damaged, and 13 percent are so severely damaged that it is questionable if repairs would be worthwhile.

At 18 percent of the bridges, parts of the reinforcement were exposed. Pockets and poorly consolidated areas in the concrete could be found in 11.5 percent of the structures. Cracks of more than 0.004 in. (0.1 mm) were found in 4.5 percent of the prestressed concrete structures, and 25.5 percent showed leaking waterproofing. Significant differences in the costs for maintenance, repair, and replacement between reinforced and prestressed bridges were not found in these examinations.

CONCLUSIONS

In evaluating the prestressed concrete construction method for road bridges as used in the Federal Republic of Germany during the last 30 years, one must bear in mind that a large amount of construction was completed using a fairly new construction method. Mistakes in design, in execution, and in the technical standards were unavoidable.

The technical standards of today incorporate the experience of the past 30 years. In design and execution, constant efforts are necessary to take into account all available experience and recent technical knowledge.

Special care must be devoted to guarantee durability under all environmental influences. Easy-to-build designs are necessary, which facilitate the pouring and compacting of the concrete so that it not only achieves the required strength but also all the other properties necessary for durability and corrosion protection. Finally, great effort must be taken in the design of the structure's waterproofing and drainage installations to ensure good functioning, simple fabrication, and good serviceability.

On-site quality control that is stricter than that which has been practiced in many cases in the past is necessary. This applies especially to the strongly weather-dependent waterproofing work, because of the effect of deicing salt.

When these prerequisites are met, prestressed concrete bridges can be constructed that are competitive and whose maintenance costs remain within an economically justifiable framework.

REFERENCES

1. F. Standfuss. Vortrag Deutscher Betontag, 1981.
2. Der Bundesminister für Verkehr-Abteilung Strassenbau-Schäden an Brücken und anderen Ingenieurbauwerken. Dokumentation. Bonn, Federal Republic of Germany, 1982.
3. Schiessl. CEB-rilem Workshop, Copenhagen, Denmark, May 1983.
4. S. Rostam and E.S. Pedersen. FIP Symposium, Bucharest, Rumania, Sept. 1980.
5. G. König and B. Wittke. IABSE Workshop, Switzerland, June 1983.
6. D. Rabe. Die Unterhaltung von Stahlbeton- und Spannbetonbrücken. Bauingenieur, Vol. 56, 1980, pp. 431-437.

Publication of this paper sponsored by Committee on Construction of Bridges and Structures.